University of Allberta

Self-Directing Organometallic Deposition of Ruthenium. Preparation, Characterization and Evaluation of Bimetallic, Ru Adatom Modified Pt Surfaces for the Electrooxidation of Methanol in Direct Methanol Fuel Cells.

By

Christopher Edward Lee

©

A thesis submitted to the Faculty of Graduate Studies and Research in partial fulfillment of the requirements for the degree of Doctor of Philosophy

Department of Chemistry

Edmonton, Alberta

Spring 2003

National Library
of Canada

Acquisitions and
Bibliographic Services

395 Wellington Street
Ottawa ON K1A 0N4
Canada

Bibliothèque nationale
du Canada

Acquisisitons et
services bibliographiques

395, rue Wellington
Ottawa ON K1A 0N4
Canada

Your file Votre référence
ISBN: 0-612-82130-7
Our file Notre référence
ISBN: 0-612-82130-7

The author has granted a non-exclusive licence allowing the National Library of Canada to reproduce, loan, distribute or sell copies of this thesis in microform, paper or electronic formats.

The author retains ownership of the copyright in this thesis. Neither the thesis nor substantial extracts from it may be printed or otherwise reproduced without the author's permission.

L'auteur a accordé une licence non exclusive permettant à la Bibliothèque nationale du Canada de reproduire, prêter, distribuer ou vendre des copies de cette thèse sous la forme de microfiche/film, de reproduction sur papier ou sur format électronique.

L'auteur conserve la propriété du droit d'auteur qui protège cette thèse. Ni la thèse ni des extraits substantiels de celle-ci ne doivent être imprimés ou aturement reproduits sans son autorisation.

Canada

University of Alberta

Library Release Form

Name of Author: Christopher Edward Lee

Title of Thesis: Self-Directing Organometallic Deposition of Ruthenium. Preparation, Characterization and Evaluation of Bimetallic, Ru Adatom Modified Pt Surfaces for the Electrooxidation of Methanol in Direct Methanol Fuel Cells.

Degree: Doctor of Philosophy

Year this Degree Granted: 2003

Permission is hereby granted to the University of Alberta Library to reproduce single copies of this thesis and to lend or sell such copies for private, scholarly or scientific research purposes only.

The author reserves all other publication and other rights in association with the copyright in the thesis, and except as herein before provided, neither the thesis nor any substantial portion thereof may be printed or otherwise reproduced in any material form whatever without the author's prior written permission.

Christopher Edward Lee
11430 32 Avenue
Edmonton, Alberta
CANADA
T6J 3H5

Date: April 14 2003

University of Alberta

Faculty of Graduate Studies and Research

The undersigned certify that they have read, and recommend to the Faculty of Graduate Studies and Research for acceptance, a thesis entitled "Self-Directing Organometallic Deposition of Ruthenium. Preparation, Characterization and Evaluation of Bimetallic, Ru Adatom Modified Pt Surfaces for the Electrooxidation of Methanol in Direct Methanol Fuel Cells" submitted by Christopher Edward Lee in partial fulfillment of the requirements for the degree of Doctor of Philosophy

Professor Steven H. Bergens

Professor Josef Takats

Professor Martin Cowie

Professor Monica Palcic

Professor Janet A.W. Elliott

Professor Richard J. Puddephatt

, 2003

Abstract

State of the art direct methanol fuel cells use Pt-Ru particles as anode electrocatalysts for the oxidation of methanol. There are two longstanding difficulties with evaluating such catalysts; first, there are no proven methods to measure their specific surface areas (number of active sites); and second, there are no proven methods to measure the surface ratio of Pt to Ru on black (rough) Pt-Ru surfaces or particles. Further, the reported methods to prepare such catalysts do not have demonstrable control over these parameters, and surface segregation may occur during the high temperature stages of the preparation. As a result of these difficulties, the optimum surface composition and chemical state of such catalysts is still under investigation nearly 40 years after their discovery. An organometallic chemistry approach to this problem was chosen. It was found that black Pt (as a gauze or as a powder) effects the hydrogenation (1 atm, - 40°C, in hexanes) of (1,5-cyclooctadiene)$Ru(C_3H_5)_2$ to result in Ru adatoms (Ru_{ad}) adsorbed by the Pt surface and the concomitant formation of cyclooctane and propane. By monitoring the reaction at low temperatures using gas chromatography or UV-Vis spectrophotometry, real time control over both the number of surface equivalents of Ru_{ad} deposited on Pt, and over the activity of the resulting Pt-Ru_{ad} surfaces was realized. This reaction was used to prepare a series of blacked Pt-Ru_{ad} gauzes and black Pt-Ru_{ad} powders of reasonably defined surface areas and surface compositions. The activities of these gauzes and powders towards the electrooxidation of methanol under typical operating conditions for a direct methanol fuel cell were determined. Remarkably, the black Pt-Ru_{ad} powders were stable towards hot pressing into Nafion® membranes and towards use in prototype direct methanol fuel cells operating at 90 °C. The optimum surface composition for operation in direct methanol fuel cells under these conditions was determined.

Bernard, Eileen, and Catherine Lee

Acknowledgement

I would like to thank my advisor, Professor Steven H. Bergens for his support and guidance throughout my studies in his laboratories and for presenting me with many interesting projects to become involved with over the years. I would also like to thank the past and present members of the Bergens group, especially, Dr. Jason Wiles, Dr. Christopher Daley, and Carolyn Leong.

I would like to thank the staff of the Spectral Services Laboratory, Glassblowing Shop, Electronic Instrument Services, and the Machine Shop. In particular, Al Chilton, Ed Feschuk, and Henry Stolk. The expertise offered by these people in the construction of the specialized equipment and further technical assistance they provided was invaluable. The assistance of Dianne Formanski, Youbin Shao, and Professor Gary Horlick with inductively coupled plasma spectrophotometry is also sincerely appreciated. In addition the assistance of Professor A. Meldrum and Greg Popowich for the TEM and EDS analysis and also the University of Alberta SLOWPOKE II Nuclear Reactor Facility and Dr. John Duke for the INAA determinations.

I would like to acknowledge and thank the friends who have supported me and been great companions over the years in Edmonton, in particular, Craig McIlhargey, Jesse Watson, Maury Richards, Katie Campbell, Dr. Dusan Ristic-Petrovic, Bryan Rowsell, and Nolan Erickson. In addition, I would like to thank Dr. Claire Mormiche and Dr. Sam Peppe who have become great friends and travelling companions, sharing in many trips throughout England and France.

I especially would like to thank my parents and my sister for their constant support throughout my studies.

Table of Contents

Chapter 1

Electrochemical Energy Conversion, Direct Methanol Fuel Cells, and Methods for the Preparation of Bimetallic Platinum-Ruthenium Surfaces for Catalysis.

Part I. Introduction

Methods for production of electrical energy from fuels 1

Conversion of chemical into electrical energy in batteries and fuel cells 2

Fuel cells and the hydrogen economy 3

The electrocatalytic reactions of a typical fuel cell. 5

The thermodynamics and kinetics of fuel cells 8

The classification of fuel cells. 13

Direct methanol fuel cells 18

The anodic oxidation of methanol on Pt-based electrocatalysts 20

Preparation of bimetallic particles composed of Pt and Ru - practical electrocatalysts 23

Characterization of bimetallic surfaces and particles 26

Preparation of bimetallic surfaces composed of Pt and Ru - model systems 29

Spontaneous deposition methods for the preparation of Pt-Ru electrocatalysts 31

Performance evaluation and optimization of Pt-Ru electrocatalysts 32

Applications of Pt-Ru surfaces beyond direct methanol fuel cells 34

Part II. Overview.

A method for the preparation of bimetallic Pt-Ru_{ad} surfaces of known surface area and defined surface composition 34

References 37

Chapter 2

Self-Directing Organometallic Deposition of Ru Adatoms on Pt. Part I. The Hydrogenation of a Ru containing Precursor on a Pt Substrate.

Introduction.....51

Results and Discussion

Electrochemical determination of the real surface area of blacked Pt gauzes.....54

Preparation of (COD)Ru(π-allyl)$_2$ and Pt substrate.....56

Hydrogenation of (COD)Ru(π-allyl)$_2$.....58

Electrochemical characterization of the Pt-Ru$_{ad}$ Surfaces.....62

Composition of the Ru Deposit.....66

Conclusions.....66

Experimental Section.....67

References.....72

Chapter 3

The Self-Directing Organometallic Deposition of Ru on Pt. Part II. The Optimization of Pt-Ru$_{ad}$ Surface Composition for the Electrooxidation of Methanol and Adsorbed Carbon Monoxide.

Introduction.....74

Results and Discussion

General Methods.....75

Electrochemical characterization of Ru$_{ad}$ modified blacked Pt gauzes.....76

Anodic stripping of adsorbed carbon monoxide.....76

Potentiodynamic oxidation of CH_3OH.....81

Potentiostatic oxidation of CH_3OH 84
Variable temperature studies 86
Stability of Ru_{ad} modified blacked Pt gauzes 87
Conclusions 88
Experimental Section 89
References 91

Chapter 4

Self-Directing Organometallic Deposition of Ru, Part III. Deposition of Ru on a Nanoscale Pt Substrates and the Evaluation of Pt-Ru_{ad} Anode Electrocatalysts in Prototype Direct Methanol Fuel Cells.

Introduction 93
Results and Discussion
Electrochemical characterization of nanoscale Pt and Pt-Ru_{ad} particles 96
Self-directing organometallic deposition of Ru_{ad} on Pt_{black} 97
Energy dispersive X-ray analysis of Ru_{ad} modified Pt_{black} and 20 wt % Pt/C 99
Electrochemical characterization of Pt_{black}-Ru_{ad} 100
Anodic stripping voltammetry of adsorbed carbon monoxide on Pt_{black} and Ru_{ad} modified Pt_{black} surfaces 102
Evolution of Ru_{ad} modified Pt_{black} surfaces 109
Evaluation of Pt_{black}-Ru_{ad} electrocatalysts in the anodes of direct methanol fuel cells 111
Electrochemical characterization of thin film anodes and cathodes 111
Direct methanol fuel cell polarization and power curves 113
The effects of surface composition on DMFC performance 116
Summary and Conclusions 118
Experimental Section 120
References 127

Chapter 5

Summary and Overview of Results 132

List of Tables

Chapter 1

Table 1.1. The classification of fuel cells.....18

Chapter 2

Table 2.1. The effects of reaction temperature on C_8 product distribution.....59

Chapter 4

Table 4.1. The bulk compositions of Pt-Ru_{ad} particles determined by EDX and GC.....99

List of Figures

Chapter 1

Figure 1.1. Galvanic electrochemical cells (a) primary, (b) secondary, and (c) fuel cells. 2

Figure 1.2. A fuel cell operating on H_2 and O_2 using an acidic electrolyte 5

Figure 1.3. The three-phase reaction zone at an electrocatalyst particle in a fuel cell anode operating on H_2.....7

Figure 1.4. A polarization curve (jV curve) for a H_2 fuel cell. 12

Figure 1.5. The power curve (PV curve) and operating efficiency (%) of a H_2 fuel cell. (The PV curve was calculated from the jV curve (Figure 1.4) using eq. 1.20. The conversion efficiency of the cell was calculated using eq. 1.22 ($\varepsilon_{thermal}$ 0.83 for a H_2 fuel cell, $\varepsilon_{voltage}$ was calculated using eq. 1.19 and the jV curve (Figure 1.4), a value of 1 was assumed for $\varepsilon_{faradaic}$).).....13

Figure 1.6. Nafion® (1) polymer electrolyte.....16

Figure 1.7. Schematic diagram of a DMFC 19

Chapter 2

Figure 2.1. A cyclic voltammogram of a blacked Pt gauze electrode at 25 °C in 1.0 M $H_2SO_{4(aq)}$. The potential is swept in the directions indicated by the arrows at 10 mV/s...55

Figure 2.2. Preparation of a Pt surface for Ru deposition 57

Figure 2.3. Number of equivalents C_8 hydrocarbons formed during hydrogenations of **1** *vs.* time for reactions carried out at 20 and -10 °C.....60

Figure 2.4. Number of equivalents of **1** consumed and total number of equivalents C_8 hydrocarbon products produced in solution versus time for a hydrogenation of **1** carried out at -10 °C.....61

Figure 2.5. (a) Cyclic voltammograms (sweep rate 5 mV/s in 1.0 M H_2SO_4(aq)) of a surface resulting from the deposition of 2.7 eq Ru_{ad}, recorded before and after saturation of the surface with CO_{ads} at 50 mV. (b) Cyclic voltammograms of a blacked Ru electrode recorded under conditions identical with those in (a). (The voltammograms in (a) and (b) are not normalized for surface area).....63

Figure 2.6. Cyclic voltammograms (sweep rate 5 $mV \cdot s^{-1}$, [H_2SO_4] = 0.5 M, [MeOH] = 0.5 M, 25 °C) of a catalyst surface generated by deposition of 3.5 eq Ru_{ad} 65

Chapter 3

Figure 3.1. Cyclic Voltammograms of blacked Pt gauze electrodes modified by the deposition of: (a) 0, (b) 0.05, (c) 0.30, (d) 0.70, and (e) 3.5 eq Ru_{ad}. These are the stable voltammograms recorded after the electrooxidation of CO_{ads} in 0.5 M H_2SO_4 at 5 mV/s (currents are scaled to illustrate the differences in morphology of the voltammograms)..77

Figure 3.2. The CO stripping voltammogram of a 0.05 eq Pt-Ru_{ad} electrode at 5mV/s..79

Figure 3.3. A plot of the CO_{ads} stripping peak potentials *vs.* eq Ru_{ad} for a series of Pt-Ru_{ad} electrodes under identical conditions.....79

Figure 3.4. Anodic sweeps of CH_3OH electrooxidation over a 0.10 eq Ru_{ad} electrode. The curves are a composite of two experiments containing the first, second, and third sweeps from one and the fourth and fifth sweeps from the other experiment 82

Figure 3.5. Third current-normalized anodic sweeps for the potentiodynamic oxidation of methanol over 0.0 (-),0.05 (- -), 0.10 (- ..-), 0.30 (- .-),0.44 (...), and 0.70 (---) eq Ru_{ad} 83

Figure 3.6. Normalized current *vs.* time for the potentiostatic oxidation of methanol over 0.0 (-),0.05 (- -),0.10 (- ..-),0.30 and 0.32 (- .-),0.44 (...), and 0.70 (---) eq Ru_{ad} at 0.40V 85

Figure 3.7. Turnover frequencies *vs.* eq Ru_{ad} for the potentiostatic oxidation of methanol over Pt-Ru_{ad} at 0.40 V.....85

Figure 3.8. Arrhenius plots of ln(j) *vs.* T^{-1} for the potentiostatic oxidation of CH_3OH over 0.05 and 0.10 eq Pt-Ru_{ad} at 0.40 V. 86

Figure 3.9. Potentiostatic oxidation of CH_3OH over 0.10 eq Pt-Ru_{ad} before and after 16 h of electrochemical activity. 87

Chapter 4

Figure 4.1. Voltammograms of Pt electrocatalyst deposits in 1.0 M H_2SO_4(aq); (a) 0.285 mg Pt_{black} at 50 mV/s, and (b) 0.279 mg of 20 wt % Pt/$C_{Vulcan\ XC\text{-}72R}$ at 20 mV/s.. 97

Figure 4.2. Surface composition (measured from the number of equivalents C_8 hydrocarbons in solution) *vs.* time for a hydrogenation of **1** over Pt_{black} at -45 °C.....98

Figure 4.3. Voltammograms of a series of Pt_{black}-Ru_{ad} deposits ((a) 0.053 (b) 0.29 (c) 0.46, and (d) 0.68 eq Ru_{ad}) recorded in 1.0 M H_2SO_4(aq) at 50 mV/s. The dashed lines are voltammograms of a Pt_{black} deposit included as a visual reference.....101

Figure 4.4. Stripping voltammogram of CO_{ads} on a Pt_{black} deposit (0.250 mg) recorded in CO free 1.0 M H_2SO_4(aq) at 50 mV/s. The solid line is the first complete sweep starting at 50 mV (in the direction indicated by the arrow) and the dashed line is the second potential cycle after removal of CO_{ads} from the deposit. 104

Figure 4.5. Stripping voltammograms of CO_{ads} on a series of Pt_{black}-Ru_{ad} deposits ((a) 0.053, (b) 0.29, (c) 0.46, and (d) 0.68 eq Ru_{ad})) recorded in CO free 1.0 M H_2SO_4(aq) at 50 mV/s. The solid lines are the first potential sweeps from the adsorption potential of 50 mV and the dashed lines are the second complete potential cycles).....106

Figure 4.6. Peak potentials for CO_{ads} stripping *vs.* surface composition for a series of Pt_{black}-Ru_{ad} deposits recorded in CO free 1.0 M H_2SO_4(aq) at 50 mV/s.....107

Figure 4.7. Stripping of Ru_{ad} from Pt_{black}-Ru_{ad} deposits during potential cycling in 1.0 M H_2SO_4(aq) at 50 mV/s ((a) 0.053, (b) 0.29, (c) 0.46, and (d) 0.68 eq Ru_{ad}). The solid lines are the initial sweeps, the dashed lines are the final sweeps, and the hairlines show the intervening sweeps.....110

Figure 4.8. Cyclic voltammograms of a series of DMFC anodes (solid lines) and cathodes (dashed lines) at 10 mV/s. The anode surface compositions are (a) 0.0535, (b) 0.29, (c) 0.46, and (d) 0.68 eq Ru_{ad}. The currents are normalized to the mass of the electrocatalyst present 112

Figure 4.9. Polarization curves recorded at 90 °C for a Pt_{black}-Ru_{ad}(0.29 eq Ru_{ad})//Nafion® 117//Pt_{black} DMFC recorded before (solid circles) and after (open circles)

several days of operation. Anode: 1.0 M methanol at 3.5 mL/min. Cathode: 20 psig O_2(g) at 600 mL/min.. 114

Figure 4.10. Cyclic voltammograms of a 0.29 eq Ru_{ad} anode before (solid line), and after (dashed line) several days of intermittent operation. The voltammograms were recorded at 10 mV/s. 115

Figure 4.11. Polarization curves for a series of Pt_{black}-Ru_{ad}//Nafion® 117//Pt_{black} DMFC at 90 °C. Anode: 1.0 M methanol at 3.5 ml/min. Cathode: 20 psig O_2(g) at 600 ml/min.116

Figure 4.12. The optimum surface composition of Ru_{ad} in operating DMFC (open circles = 60 °C, filled circles = 90 °C).. 117

Figure 4.13. Photos of fuel cell hardware and of the heated press used for MEA fabrication; (a) Graphite cell block, (b) heated press showing the heated aluminum blocks, hydraulic press and the power regulators for heating the assemblies, (c) a completed MEA laid over a Teflon® gasket and the cell block shown in (a), and (d) the assembled fuel cell hardware showing connections to test-stand apparatus (not shown), fuel and oxidant feeds.).....126

List of Abbreviations and Symbols

A	area	cm^2
α	transfer coefficient	
D	dispersion	%
ΔG	Gibbs free energy change	kJ/mol
ΔH	enthalpy change	kJ/mol
ΔS	entropy change	kJmol K
ε	efficiency	
$\varepsilon_{faradaic}$	faradaic efficiency	
$\varepsilon_{fuelcell}$	overall efficiency of a fuel cell	
$\varepsilon_{thermal}$	thermodynamic efficiency	
$\varepsilon_{voltage}$	voltage efficiency	
E	potential	mV, V
E_{an}	anode potential	mV,V
E_{an}°	standard anode potential	mV,V
E_{cath}	cathode potential	mV,V
E_{cath}°	standard cathode potential	mV,V
E_{cell}	cell potential	mV,V
E_{cell}°	standard cell potential	mV,V
E_{open}	open circuit potential	mV, V
E_{open}°	standard open circuit potential	mV, V
F	charge per mole of electrons (Faraday)	96485 C/mol e-
i	current	mA,A
$i_{\circ}$	exchange current	mA, A
j	current density	mA/cm^2
$j_{geometric}$	current per unit of geometric electrode area	mA/cm^2
j_{real}	current per unit of real catalyst surface area	mA/cm^2, $\mu A/\mu mol$
$j_{specific}$	current per gram of catalyst	mA/mg
n	number of moles of electrons transferred	mol

n_{Ruad}	number of moles of Ru adatoms	mol
$n_{Ptsurface}$	number of moles of Pt surface atoms	mol
$n_{surface}$	number of moles of surface atoms	mol
n_{total}	total moles of catalyst	mol
P	power	mW, W
Q	charge	mC, C
Q_{CO}	charge due to CO oxidation	mC
Q_{CO+O}	charge due to surface oxide formation and CO oxidation	mC
Q_O	charge due to surface oxide formation	mC
R	resistance	Ω
θ_{CO}	surface coverage by CO_{ads}	
θ_{OH}	surface coverage by OH_{ads}	
θ_{Ru}	surface coverage by Ru_{ad} (fraction of surface atoms that are Ru atoms)	
T	temperature	°C, K
t	time	s
ν	sweep rate	mV/s
v	reaction rate	mol/s cm^2
ad	Adatom	
ads	Adsorbed Species	
AES	Auger Electron Spectroscopy	
AFC	Alkaline Fuel Cell	
ALE	Atomic Layer Epitaxy	
CV	Cyclic Voltammetry	
CVD	Chemical Vapor Deposition	
DEMS	Differential Electrochemical Mass Spectrometry	
DMFC	Direct Methanol Fuel Cell	
EDX	Energy Dispersive X-Ray Analysis	
EXAFS	Extended X-Ray Adsorption Fine Structure	
FC	Fuel Cell	
GC	Gas Chromatography	

GC-IR	Gas Chromatography - Infrared Spectroscopy
GC-MS	Gas Chromatography - Mass Spectroscopy
GDE	Gas Diffusion Electrode
HRTEM	High Resolution Transmission Electron Microscopy
ICE	Internal Combustion Engine
LEED	Low Energy Electron Diffraction
LEIS	Low Energy Ion Scattering
LSV	Linear Sweep Voltammetry
MCFC	Molten Carbonate Fuel Cell
MEA	Membrane Electrode Assembly
MOCVD	Metallorganic Chemical Vapor Deposition
MVD	Metal Vapor deposition
NAA	Neutron Activation Analysis
PAFC	Phosphoric Acid Fuel Cell
PEM	Polymer Electrolyte Membrane
PEMFC	Polymer Electrolyte Membrane Fuel Cell
PVD	Physical Vapor Deposition
RHEED	Reflection High Energy Electron Diffraction
SEM	Scanning Electron Microscopy
SOFC	Solid Oxide Fuel Cell
SOMC	Surface Organometallic Chemistry
STM	Scanning Tunneling Microscopy
TEM	Transmission Electron Microscopy
TN	Turnover Number
UHV	Ultra High Vacuum
upd	Underpotential Deposition
XANES	X-ray Absorption Near Edge Spectroscopy
XPS	X-Ray Photoelectron Spectroscopy
XRD	X-Ray Diffraction
YSZ	Yttrium Stabilized Zirconia

Chapter 1

Electrochemical Energy Conversion, Direct Methanol Fuel Cells, and Methods for the Preparation of Bimetallic Platinum-Ruthenium Surfaces for Catalysis.

Part I. Introduction

Methods for production of electrical energy from fuels. A fuel cell is an electrochemical device in which the free energy change of a combustion reaction is directly converted into electrical energy.[1] The first fuel cell was invented in 1839 by Sir W.R. Grove. Grove observed minute currents due to reaction of H_2 and O_2 at Pt electrodes immersed in H_2SO_4(aq).[2, 3] The net chemical reaction for thermal, catalytic, and electrocatalytic combustion of a fuel is the same. The fuel (e.g., H_2) reacts with an oxidant (O_2) to produce combustion products and energy (eq. 1.1).

$$H_2 + 1/2\ O_2 \longrightarrow H_2O + \text{energy} \qquad \text{(eq. 1.1)}$$

Energy is released as heat and light during thermal and catalytic combustion of H_2. The heat released can be converted to mechanical work. The amount of heat that is converted into mechanical work is limited by the Carnot principle. According to the Carnot principle the efficiency of any reversible heat engine depends on the temperature range over which it operates, and not on the properties of the working substances.[4] In practice, the efficiency of a heat engine (e.g., an internal combustion engine) is ~ 20 %.[5] A generator could then be used to convert the mechanical work into electrical energy. The typical overall efficiency of this process is ~ 18%. In 1894 Ostwald noted that, unlike heat engines, the maximum efficiency of an electrochemical conversion process (e.g., combustion of H_2 in a fuel cell) is not limited by the Carnot principle.[6] In fact, depending on the entropy change of the reaction, it is theoretically possible for a fuel cell to operate with conversion efficiencies in excess of 100 %. In practice, electrochemical conversion efficiencies of 60 to 80 % have been obtained using fuel cells.[7] Even in 1894

Ostwald warned that intolerable pollution would result if direct electrochemical conversion was not developed as an alternative to thermal combustion methods for the production of electricity.[5]

The major advantage to the use of fuel cells for the production of electrical power over thermal methods is the promise of higher energy conversion efficiencies. This higher efficiency would lead to a reduction of CO_2 emissions, and could eliminate emissions of NO_x, SO_2, CO, hydrocarbons, and particulates.[7-9] Other advantages of the use of fuel cells over heat engines include their simple construction (no moving parts), that they are scaleable to meet a wide range of power requirements, and their quiet operation.[1, 7]

Conversion of chemical into electrical energy in batteries and fuel cells. A galvanic electrochemical reaction converts chemical energy into electrical energy. Galvanic cells either produce electricity directly from chemical energy (primary cells and fuel cells) or they store electricity in the form of chemical energy (secondary cells). Figure 1.1 illustrates the fundamental differences between primary batteries, secondary batteries, and fuel cells. In a primary or secondary battery the fuel, oxidant, and

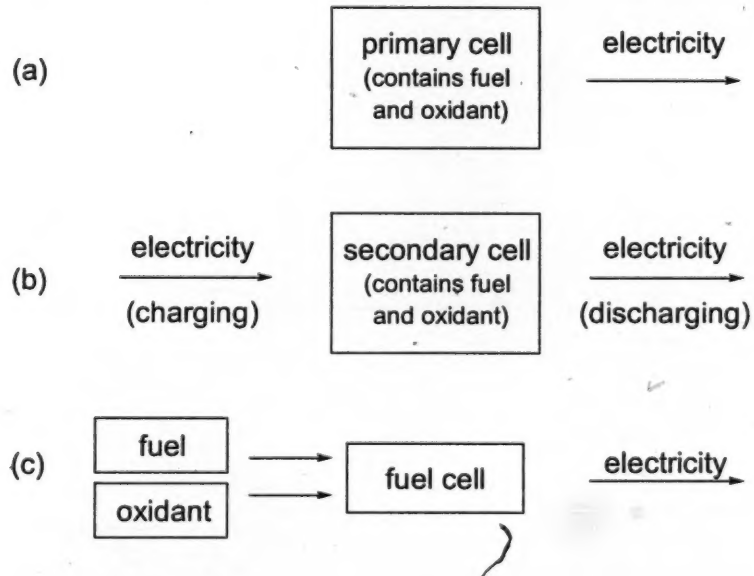

Figure 1.1. Galvanic electrochemical cells (a) primary, (b) secondary, and (c) fuel cells.

electrodes form a self-contained (closed) system. A primary cell is one in which the electrodes are consumed during the reaction and the reaction is irreversible. In a secondary cell the electrodes are consumed during the reaction, however, they can be regenerated (recharged) by the application of an external power source that provides electric current and drives the galvanic reaction in the reverse direction. The fundamental difference between primary or secondary batteries and fuel cells is the nature of the electrodes and their relation to the reactants. A fuel cell consists of an anode and a cathode containing suitable electrocatalysts, an electrolyte, and an external circuit. The fuel and oxidant are stored outside the fuel cell. The fuel and oxidant are fed to the cell as required by the electric load. The reactions that occur in operating fuel cells are electrocatalytic. The operating life span of a fuel cell is therefore not limited by the amount of reactants it contains (such as in primary cells), nor by the number of recharge cycles that the electrodes can tolerate (such as in secondary cells).

Fuel cells and the hydrogen economy. The selection of a fuel for use in a fuel cell requires consideration of the activity of the fuel towards electrooxidation, ease of storage, processing, and availability.[10] The fuel with the highest electrochemical activity is H_2 and all fuel cells are capable of operating using H_2. As a result of its activity in fuel cells, there is considerable interest in the development of an energy economy based on H_2.[11, 12] Unfortunately, practical methods for the large-scale production, storage, and widespread distribution of H_2 do not exist.[13, 14] The storage and distribution of H_2 requires the use of high pressure apparatus or cryogenic liquefaction of the fuel. In addition, there is a serious risk of fire and/or explosion if H_2 is used. The onsite decomposition of H_2 carriers (e.g., NH_3BH_3, $LiAlH_4$, and $NaBH_4$) has been investigated.[15] None of these are attractive alternatives due to the amount of energy lost during the production and processing of the H_2.

The common carbon containing fuels (e.g., coal, natural gas, methanol, and gasoline) can be converted into mixtures of H_2 and CO_2 by steam reforming, partial oxidation, or by autothermal reforming.[16-18] These processes are shown in eq. 1.2, 1.3., and 1.4, respectively, for the conversion of CH_3OH, since it is the most active of the

common fuels towards these conversions. For example, the steam reforming of CH_3OH

$$CH_3OH + H_2O \longrightarrow CO_2 + 3\,H_2 \qquad \text{(eq.1.2)}$$

$$CH_3OH + 1/2\,O_2 \longrightarrow CO_2 + 2\,H_2 \qquad \text{(eq.1.3)}$$

$$4\,CH_3OH + 3\,H_2O + 1/2\,O_2 \longrightarrow 4\,CO_2 + 11\,H_2 \qquad \text{(eq.1.4)}$$

can be carried out at lower temperatures (i.e., 250 °C) than are required for natural gas or gasoline (i.e., 1000 °C).[19, 20] In addition, CH_3OH does not contain sulphur impurities (e.g., H_2S) that are known to poison steam reforming catalysts.

The conversion of CH_3OH into H_2 and CO_2 does not go to completion in a single step. Depending on the method used various amounts of CO remain in the fuel stream. It is well known that CO is an excellent poison for the electrocatalysts (e.g., Pt) used in fuel cells.[7] Additional stages, such as water gas shift reaction (eq. 1.5) or preferential

$$CO + H_2O \longrightarrow H_2 + CO_2 \qquad \text{(eq. 1.5)}$$

oxidation are therefore required to remove even trace amounts of CO from the fuel stream before the processed fuel can be used in most fuel cells. The conversion of any fuel into H_2 thus requires several stages and it requires energy. This reduces the overall energy conversion efficiency of the fuel cell system, increases its complexity, and adds to the overall monetary cost of the system. In addition to catalyst poisoning by CO, the loss of energy due to the conversion of the fuel, the thermal integration of high temperature fuel reforming unit and low temperature fuel cells is a technical challenge.

The only other possible fuel molecule that displays promising electrochemical activity to an extent that makes it a suitable alternative to H_2 for direct electrooxidation in fuel cells is CH_3OH (*vide infra*). CH_3OH is a liquid under most conditions and thus has a higher energy density than H_2; the energy density of CH_3OH is 17.4 MJ/L and that of H_2

(stored at 160 atm) is only 1.55 MJ/L.[7] Furthermore, the transportation and storage of CH_3OH is easier and safer than for H_2.

The electrocatalytic reactions of a typical fuel cell. The electrocatalyst used in the majority of fuel cells is Pt because it is the most active and stable electrocatalyst for oxidation of H_2 and for the reduction of O_2. Figure 1.2 is a schematic diagram of a fuel cell operating on H_2 and O_2 using an acidic electrolyte. The fuel (H_2) is oxidized at the anode to generate electrons and protons (eq. 1.6). The electrons are transported to the cathode through the external circuit, and protons are transferred to the cathode through the electrolyte. Oxygen is reduced to O^{2-} and reacts with protons to generate H_2O at the cathode (eq.1.7). The complete cell reaction (eq. 1.1) is obtained by adding the oxidation (eq. 1.6) and reduction (eq. 1.7) half-cell reactions.

$$H_2 \longrightarrow 2\,H^+ + 2\,e^- \qquad \text{(eq. 1.6)}$$

$$1/2\,O_2 + 2\,H^+ + 2\,e^- \longrightarrow H_2O \qquad \text{(eq. 1.7)}$$

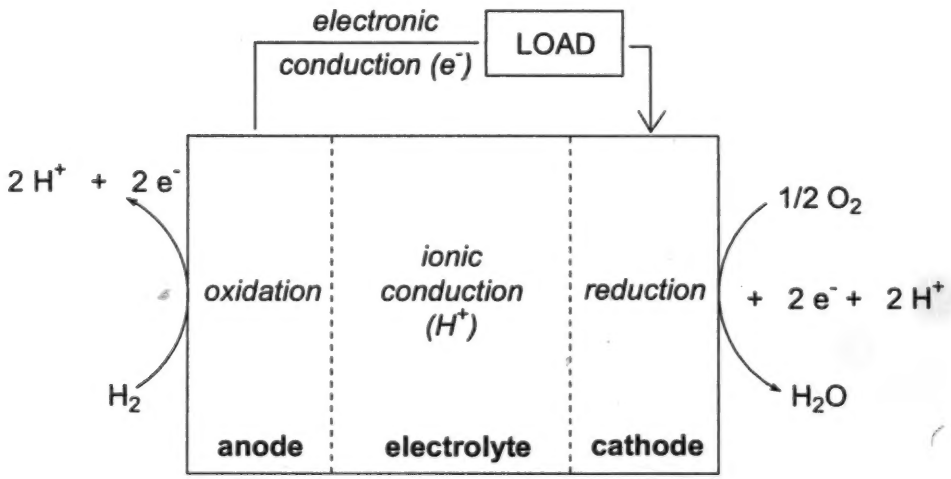

Figure 1.2. A fuel cell operating on H_2 and O_2 using an acidic electrolyte.

The rate of an electrocatalytic reaction is proportional to the number of active sites on the electrocatalyst. The number of active sites is often designated by the real surface area (A_{real}, cm^2) of the electrocatalyst. The average surface packing density of flat polycrystalline Pt (nmol surface atoms per cm^2 of surface area) is 2.18 $\mu mol/cm^2$.[21] The current per mol of active sites is often expressed as the current per cm^2 (mA/cm^2), where the surface area used is that obtained from the number of moles of Pt atoms on the surface of the catalyst and assuming the surface has the same packing density as flat polycrystalline Pt. The specific current density ($j_{specific}$) and the real current density (j_{real}) are related by the specific surface area of the catalyst (e.g., ~28 m^2/g for nanoscale unsupported Pt). The intrinsic activity of an electrocatalyst can be evaluated only via measurements of the real current density. These measures of current density can be used to make meaningful activity comparisons among electrocatalysts. The *intrinsic* and *specific* activities of a Pt electrocatalyst are related by the dispersion of the metal. The dispersion (D, %) of a metal is the ratio of the number of surface sites ($n_{surface}$, mol) relative to the total amount of metal (n_{total}, mol) (eq. 1.8).

$$D(\%) = \frac{n_{surface}}{n_{total}} \times 100 \qquad \text{(eq. 1.8)}$$

The rate of an electrochemical reaction (υ, mol/s cm^2) is directly proportional to the observed current (i, A) as shown by eq. 1.9, where n is the moles of electrons transferred per mole of reactant (e.g., n is 2 for H_2 combustion, eq. 1.1), F is Faradays constant (i.e., 96485 C/mol e^-).

$$\upsilon = \frac{i}{n F A_{real}} \qquad \text{(eq. 1.9)}$$

The electrochemical reactions in a fuel cell occur only on the surface of the electrocatalyst. To make effective use of this expensive noble metal, nanoscale (i.e., high dispersion) Pt particles must therefore be used in the construction of fuel cell electrodes.

State-of-the-art Pt electrocatalysts are between ~ 10 nm (unsupported) and ~ 2 nm (supported on carbon) in diameter, corresponding to dispersions ranging from 10 to 40 %.[21] Figure 1.3 is a summary of the physical states and functions of a single electrocatalyst particle and its immediate surroundings (i.e., the three-phase reaction zone), in a fuel cell anode. The electrodes of a fuel cell are porous to maximize contact between the electrolyte, reactants, active sites on the electrocatalyst, and the electronic conductor. Further, in order to be effective, the microstructure of the electrode must facilitate the transport of reactants to the catalyst surface and removal of the reaction products (e.g., protons, electrons, and neutral molecules, H_2O or CO_2).[7] The electrolyte, electronic conductor, and channels for the transport of the reactants and products must all be in contact with the catalyst particles.

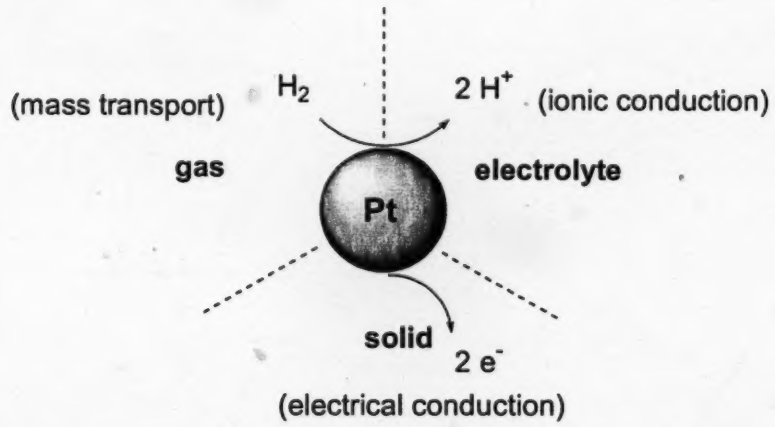

Figure 1.3. The three-phase reaction zone at an electrocatalyst particle in a fuel cell anode operating on H_2.

The rate of an electrochemical reaction depends, among other things, on the number of *available* active surface sites. The utilization of nanoscale Pt electrocatalysts in fuel cells (i.e., the fraction of electrocatalyst particles that satisfy the criteria outlined above) is often significantly less than 100 %. In light of the considerations outlined above, the construction of fuel cells requires that substantial attention be given to the electrode structure on a microscopic scale.

The thermodynamics and kinetics of fuel cells. The standard cell potential ($E°_{cell}$, V) is the difference between the standard reduction potentials for the cathode (e.g., $E°_{cat}$ = 1.229 V (eq. 1.8)), and anode (e.g., $E°_{an}$ = 0 V (eq. 1.7)) half-cell reactions (eq.1.10).

$$E^{o}_{cell} = E^{o}_{cat} - E^{o}_{an} \qquad \text{(eq. 1.10)}$$

The maximum amount of electrical work that can be obtained from a fuel cell is equal to $\Delta G°_{cell}$. The change in free energy of an electrochemical reaction ($\Delta G°_{cell}$, KJ/mol) can be calculated from $E°_{cell}$ by eq. 1.11.

$$\Delta G^{o}_{cell} = -nFE^{o}_{cell} \qquad \text{(eq. 1.11)}$$

The maximum thermal efficiency of a fuel cell under standard conditions ($\varepsilon_{thermal}$) is given by eq. 1.12.

$$\varepsilon_{thermal} = \frac{\Delta G^{o}}{\Delta H^{o}} \qquad \text{(eq. 1.12)}$$

The open circuit potential (E_{open}) of a fuel cell is the potential difference observed between the anode and cathode when there is no net combustion occurring. Under ideal conditions E_{open} is equal to the Nernst potential (E_{cell}) given by eq. 1.13, where R is 8.314 J/mol K, T is temperature in K, and Q is the reaction quotient.

$$E_{open} = E_{cell} = E^{o}_{cell} - \frac{nF}{RT} \ln Q \qquad \text{(eq. 1.13)}$$

The operating voltage of a fuel cell under load ($E_{cell}(j)$) is always lower than E_{open} (E_{cell} or $E°_{cell}$) because of electrode polarization (eq. 1.14).[22] The magnitude of the cell polarization (η_{cell}) reflects the changes in the potentials of the electrodes required to

increase the rate of the electrochemical reaction from zero (i.e., equilibrium values of E_{an} and E_{cat}).[23]

$$\eta_{cell} = E^{o}_{cell} - E_{cell}(j) \qquad \text{(eq. 1.14)}$$

There are several types of overpotential encountered in fuel cells; activation overpotential (η_{act}), ohmic overpotential (η_{ohm}), and concentration overpotential (η_{conc}). Ohmic overpotential arises from resistance to electric and ionic conduction within the cell components. Concentration overpotential arises from mass transport of reactants to the active sites on the electrodes. The values of η_{ohm} and η_{conc} depend on the construction of the fuel cell and on the operating conditions. The value of η_{act} depends on the activities of the electrocatalysts used.[24-26] The value of η_{cell} is the sum of all of the types of overpotential for the anode and the cathode reactions (eq. 1.15).

$$\eta_{cell} = \eta_{act} + \eta_{ohm} + \eta_{conc} \qquad \text{(eq. 1.15)}$$

The Tafel equation (eq. 1.16) is an empirical relation that describes the behavior of η_{act} under irreversible electrochemical reaction conditions.[27] According to eq. 1.16 the rate of an electrochemical reaction increases exponentially as the electrode potential (E(j)) is displaced from its equilibrium value (i.e., the Nernst potential (E_{cell})).

$$\eta_{act} = a + b \log(j) \qquad \text{(eq. 1.16)}$$

The values of "a" and "b" in eq. 1.16 can be determined from measurements of the observed activation overpotentials as a function of current density. The empirical constant "a" is related to the exchange current density, and "b" is the Tafel slope for the electrode reaction. The exchange current density (j_o) is a measure of the intrinsic activity of an electrocatalyst under reversible (i.e., equilibrium) conditions (i.e., j is zero so the forward and reverse reaction rates at the electrode are equal). The Tafel slope is a

measure of the amount of activation overpotential required to increase j by a factor of 10. An effective electrocatalyst exhibits a high j_o and a low Tafel slope.[22]

The limiting current density (j_l) is the maximum rate for an electrode reaction for a given set of mass transport conditions.[22] The concentration overpotential is related to the mass transport of reactants to the electrodes and can be calculated if j_l is known using eq. 1.17.[28] The ln term of eq. 1.17 accounts for the difference between the bulk concentration of a reactant and its concentration at the electrode surface as a fraction of j_l.

$$\eta_{conc} = \frac{RT}{nF} \ln\left(\frac{j_l}{j_l - j}\right) \qquad \text{(eq. 1.17)}$$

The ohmic overpotential (η_{ohm}) is due to the linear increase of the voltage drop (jR drop) across the cell. It is caused by resistance in the electrodes, the electrolyte, and the electronically conducting components of the fuel cell. The magnitude of η_{ohm} is given by eq. 1.18 (i.e., Ohms law).

$$\eta_{ohm} = jR \qquad \text{(eq. 1.18)}$$

The ratio of the observed cell potential under load ($E_{cell}(j)$) to the potential under reversible conditions (i.e., Nernst potential, E_{cell}) reflects the fraction of electrochemical potential energy that is being converted into electricity. It is called the voltage efficiency factor ($\varepsilon_{voltage}$, eq. 1.19).

$$\varepsilon_{voltage} = \frac{E_{cell}(j)}{E_{cell}} \qquad \text{(eq. 1.19)}$$

The power output (i.e., power density (P_{cell}, W)) of a fuel is the product of j and $E_{cell}(j)$ according to eq. 1.20.

$$P_{cell} = j_{cell}E_{cell}(j) \qquad \text{(eq. 1.20)}$$

There is a balance between j and $E_{cell}(j)$ that determines the maximum power output of a fuel cell. The primary goal of fuel cell research in to maximize P at the lowest possible η_{act}. The polarization of electrodes during the operation of a fuel cell is one of the most significant barriers to the construction of practical fuel cells.

There is one additional factor to consider that affects the energy conversion efficiency of a fuel cell, that is the faradaic efficiency ($\varepsilon_{faradaic}$). The faradaic efficiency (eq. 1.21) accounts for any non-electrochemical routes for the electrode reactions to proceed. For instance, the crossover of fuel to the cathode results in the direct reaction (catalytic combustion) of H_2 on the cathode electrocatalyst. This process is a chemical short circuit in the fuel cell. The incomplete electrooxidation of the fuel at the anode may also decrease $\varepsilon_{faradaic}$.

$$\varepsilon_{faradaic} = \frac{\text{coulombs obtained}}{(\text{moles consumed})nF} \qquad \text{(eq. 1.21)}$$

The overall efficiency of a fuel cell (ε_{cell}) is the product of the each of the efficiency terms described above (eq. 1.22).

$$\varepsilon_{fuel\ cell} = \varepsilon_{thermal}\varepsilon_{voltage}\varepsilon_{faradaic} \qquad \text{(eq. 1.22)}$$

In order to optimize the operating efficiency of a fuel cell each individual efficiency factor must be considered. In general $\varepsilon_{thermal}$ is a constant, and $\varepsilon_{faradaic}$ can be increased by careful optimization of operating conditions. Improvements in $\varepsilon_{voltage}$ would allow the actual operating efficiencies of fuel cells to more closely approach their thermodynamic limits.

The performance of a fuel cell is represented by polarization (i.e., jV) and power (i.e., PV) curves. Figures 1.4 and 1.5 show the calculated jV and PV responses of a real H_2 - O_2 fuel cell constructed by Neidrach *et al.*[29] The jV curve in Figure 1.4 was

calculated using eq. 1.23 (a = 0.102 V, b = 5.7 x 10^{-4} kΩ/cm^2, c = 0.088 V, d = 0.16 V, and j_l = 620 mA/cm^2) and eq. 1.14.[30]

$$\eta_{cell} = a \log(j) + b(j) + c \log\left(\frac{j_l - j}{j_l}\right) + d \qquad \text{(eq. 1.23)}$$

The relative contributions of the three types of overpotential to the total cell overpotential vary according to the position along the cell polarization curve. In region (a) it is η_{act} that limits the performance, in region (b) it is the total resistance (R) that limits the performance, and finally in region (c) (at the highest current densities) it is η_{conc} that limits the performance. The power curve shows that the maximum P_{cell} requires a significant η_{cell} and that a fuel cell operates most efficiently at low power loads.

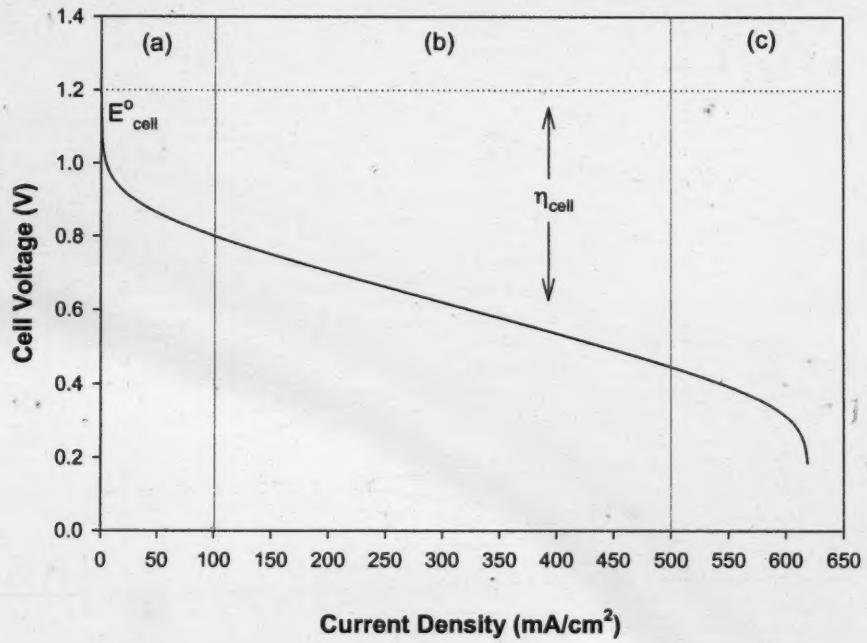

Figure 1.4. A polarization curve (jV curve) for a H_2 fuel cell.

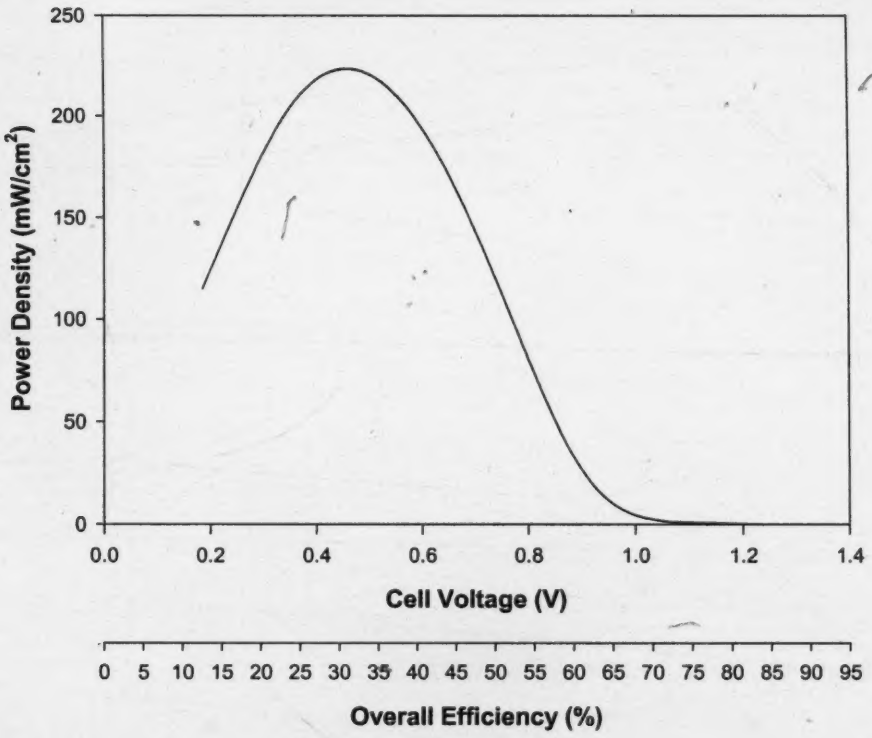

Figure 1.5. The power curve (PV curve) and operating efficiency (%) of a H_2 fuel cell. (The PV curve was calculated from the jV curve (Figure 1.4) using eq. 1.20. The conversion efficiency of the cell was calculated using eq. 1.22 ($\varepsilon_{thermal}$ 0.83 for a H_2 fuel cell, $\varepsilon_{voltage}$ was calculated using eq. 1.19 and the jV curve (Figure 1.4), a value of 1 was assumed for $\varepsilon_{faradaic}$).).

The classification of fuel cells. The classification of fuel cells is based primarily on the type of electrolyte they use. There are five common types of fuel cells. In order of increasing operating temperature they are proton exchange membrane fuel cells (PEMFC), alkaline fuel cells (AFC), phosphoric acid fuel cells (PAFC), molten carbonate fuel cells (MCFC), and solid oxide fuel cells (SOFC).[31, 32] Table 1.1 (page 18) is a summary these types of fuel cells and their components. The medium and high temperature fuel cells (i.e., PAFC, MCFC, and SOFC) are complex systems only suitable for stationary, large scale and remote applications. Low temperature cells (AFC and

PEMFC) are well suited to mobile applications on a scale ranging from cellular telephones to automobiles and spacecraft.[33, 34]

The electrolytes used in solid oxide fuel cells are ceramics. The first solid oxide electrolyte was a yttria stabilized zirconium oxide (e.g., 15 wt % Y_2O_3-ZrO_2 (YSZ)) discovered in 1899 by Nernst.[35] This electrolyte remains the electrolyte of choice for use in SOFC's.[36] The electrodes are composed of cerments. A cerment is a combination of sintered metal and ceramic that is conductive to ions and electrons, and has high thermal stability.[37] The half-cell reactions for a SOFC operating on H_2 and O_2 are shown in eq. 1.24 (anode) and eq. 1.25 (cathode). In order to achieve the required ionic conductivity, SOFC's operate at temperatures ranging from 600 to 1000 °C. The electrode kinetics are facile at these high operating temperatures, and so certain carbon containing fuels (e.g., CO, natural gas, CH_3OH) can be used directly in place of H_2.[38]

$$2\,H_2 + 2\,O^{2-} \longrightarrow 2\,H_2O + 4e^- \qquad \text{(eq. 1.24)}$$

$$O_2 + 4\,e^- \longrightarrow 2\,O^{2-} \qquad \text{(eq. 1.25)}$$

It is worthwhile to note that the direct use of carbon containing fuels results in formation of carbon deposits on the anode. The accumulation of carbon deposits can be avoided by the addition of H_2O to the fuel feed.[39] One practical advantage of SOFC's is that the waste heat can be utilized for other purposes (e.g., the production of useful heat and more electricity using a steam turbine generator). The primary disadvantages of SOFC's are their excessive manufacturing costs, the lack of thermal compatibility or long-term stability of the materials used for their construction, and that they are only suitable for stationary applications.

The molten carbonate fuel cell is also a high temperature device. As such, co-generation and facile reaction kinetics are used as in SOFC's. The electrolytes used in molten carbonate fuel cells are eutectic mixtures of alkali metal carbonates (e.g., Li_2CO_3/Na_2CO_3) in a γ-$LiAlO_2$ matrix at 650 to 700 °C. The electrodes used are

cerments (e.g., NiO-YSZ (anode)).[31] The half-cell reactions for a MCFC operating on H_2 and O_2 are shown in eq. 1.26 (anode) and eq. 1.27 (cathode).

$$H_2 + CO_3^{2-} \longrightarrow H_2O + CO_2 + 2\,e^- \qquad \text{(eq. 1.26)}$$

$$1/2\,O_2 + CO_2 + 2\,e^- \longrightarrow CO_3^{2-} \qquad \text{(eq. 1.27)}$$

The conversion of the electrolyte into CO_2 at the anode causes a significant technical problem. The anode reaction consumes the electrolyte (CO_3^{2-}) to generate CO_2. CO_2 is consumed at the cathode to regenerate CO_3^{2-}. The CO_2 formed at the anode must therefore be recycled back to the cathode. This represents a significant technical problem in the use of MCFC's. As is the case for SOFC's the manufacturing costs of MCFC's are excessive, and their high operating temperatures limits their use to stationary applications.

Phosphoric acid fuel cells operate at intermediate temperatures (~ 200 °C). PAFC's are the only type of fuel cell to be used on a large commercial scale.[7] PAFC's can only operate using H_2 (or reformate) as fuel. At the operating temperature of PAFC's the anode electrocatalyst, Pt supported on carbon, can tolerate up to 5 % CO in the fuel.[40] The half-cell reactions of a PAFC are the same as those in any fuel cell operating with an acidic electrolyte (eq. 1.7 (anode) and eq. 1.8 (cathode)). Sintering, a decrease in the specific surface area of the Pt electrocatalysts caused by particle agglomeration at the operating temperature of ~ 200 °C is the most significant problem with PAFC's.[41]

The electrolytes used in polymer electrolyte membrane fuel cells are acidic, proton conducting ion exchange membranes. The electrolyte transports protons from the anode to the cathode. An ideal polymer electrolyte membrane (PEM) has high proton conductivity, negligible electron conductivity, high chemical and thermal stability, and it is impermeable to the fuel and oxidant.[42] The advantages to use of a PEM over liquid electrolytes (e.g., aqueous H_2SO_4 or H_3PO_4) in fuel cells include simplified construction, reduced size, and minimal corrosion of the fuel cell. The use of an immobilized electrolyte also eliminates the dilution or leaching of the electrolyte by H_2O.

The PEM fuel cell was pioneered in the 1960's by Grubb and Neidrach at General Electric, Inc. for use in the Gemini space missions.[7] The maximum lifetime (~ 500 h) of these early membranes was too short for commercial applications. Perfluorosulfonic acid membranes (e.g., Nafion® (**1**), Figure 1.6)) were introduced by DuPont, Inc. in 1968.[7] Nafion® has a significantly longer lifetime as a PEM (~ 57 000 h) than its predecessors, and it has high proton conductivity, electrical resistance, as well as chemical, mechanical, and thermal stability.[7] Since its introduction, a significant effort has been focused on the development of practical PEM fuel cells using Nafion®.

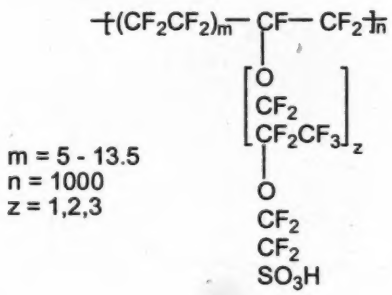

Figure 1.6. Nafion® (**1**) polymer electrolyte

The central component of a PEM fuel cell is the membrane electrode assembly (MEA). A membrane electrode assembly is composed of two porous electrodes bonded to opposite sides of a PEM. The backsides of the electrodes are in contact with electronically conducting plates that contain fuel and oxygen flow fields.[43] The most common type of electrode used in PEM fuel cells is the gas diffusion electrode (GDE). A gas diffusion electrode is a porous electrode composed of a semi-hydrophobic reaction layer containing the electrocatalyst and a hydrophobic gas-permeable layer that contains carbon and Teflon®.[7, 44] The gas diffusion layer is made hydrophobic to prevent H_2O from blocking the pores, and the electrocatalyst layer is less hydrophobic to facilitate contact among the reaction zone components and maintain the electrolyte conductivity. There are a number of methods to fabricate such electrodes and to incorporate them into membrane electrode assemblies. These methods are reported to improve the utilization of

the expensive Pt catalysts by optimizing the structure of the three-phase reaction zone (Figure 1.3, page 7).[45-58] The factors that limit the performance of a PEM fuel cell are primarily related to its operating temperature. The upper operating temperature in PEM fuel cells is limited to ~ 100 °C to avoid drying out the PEM. Further, PEM fuel cells operate at the highest real efficiencies using H_2 as fuel. Since hydrocarbon reforming is the only feasible source of H_2, and PEM fuel cells operate at relatively low temperatures, the anode catalysts suffer from poisoning by the trace amounts of CO present in even the most highly purified reformate.[7]

Alkaline fuel cells can operate at low temperatures and they can use non-noble metal electrocatalysts (e.g., Ni (anode) and Ag (cathode)).[40] The kinetics for O_2 reduction over Ag are facile in an AFC. The half-cell reactions for an AFC operating on H_2 and O_2 are shown in eq. 1.28 (anode) and eq. 1.29 (cathode).

$$H_2 + 2\,OH^- \longrightarrow 2\,H_2O + 2\,e^- \qquad \text{(eq.1.28)}$$

$$1/2\,O_2 + H_2O + 2\,e^- \longrightarrow 2\,OH^- \qquad \text{(eq. 1.29)}$$

Carbon dioxide must be removed from the fuel and oxidant to avoid the formation of carbonates (eq. 1.30), which consumes the electrolyte of an AFC, and the insoluble

$$CO_2 + 2\,OH^- \longrightarrow CO_3^{2-} + H_2O \qquad \text{(eq.1.30)}$$

carbonates foul the electrodes. In addition, the H_2O product of combustion must be removed in order to prevent dilution of the electrolyte. The Apollo spacecraft used, and the Space Shuttle currently uses AFC's because of their high power to weight ratio and in these limited cases, the use of pure H_2 and O_2 is not prohibitively expensive.[7]

Table 1.1. The classification of fuel cells.[59]

Type	Temperature (°C)	Electrolyte	Electrocatalyst(s)	
			anode	cathode
AFC	25-250	KOH	Pt-Au, Pt, Raney Ni	Pt-Au, Pt, Ag
PEMFC	60-130	Nafion®	Pt, Pt-Ru	Pt
PAFC	190-210	H_3PO_4	Pt	Pt-Cr-Co, Pt-Ni
MCFC	650	Li_2CO_3/K_2CO_3	Ni, Ni-Cr	Li-NiO
SOFC	1000	Y_2O_3-ZrO_2	Ni-ZrO_2	$LaSrMnO_3$

Direct methanol fuel cells. The only fuel cell that is classified by the fuel it uses is the direct methanol fuel cell (DMFC). A variety of electrolytes (e.g., KOH(aq) and H_2SO_4(aq)) have been used in direct methanol fuel cells.[60] To facilitate the application of DMFC's to scaleable portable power generation the electrolytes used at present are polymer membrane electrolytes, such as Nafion®. As such, the direct methanol fuel cell is at present a variant of the PEMFC in which CH_3OH is oxidized to CO_2 at the anode (eq. 1.31).[61] The most notable advantage of the DMFC over the PEMFC is the use

$$CH_3OH + H_2O \longrightarrow CO_2 + 6\,H^+ + 6\,e^- \qquad \text{(eq. 1.31)}$$

of a liquid fuel instead of gaseous H_2. The advantages of the PEMFC (*vide supra*) are all applicable to a DMFC. As such there is an intense interest in the development of a practical DMFC. Figure 1.7 is a schematic of a DMFC showing the anode and cathode half-cell reactions. The $E°_{cell}$ for a DMFC (eq. 1.32) is 1.214 V, which is comparable to that of a PEMFC operating on H_2 (1.229 V, eq. 1.1). According to eq. 1.12 the maximum

thermal efficiency of a DMFC is 97 %. The maximum thermal efficiencies of DMFC's are significantly higher than those of PEMFC's operating on pure H_2 as fuel (i.e., 83 %).[62]

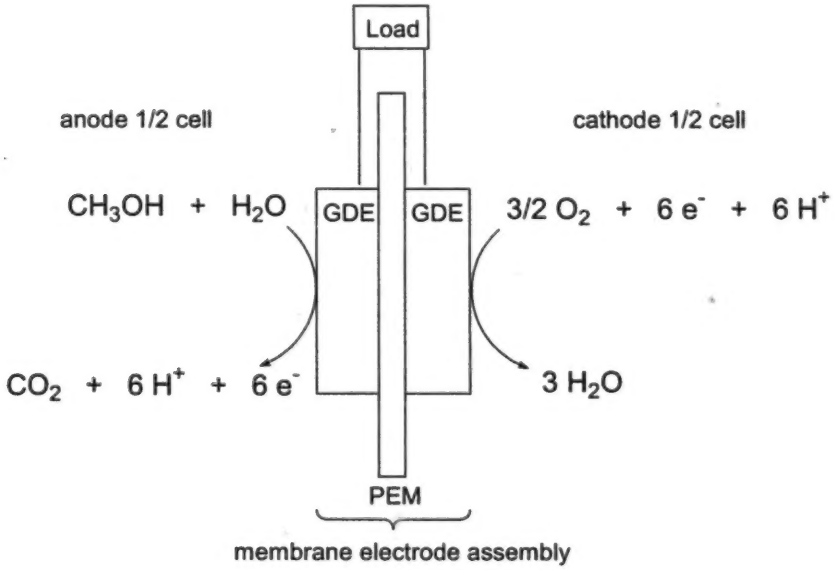

Figure 1.7. Schematic diagram of a DMFC.

$$CH_3OH + 3/2\ O_2 \longrightarrow CO_2 + 2\ H_2O + \text{energy} \qquad \text{(eq. 1.32)}$$

DMFC systems are less complex than PEMFC systems (operating on pure H_2 or reformate) due to the ease of liquid fuel storage and the elimination of fuel conversion stages. The simplified construction of DMFC's, and high energy density of CH_3OH therefore results in higher power to weight ratios for DMFC's. These features make the DMFC an attractive alternative to the use of secondary batteries (e.g., NiCd and Li ion batteries) in portable electronic devices (e.g., cellular phones and laptop computers).[63] These advantages of DMFC's also make them a promising alternative to internal combustion engines or PEMFC's in automobiles.[64]

There are two major factors that limit the performance of a DMFC. The first limitation is that the currently available polymer electrolytes are permeable to CH_3OH. As a result, CH_3OH is transported through the PEM from the anode to the cathode to

leading to a chemical short circuit that reduces the cathode potential, and a loss of fuel through the cathode exhaust. The deleterious effects of CH_3OH crossover would be reduced by using CH_3OH impermeable membranes, optimizing the operating conditions to consume CH_3OH at the anode (i.e., lean feed), or by employing a cathode electrocatalyst that does not react with CH_3OH.[65-68] The use of cathode catalysts that do not react with CH_3OH is of limited use since the fuel would still be wasted via the cathode exhaust. The second limitation is that the anodes electrocatalysts (e.g., Pt) are poisoned by a strongly adsorbed intermediate derived from CH_3OH electrooxidation.[69] The nature of the strongly adsorbed intermediate (poison) has been studied in considerable detail and it is believed to be CO (CO_{ads}).[70, 71] At present, the major obstacle to the development of a practical DMFC is the lack of a suitable alternative to Pt capable of sustaining rapid, and complete electrooxidation of CH_3OH (eq. 1.31).[72]

The anodic oxidation of methanol on Pt-based electrocatalysts. A suitable anode electrocatalyst for a DMFC must effect the complete electrooxidation of CH_3OH to CO_2 (eq. 1.31) at a potential near the standard potential ($E°_{an}$ = 0.016 V) for CH_3OH oxidation. The most active single component electrocatalyst for the anodic oxidation of CH_3OH is Pt.[71] The electrooxidation of CH_3OH over Pt electrodes quickly self-poisons to give negligible steady-state currents at potentials useful for a DMFC.[73-75] The mechanism of CH_3OH electrooxidation on Pt has been extensively studied over the past 40 years, and the pertinent details are summarized below.[71, 76-78] The oxidation of CH_3OH occurs via a rapid stepwise dehydrogenation that is initiated by cleavage of a methyl C-H bond (eq. 1.33).[79] Subsequent rapid dehydrogenations of $(CH_2OH)_{ads}$ forms adsorbed CO (CO_{ads}) and adsorbed H (H_{ads}) (eq. 1.34). As the electrooxidation of H_{ads} on Pt surfaces (eq. 1.35) is a rapid reaction, H_{ads} does not accumulate and block the surface towards further reactions, eq. 1.33 or 1.34. The oxidation of CO_{ads} is the slowest step in the process, and CO_{ads} accumulates on the surface as the reaction proceeds, eventually blocking all surface sites towards further reaction with CH_3OH.[71, 77, 80] The oxidation of CO_{ads} to CO_2 requires a co-adsorbed oxide species (most likely OH_{ads}) that is formed by the activation of H_2O (eq. 1.36 and 1.37). The activation of H_2O to form Pt oxides does not occur below 0.5 to 0.6 V, and potentials in excess of ~ 0.8 V are required for the

formation of significant amounts of Pt oxide surface.[81, 82] Thus, the rate of CH_3OH electrooxidation over Pt is accelerated by facilitating the oxidative removal of CO_{ads} as CO_2 (eq. 1.38).

$$CH_3OH \xrightarrow[Pt]{} (CH_2OH)_{ads} + H_{ads} \qquad \text{(eq. 1.33)}$$

$$(CH_2OH)_{ads} \rightarrow \rightarrow \rightarrow CO_{ads} + 3\,H_{ads} \qquad \text{(eq. 1.34)}$$

$$H_{ads} \longrightarrow H^+ + e^- \qquad \text{(eq. 1.35)}$$

$$H_2O \longrightarrow H_{ads} + OH_{ads} \qquad \text{(eq. 1.36)}$$

$$CO_{ads} + OH_{ads} \longrightarrow CO_2 + H_{ads} \qquad \text{(eq. 1.37)}$$

$$CO_{ads} + H_2O \longrightarrow CO_2 + 2\,H^+ + 2\,e^- \qquad \text{(eq. 1.38)}$$

The electrooxidation of CH_3OH on Pt in acidic electrolytes is a structure sensitive reaction. The rate of a structure sensitive reaction depends on the surface crystallography of the catalyst used. The electrooxidation of CH_3OH on Pt(111), Pt(110), and Pt(100) has been studied in considerable detail.[83-87] The activity of single crystal Pt surfaces towards the electrooxidation of CH_3OH increases in the order Pt(111) < Pt(100) < Pt(110), and the 110 plane consistently displays the highest intrinsic activity and rate of poisoning.[86] The surface of polycrystalline Pt (solid electrodes and nanoscale particles) is assumed to be a composite of the low index crystal surfaces. There are no methods available for the preparation of nanoscale Pt particles with controlled crystallography. The effects of surface structure of nanoscale electrocatalysts are believed to be responsible for the observed crystallite size effects. There are conflicting reports as to the existence of a particle size effect on the electrooxidation of CH_3OH.[88, 89] A maximum in the intrinsic activity of nanoscale Pt particles on carbon has been observed for Pt particles with a diameter of ~ 3 nm, corresponding to a specific surface area of ~ 80 m^2/g Pt, during the

potentiostatic electrooxidation of CH_3OH in H_2SO_4(aq).[89] The methods used to prepare nanoscale Pt particles produce a distribution of particle sizes and methods for the preparation of monodisperse nanoscale Pt particles do not exist.[90]

The activity of Pt towards the electrooxidation of CH_3OH has been increased using co-catalysts that reduce the potential for the activation of H_2O and thereby factilitate the oxidative removal of CO_{ads}.[83] The most active anode electrocatalysts for CH_3OH oxidation in polymer electrolyte fuel cells are nanoscale particles composed of Pt and Ru.[91] It is known that the potential for CO oxidation is lower on Ru and on Pt-Ru surfaces than on pure Pt.[92] Nanoscale particles composed of Pt and Ru are also the most active catalysts for the oxidation of CO containing reformate in the PEMFC's and the PAFC's.[93, 94]

There are numerous studies of Pt-Ru electrocatalysts for the direct electrooxidation of CH_3OH.[92, 95-136] There are also a number of other binary, ternary, and quaternary metal combinations that have been studied for the anodic oxidation of CH_3OH in a DMFC.[83, 137] Other systems studied for CH_3OH electrooxidation include Pt-Re,[138, 139] Pt-Sn,[114, 140-143] Pt-Mo,[144, 145] Pt/WO_x,[146, 147] $Pt\text{-}Ru/WO_x$,[148], Pt-Ru-Sn,[149] Pt-Ru-Os,[150] Pt-Ru-Os-Ir,[151, 152] and Pt-Ru-Sn-W.[153] In all cases Pt remains an essential component.

It is believed that bimetallic, Pt-based catalysts (e.g., Pt-Ru surfaces) accelerate the rate of CH_3OH electrooxidation by a bifunctional mechanism.[136, 154] According to the bifunctional mechanism it is the Pt surface sites that activate CH_3OH to form CO_{ads} and H_{ads} (eq. 1.39), and the Ru surface sites are believed to activate H_2O to form surface oxides (eq. 1.40). It is known that the formation of Ru surface oxides commences at ~ 0.2 V whereas potentials in excess of 0.5 V are required to activate H_2O on Pt surfaces.[155-157]

$$CH_3OH \xrightarrow[Pt]{} Pt\text{-}CO_{ads} + 4\ Pt\text{-}H_{ads} \qquad \text{(eq. 1.39)}$$

$$H_2O \xrightarrow[Ru]{} Ru\text{-}OH_{ads} + Ru\text{-}H_{ads} \qquad \text{(eq. 1.40)}$$

The bifunctional mechanism is a modification of the Langmuir-Hinselwood model of heterogeneous reactions.[158] According to the Langmuir-Hinselwood model of surface reactions, the rate of electrooxidation of CO_{ads} (derived from CH_3OH) on Pt-Ru surfaces (eq. 1.41) depends upon the relative surface coverage's of CO_{ads} (θ_{CO}) and OH_{ads} (θ_{OH}). The removal of CO_{ads} according to eq. 1.41 occurs at the interfaces between Pt and Ru on

$$Pt\text{-}CO + Ru\text{-}OH \longrightarrow Pt + Ru + CO_2 + H^+ + 1\,e^- \qquad \text{(eq. 1.41)}$$

the surface. The relative surface concentrations (*vide infra*) of Pt, Ru, and Pt-Ru determine the steady state values of θ_{CO} and θ_{OH} during CH_3OH electrooxidation. The surface concentrations, distributions of Ru and Pt surface sites, and the mobility of surface adsorbed species (e.g., CO_{ads} and OH_{ads}) alter the intrinsic activity of these electrocatalysts.[159] The presence of an additional electronic effect on the reactivity of Pt-Ru surfaces has also been discussed, but its contribution relative to the bifunctional effect is believed to be small.[160-162] The development of a practical DMFC requires an anode electrocatalyst capable of sustaining the rapid, and complete anodic oxidation of CH_3OH (eq. 1.31). The requirements for a suitable electrocatalyst for a DMFC anode are its intrinsic activity, stability, selectivity, and cost. The intrinsic activity of an electrocatalyst can only be determined by measuring the rate of the electrochemical reaction per active site under reaction rate limiting conditions. The activity of Pt-Ru surfaces towards CH_3OH, and CO electrooxidation, depends primarily on the number and the composition of active surface sites. The surface composition (θ_{Ru}) is the stoichiometric ratio of the number of Ru surface atoms (N_{Ru}) to the total number of surface atoms ($N_{surface}$). The bulk composition (X_{Ru}) of a Pt-Ru catalyst is the mole fraction of Ru in the Pt-Ru particles. It is important to realize that, in accordance with the bifunctional mechanism, the electrocatalytic activity of a Pt-Ru surface depends on θ_{Ru} not X_{Ru}.

Preparation of bimetallic particles composed of Pt and Ru - practical electrocatalysts. In order to prepare Pt-Ru electrocatalysts of high intrinsic activity for use in a DMFC the amount of available surface must be maximized and the surface composition must be optimized for the electrooxidation of CH_3OH. The distribution of

particle diameters and surface compositions must be narrow in order to maintain uniform catalytic activity throughout the catalyst sample. There are a number of methods for the preparation of catalytic materials ranging from the direct precipitation of the catalyst or impregnation of a suitable support and subsequent conversion of the catalyst precursor(s) on the support.[163, 164] There are two general approaches to the preparation of nanoscale Pt-Ru particles for use as electrocatalysts. They are the preparation of bimetallic Pt-Ru alloy nanoparticles and the modification of single component nanoparticles by deposition of Ru_{ad} on Pt particles. In general, nanoscale Pt-Ru particles are prepared via the chemical co-reduction of mixtures of Pt and Ru chloride salts with a variety of reducing agents (e.g., H_2, $NaBH_4$, H_4N_2, formaldehyde, sodium formate) followed by thermal treatment of the bimetallic composite in a reducing or inert atmosphere.[97, 165-169] Nanoscale Pt-Ru particles have also been prepared by mechanical methods. For example, the ball milling of a mixture of the pure metals in combination with additional agents (Al and NaF), results in the formation of relatively large Pt-Ru alloy particles with heterogeneous distributions of particle sizes and compositions.[170, 171] These methods are not suitable for the preparation of bimetallic alloy nanoparticles with control over the surface composition. There is a distribution of particle sizes and bulk compositions that arises due to problems inherent to the preparation techniques. Such problems include, variations in the rates of mass transport to the sites of particle growth which cause a distribution of particle sizes and compositions, interactions of the precursors with the support, and surface segregation during thermal stages of the catalyst preparation procedures.[172]

The chemical co-reduction of binary mixtures of the metal-containing precursors does not result in the formation of homogeneous alloy nanoparticles. In order to obtain homogeneous alloyed metal particles high temperature thermal annealing of the chemically produced bimetallic composite nanoparticles is required.[163] During the cooling stage the components of the bimetallic particles may arrange into a homogeneous (i.e., ordered alloy). There is a tendency for surface enrichment phenomena to occur in Pt-Ru and particles during thermal treatments.[173, 174] In the case of Pt-Ru an enrichment of the surface in Pt occurs if annealed in H_2 or inert atmosphere, on the other hand if the

atmosphere contains O_2 then Ru enrichment is observed.[175] There is also a tendency for phase separation of the components during thermal treatments of Pt-Ru alloy particles.[176]

The state-of-the-art procedure for the preparation of carbon supported Pt-Ru was developed by Watanabe *et al.*[97] They used the co-deposition of fine oxides of Pt and Ru by reaction of H_2O_2 with metal-containing precursors ($Na_6Pt(SO_3)_4$ and $Na_4Ru(SO_3)_3$). Subsequent thermal treatment in a H_2 atmosphere reduces these combined oxide precursors to high surface area Pt or Pt-Ru alloy nanoparticles.[97]

Bonnemann *et al.* have prepared surfactant-stabilized colloidal nanoparticles via reduction of mixtures of Pt and Ru chlorides using tetraalkylammonium hydro-triorganoborates.[177] A reactive annealing pretreatment was required to remove the surfactant prior to use of these nanoparticles as electrocatalysts. These colloidal particles have been used as precursors for unsupported, and carbon supported Pt-Ru electrocatalysts for the electrochemical oxidation of CH_3OH and H_2 contaminated with CO.[178-181] The structure and chemical composition of the particles were studied and, as expected, particle segregation and separation was observed upon high temperature treatment.[182, 183] Chaudret *et al.* developed a method to prepare nanoscale Pt-Ru alloy particles via the decomposition of Pt(dibenzylideneacetone)$_2$ and (1,5-cyclooctadiene)Ru (cyclooctatriene) mixed in various ratios in THF solutions under a H_2 atmosphere.[184] Polyvinylpyrolidone was added to prevent aggregation of the colloidal metal particles.[184] It is important to note that in order to prepare active electrocatalysts for use in fuel cells any surfactants or protective polymer layers must be eliminated from the surface prior to fabrication of the electrodes. Therefore, in order for these catalysts to be used in fuel cells a method for the removal of the PVP coating must be employed. To date these catalysts have only been characterized and their evaluation towards electrochemical reactions has not been reported.

The thermal decomposition of bimetallic organometallic compounds to prepare nanoscale Pt-Ru particles has been studied by the Nuzzo and Lukehart groups. Nuzzo *et al.* found that thermal decomposition of bimetallic Pt-Ru cluster compounds (e.g., $PtRu_5C(CO)_{16}$ and $PtRu_4(CO)_{16}$) results in the formation of bimetallic nanoparticles with a controlled bulk composition that is predetermined by the composition of the metal

containing precursor and with a narrow size distribution about an average particle size of 1.5 nm.[173, 185] Lukehart *et al.* have also reported that the thermal decomposition caused by microwave dielectric heating of a single source molecular precursor ((η^2-C_2H_4)(Cl)Pt(μ-Cl)$_2$Ru(Cl)(η^3:η^3-2,7-dimethyloctadienediyl)) supported on carbon enables control of the distribution of bulk compositions of Pt-Ru nanoparticles for use in DMFC's.[186] Although these methods are able to control the bulk Pt to Ru ratio, the surface compositions remained uncontrolled. In addition, the decomposition of bimetallic precursors is of limited utility due to the lack of suitable precursors of readily variable Pt and Ru contents.

Characterization of bimetallic surfaces and particles. There are a number of spectroscopic techniques available for the elemental analysis and physical characterization of Pt-Ru electrocatalysts.[187] Techniques for the determination of surface composition must be used in concert with techniques for the determination of the real surface area to facilitate the evaluation of the intrinsic activity of Pt-Ru electrocatalysts. The primary distinction among the elemental analysis methods is the degree of surface selectivity. The techniques can be classified as surface specific, surface sensitive, or as bulk elemental analysis methods.

The composition of Pt-Ru surfaces can only be measured using surface specific spectroscopic techniques for elemental analysis. The use of surface specific spectroscopic techniques (e.g., low energy ion scattering (LEIS) or low energy electron diffraction spectroscopy (LEEDS)) is limited to the analysis of smooth surfaces under ultra high vacuum conditions (UHV). The use of physical techniques (e.g., scanning tunneling electron microscopy (STM)), although surface specific, is also limited to smooth surfaces (e.g., single crystals). Surface sensitive techniques (e.g., X-ray photoelectron spectroscopy (XPS) and Auger electron spectroscopy (AES)) can only be used to approximate θ_{Ru} due to penetration of the incident X-rays or electrons that excite emission from variable depths within the bulk of the sample. The signals produced by the bulk and surface atoms of the sample cannot be separated from each other. The use of solid state ^{195}Pt NMR is reported to be capable of distinguishing the surface and bulk Pt resonances.[188] The Wieckowski group and others have developed electrochemical

nuclear magnetic resonance spectroscopy (EC-NMR) as a probe of the electronic structure of Pt and Pt-Ru surfaces.[189]

The bulk composition of nanoscale Pt-Ru particles can be measured using neutron activation analysis (NAA) or energy dispersive X-ray analysis (EDX). The combined use of high-resolution electron microscopy (HRTEM) and EDX is often used to determine the particle size and bulk composition distributions for Pt-Ru nanoparticles. Alternatively X-ray based techniques may be used that enable additional structural information to be gathered. The average bulk composition and particle diameter of nanoscale Pt-Ru alloy crystallites can be determined using X-ray diffraction (XRD).[190] The particle size is determined from the broadening of selected lines using the Scherrer method, and the composition of the particles can be determined from the average lattice spacing, assuming that Vergard's law is valid.[191] The analysis of particles using this method has been criticized for its lack of sensitivity to amorphous phases of hydrous Ru oxide that are believed, by some, to be a required component for an active CH_3OH electrooxidation catalyst.[100, 192] It is important to note that the proposed hydrous oxide component has recently been shown to be responsible for increases in the conductivity of the electrocatalyst layer in DMFC anodes and that the active surface for CH_3OH electrooxidation in fuel cells is composed of metallic Pt and Ru surface sites (*vide infra*). The crystallographic characterization of nanoscale Pt-Ru alloy particles can also be determined by extended fine structure X-ray analysis (EXAFS).[173,193, 194] The advantages of the X-ray based methods are that they allow the distinction between the formation of supported bimetallic electrocatalysts and supported alloy electrocatalysts.[195]

The electrochemical determination of the surface composition of Pt surfaces modified by Ru adatoms or Pt-Ru alloys is not a trivial matter.[196] The number of Pt active sites can be determined using standard electrochemical methods, such as cyclic voltammetry in aqueous acid as described in Chapter 2. The surface area of Ru cannot be measured by cyclic voltammetry due to the overlap of the potential ranges for surface reactions involving hydrogen and oxygen in the cyclic voltammogram. The use of electrochemical methods to characterize Pt-Ru surfaces is impeded by the lack of a well-defined electrochemical response in the cyclic voltammogram of Ru surfaces, and the

overlap of the electrochemical responses of Pt and Ru surfaces in the voltammogram. As a result, neither θ_{Ru} nor $N_{surface}$ are measurable using standard electrochemical methods for Ru or Pt-Ru surfaces. Studies by Watanabe *et al.* indicated that θ_{Ru} could be determined by integrating the charge associated with Ru oxide formation during the anodic sweeps of cyclic voltammograms recorded in HCl(aq). However the number of electrons involved and the nature of the surface oxide species are both poorly defined, leading to difficulties in the reliable use of this method. Subsequent studies by van Veen *et al.* indicated that the shift in the peak potential for the reduction of the surface oxides during the cathodic sweep of the cyclic voltammogram is diagnostic of θ_{Ru} up to a surface composition of ~ 40 % Ru, unfortunately these measurements result in the destruction of the surface due to an upper potential limit of 1.2 V. These authors were able to correlate their results to the mass of Ru deposited, measured using a quartz crystal microbalance.

The indirect measurement of surface composition using probe molecules was reported by the Gonzalez group. They measured the relative IR band intensities of co-adsorbed CO and NO,[197] and performed gas titrations using CO-O_2 on silica supported Pt-Ru nanoparticles.[198] These authors concluded, based on a comparison of their methods, that NO adsorption on Pt-Ru caused adsorbate induced enrichment of the Ru content on the surface.[198] The use of CO_{ads} as a probe for surface characterization has been explored by several groups using electrochemical (e.g., CO stripping voltammetry) and spectroscopic (e.g., Fourier Transform Infrared Spectroscopy (FTIR)) methods. The results of such analysis appear to be dependent on the distribution of the surface components (*vide infra*). Thus, surfaces of alloys are not equivalent to the surfaces of adatom modified substrates.

Stimming *et al.* observed distinct CO bands for CO_{ads} on Pt or Ru and proposed that these CO bands could be used to define the surface composition of Ru_{ad} modified Pt(111) surfaces.[199] The FTIR studies of Ru modified Pt surfaces exhibit two peaks that are attributed to the presence of pure Ru and pure Pt domains. However, FTIR studies of CO on Pt-Ru alloys showed only a single band for CO_{ads}.

The electrooxidation of adsorbed CO has been examined on Ru modified single crystal Pt surfaces and on nanoscale Pt particles modified by Ru_{ad} deposition.[200-203] In

cases of Ru island formation, multiple CO stripping peaks have been observed in voltammograms recorded in H_2SO_4(aq) electrolytes. Baltruschat *et al.* observed two CO peaks during the anodic stripping of CO_{ads} from Ru_{ad} modified Pt(111) and Pt(332) and concluded that the mobility of CO on Pt is low.[204] In $HClO_4$(aq) only a single CO_{ads} stripping peak is observed, and this was attributed to the weakly adsorption of perchlorate anions that do not inhibit the surface diffusion of CO_{ads} during the potential sweep experiments.[205] In cases where island formation is apparent the authors believe that CO_{ads} oxidation occurs either on large ensembles of Pt surface atoms or at Pt-Ru ensembles. This implies that the mobility of CO_{ads} on Pt and Pt-Ru surfaces is slower than the rate of electrooxidation of CO to CO_2 and that it is inhibited by adsorbed anions (e.g., SO_4^{2-}). This has been confirmed by ^{13}C NMR studies of Wieckowski *et al.* The electrochemical stripping of CO_{ads} has been used by some authors to define the surface areas of co-electrodeposited Pt-Ru alloys and the surface compositions of nanoscale Pt-Ru particles.[106, 206] The validity of these results is still to be confirmed. Recently, Wieckowski *et al.* showed that the presence of Ru on the surface increases the mobility of CO_{ads} on Pt-Ru. The Wieckowski group have proposed that CO stripping voltammetry and ^{13}CO solid state NMR spectroscopy may also be used to measure the surface composition of Ru adatom modified Pt particles.[203]

Due to the difficulties associated with the characterization of Pt-Ru electrocatalysts (*vide supra*), a method for the fabrication of nanoscale Pt-Ru particles with defined and controlled surface areas and compositions is required for the optimization of DMFC anodes. A useful method for the deposition of Ru on Pt should also be suitable for use on model surfaces (e.g., polycrystalline Pt electrodes) and practical substrates (e.g., nanoscale Pt particles) to enable rapid catalyst screening prior to final evaluation in a real DMFC.

Preparation of bimetallic surfaces composed of Pt and Ru - model systems. The preparation of model Pt-Ru surfaces has been accomplished by synthesis of well-defined alloys by arc melting mixtures of the pure metal in the desired ratio, by the deposition of adatoms, and by the co-electrodeposition of Pt and Ru onto a supporting electrode.

The deposition of Ru adatoms (Ru_{ad}) onto Pt substrates of known surface area can, in principle, be used to prepare Pt-Ru surfaces of known surface composition. The minimum requirements of such a method are that the deposition process must not alter the real surface area of the Pt substrate and that the amount of Ru_{ad} deposited be measurable. The Pt substrates used include single crystals (e.g., Pt(111), Pt(110), or Pt(100)), polycrystalline Pt surfaces, or nanoscale Pt particles, unsupported or supported. The degree of control over the amount of Ru_{ad} deposited and the techniques that can be used to characterize the resulting Pt-Ru_{ad} surfaces (*vide infra*) depend on the nature of the Pt substrate and on the method used to deposit the Ru adatoms. The methods that have been used to deposit Ru_{ad} on Pt include metal atom vapor deposition (MVP),[200, 240, 207] chemical adsorption/thermal decomposition,[208] chemical vapor deposition (CVD),[209] and electrodeposition.[114, 115, 162, 210-217] These methods do not provide precise control over the amount of Ru_{ad} deposited, and the distribution of the deposited Ru_{ad} can not be controlled.

The deposition of Ru using MVD or CVD is restricted to use on single crystal or smooth (on the atomic scale) polycrystalline Pt surfaces. The amount of Ru deposited is difficult to control, and in most cases it is determined after the deposition is complete using surface specific spectroscopic methods (e.g., low energy ion scattering (LEIS)). Additional limitations of these methods are that both the preparation and characterization stages require expensive and complex instrumentation (i.e., ultra high vacuum (UHV) systems).

The electrodeposition of Ru_{ad} on Pt is controlled by the potential and current distribution on the electrode surface. Therefore the deposition of Ru_{ad} on the electrode results in the formation of islands and towers of Ru_{ad} on the surface. Variations in the rates of mass transport of Ru ions to the surface sites also result in non-uniform deposits. Further, the commonly used Ru containing precursors contain anions that strongly adsorb to the electrode and block surface sites. The presence of chloride ions is known to poison Pt surfaces towards CH_3OH oxidation.[218, 219] The electrodeposition of metal adatoms onto smooth Pt surfaces of known real surface area can be used to prepare model Pt-Ru_{ad} systems of known surface compositions and surface areas but is unsuitable for the

fabrication of practical electrocatalysts. Electrodeposition can not be used for the preparation of practical nanoscale Pt-Ru_{ad} particles because of the difficulties associated with maintaining uniform electrical contact amongst the particles, and with the supporting electrode during the deposition process.

The preparation of bimetallic surfaces using co-electrodeposition has also been explored in considerable detail.[107, 220-222] The co-electrodeposition of Pt-Ru onto supporting electrodes (e.g., C, Pt, Au) from electrolytes containing Pt (e.g., H_2PtCl_6) and Ru (e.g., $K_2Ru(NO)Cl_5$, $RuCl_3$) salts produces rough polycrystalline surfaces. As such, these rough surfaces are more accurate models of practical nanoscale Pt particles. Unfortunately, the preparation of Pt-Ru surfaces by co-electrodeposition results in significant and unpredictable changes in the real surface area and since the real surface area of Pt-Ru surfaces can not be measured directly (*vide supra*) comparisons among catalysts of different compositions are tenuous at best.[106]

Spontaneous deposition methods for the preparation of Pt-Ru electrocatalysts. The spontaneous deposition process was first reported by Szabo *et al.*, these authors observed the deposition of a Ru species onto Pt electrodes that were first polarized to 50 mV in H_2SO_4(aq), or HCl(aq) prior to the addition of a small amount of a $RuCl_3$ solution, the Ru deposition occurred under open circuit conditions and a final open circuit voltage of 0.85 V was observed.[223, 224] The spontaneous deposition of Ru_{ad} on Pt was used by Franaszczuk *et al.* to prepare Pt-Ru_{ad} electrodes for the voltammetric oxidation of CH_3OH.[123] Subsequently, Wieckowski *et al.* have exploited the spontaneous deposition of Ru_{ad} on a variety of Pt substrates and studied the effects of Ru_{ad} on the electrooxidation of CH_3OH and CO_{ads}.[203, 225-233] These depositions are typically carried out by immersing the Pt substrates (electrodes, or powders) into a solution containing a Ru precursor (e.g. $RuO(H_2O)_4^{2+}$) under open circuit conditions (at an initial potential of ~ 0.40 V), after removal of the substrate (at a final open circuit potential of ~ 0.85 V), the Ru deposit is reduced by electrochemical reduction in blank electrolyte. This method of Ru_{ad} deposition is capable of producing sub-monolayer coverages of Ru_{ad} on a wide variety of Pt substrates; single crystal surfaces, polycrystalline surfaces and nanoscale Pt particles. The deposition process self-terminates and the saturation coverages ranges from 5 to 24%

depending on the crystallography of the Pt substrate. The amount of Ru deposited can be increased by further electrodeposition (used on bulk Pt electrodes) or by repeating the entire procedure (used on nanoscale Pt particles).

The Vielstich group have also used a spontaneous deposition method to prepare Ru_{ad} modified Pt(111) for the electrooxidation of CO_{ads} and CH_3OH.[234, 235] According to their procedure freshly prepared $RuCl_3$ solutions are used and they believe that the deposition proceeds via the formation of adsorbed Cl anions and co-adsorbed Ru cations (eq. 1.42) the final Ru_{ad} deposit is obtained by reducing the adsorbed layer at 50 mV prior to use.[235]

$$3\,Pt + RuCl_3 \longrightarrow 3\,Pt(Cl)_{ads} + (Ru^{3+})_{coads} \qquad \text{(eq. 1.42)}$$

Spontaneous deposition of Ru on single crystal Pt substrates results in the formation of Ru_{ad} as islands, and multilayer deposits (towers) have also been observed by STM.[228, 229, 235] Due to the uncontrolled growth of the Ru_{ad} deposit the spontaneous deposition of Ru_{ad} does not enable fine control over the surface composition during the deposition.

The Adzic group have recently reported preliminary results on the modification of Ru single crystals and carbon supported Ru nanoparticles by Pt adatoms (Pt_{ad}) using a spontaneous deposition procedure.[236, 237] Behm *et al.* have also examined the effects of Pt_{ad} deposited on Ru(0001) surface on CO adsorption and oxidation using temperature programmed desorption and reaction studies.[238]

Performance evaluation and optimization of Pt-Ru electrocatalysts. The optimization of the composition of Pt-Ru electrocatalysts (primarily using model electrodes) has been studied in considerable detail over the past 40 years. The effects of Pt-Ru surface composition have been examined for Ru adatom (Ru_{ad}) modified Pt surfaces, for thermally prepared smooth alloys of Pt and Ru, and for co-electrodeposited Pt-Ru on a number of substrates. There are several examples where smooth bulk alloys of known surface composition have been prepared for the electrooxidation of CH_3OH and/or CO_{ads}.[239-244] There remain differences between the results reported regarding the

composition of the most active Pt-Ru electrocatalysts. The reported optimum surface compositions for the oxidation of CH_3OH range from 5 to 50 %. The earliest studies of the effects of Pt-Ru catalyst composition on the electrooxidation of CH_3OH indicated that the highest activity is obtained at a Ru content of 5 to 10 %.[75] Watanabe *et al.* concluded that the optimum surface composition of Ru_{ad} modified Pt electrodes is 50 %.[136] The studies by Gasteiger *et al.* indicated that optimum surface composition of Pt-Ru alloys towards CH_3OH oxidation ranges from 7 to 30 % depending upon the electrode potential and the temperature.[245, 246] The results of Chu *et al.* using nanoscale Pt-Ru alloy particles indicated that the highest activity was obtained using 50 % Ru particles at 25 and 60 °C.[107] An optimum surface composition of ~ 15 % was reported by van Veen *et al.* using co-electrodeposited Pt-Ru.[162] Recent studies by the Vielstich group led to the conclusion that the optimum composition is between 10 and 40 % Ru and that it is independent of surface composition within this range.[106] The Wieckowski group have examined the effects of surface structure and composition on methanol electrooxidation and found that the optimum surface composition ranges from 15 to 30 % and its exact value depends on the surface crystallography of the underlying Pt substrate (*vide infra*).[247-249] The sources of conflict among these determinations are the lack of control over θ_{Ru} during catalyst preparation, and the lack of techniques available to measure the real surface area and composition of Pt-Ru electrocatalysts. Therefore the primary control variables used are the dispersion of the catalyst and its bulk composition (X_{Ru}). In order to evaluate the intrinsic activity of an electrocatalyst, the number of active surface sites and their composition must be known.

The chemical state of the active components of Pt-Ru catalysts has been investigated. The chemical state of the components can be controlled by the preparation or pretreatment procedures. There are claims in the patent literature that indicate that separated Pt and Ru particles are the most active.[250] Others have indicated that an intimate mixture of Pt and Ru with activity that does not depend on the surface composition or chemical state of the components provided the catalyst contains 50 to 75 wt % Pt is the most active.[251] The presence of metallic Ru, Ru oxide (RuO_2), and a hydrous Ru oxide (RuO_xH_y) components has been confirmed in the commercial anode

electrocatalysts.[100, 252] Studies by the Gottesfeld[253] and Maricle[254] groups tackled the issue of the chemical state of the active catalyst (in the commercial electrocatalysts); they concluded that the active electrocatalyst component for CH_3OH electrooxidation in fuel cells is metallic Pt-Ru alloy and that there is a hydrous Ru component that increases the electrical and ionic conductivity of the electrocatalyst layer inside an operating DMFC. The results of Gottesfeld *et al.* also indicated that the surface composition of the alloy component of the conditioned commercial catalyst ($PtRuO_x$) is ~ 30 % Ru.[253]

Particle size effects have been observed for the electrooxidation of CH_3OH on nanoscale Pt and Pt-Ru particles. The optimum particle size for a Pt-Ru (1:1 atomic ratio) was reported to be 3 nm for the potentiostatic electrooxidation of CH_3OH in H_2SO_4(aq) at 60 °C.[255] The origin of particle size effects is uncertain, though most likely to be a result of changes in surface structure as particle size decreases. There are no methods for the preparation of practical nanoscale particles of controlled surface composition and particle sizes.

Applications of Pt-Ru surfaces beyond direct methanol fuel cells. Nanoscale bimetallic particles composed of Pt and Ru are useful in a variety of heterogeneous reactions. Bimetallic clusters of Ru and Pt have been used to catalyze the hydrogenation of arenes,[256, 257] hydrogenolysis of propane and isomerization of alkanes,[258] the hydrogenation of CO,[259] and in chemical heat pump systems based on the interconversion of 2-propanol and acetone-hydrogen mixtures.[260] It is known that Pt-Ru is among the most active catalysts for the visible light induced hydrogen generation.[261] The most well documented application is the increased activity of Pt-Ru relative to Pt or Ru alone towards the oxidation of CH_3OH and CO_{ads} (*vide supra*).

Part II. Overview.

A new method for the preparation of bimetallic Pt-Ru_{ad} surfaces of known surface area and defined surface composition. The catalytic activity of bimetallic Pt-Ru surfaces towards the electrooxidation of CH_3OH is known to depend, among other things, on the

relative amounts of Pt and Ru at the surface (i.e. the surface composition). Present methods to prepare practical Pt-Ru electrocatalysts do not have demonstrable control over surface composition. This lack of control over surface composition is a major limiting factor in the development of useful DMFC. The self-directing deposition of Ru_{ad} on Pt substrates that is described in the following chapters is a heterogeneous reaction system that deposits controlled amounts of Ru_{ad} onto Pt surfaces (*vide infra*).

Whitesides *et al.* have shown that Pt surfaces (e.g., Pt_{black}) effect the hydrogenation of compounds with the general formula (diolefin)Pt(alkyl)$_2$ (e.g., η^4-1,5-cyclooctadiene)Pt(methyl)$_2$) and that the hydrogenation results in the deposition of Pt adatoms (Pt_{ad}) on the surface of the Pt_{black} substrate (eq. 1.43).[262-264]

$$\text{(diolefin)Pt(alkyl)}_2 + 3\,H_2 \xrightarrow{Pt_{black}} Pt_{ad} + \text{saturated hydrocarbons} \qquad \text{(eq. 1.43)}$$

The replacement of the (diolefin)Pt(II)(alkyl)$_2$ precursor with an organometallic Ru containing precursor (eq. 1.44) resulted in a clean and controlled metal deposition reaction for the preparation of bimetallic surfaces. The resulting surfaces are

$$\text{(diolefin)Ru(allyl)}_2 + 5\,H_2 \xrightarrow{Pt_{black}} Ru_{ad} + \text{saturated hydrocarbons} \qquad \text{(eq. 1.44)}$$

composed of exposed substrate (Pt) and deposited adatoms (Ru_{ad}). This method is a bench-top chemical process that will self-direct the deposition of ultra-thin films and sub-monolayer amounts of Ru_{ad} on Pt substrates. The Ru containing precursor does not contain ligands known to poison Pt surfaces (e.g., Cl^-, CO, amines, or phosphines). The reaction requires a Pt initiator, therefore the deposition will self-direct onto Pt clusters in the presence of an inert support. The reaction conditions were tuned to ensure reaction-rate-limiting conditions and not mass-transport limited. Carrying out the depositions under reaction rate limiting conditions ensured narrow distributions in the ratios of Pt

surface to Ru surface atoms on the Pt substrates. The coverage of the Pt substrate by Ru_{ad} can be controlled by varying the reaction time. The amount of Ru deposited was optimized for CH_3OH electrooxidation in fuel cells.

The Pt substrate can be a single crystal, polycrystalline, or nanoscale Pt particles. The nanoscale Pt particles can be unsupported or supported upon and inert support (e.g., carbon). The reaction developed during these studies can be applied to both model Pt electrodes and to nanoscale Pt particles. The application of a catalyst preparation method to model and real catalysts adds merit to model studies that are often plagued by a lack of similarity to the real, desired product.

Surface enrichment, segregation, and sintering of nanoscale particles prepared by the method described was avoided by limiting the exposure of the catalysts to high temperatures. The lifetime of adsorbed metal adatoms on the nanoparticle surface will control the utility of these bimetallic surfaces in practical heterogeneous systems. Since the annealing stage of bimetallic catalyst formation is omitted from the self-directing Ru deposition system surface enrichment is not expected.

The ability to prepare rough Pt-Ru surfaces of known surface area and controlled surface composition was be exploited for the optimization of Pt-Ru surfaces for the electrooxidation of CH_3OH in a DMFC. The Pt-Ru_{ad} surfaces were used for a systematic study of the effects of Pt-Ru_{ad} surface composition on the intrinsic activity of bimetallic electrocatalysts towards the electrooxidation of CH_3OH using high surface area Pt substrates. The results were applied to the preparation of nanoscale Pt-Ru_{ad} electrocatalysts. The activity and stability of adatom modified Pt particles was determined in a prototype DMFC. The activities of Pt-Ru_{ad} surfaces prepared using this methodology was determined using standard electrochemical techniques and prototype DMFC's.

References

(1) Liebhafsky, H.A.; Cairns, E.J. *Fuel Cells and Fuel Batteries*, John Wiley & Sons, Inc., 1968.

(2) Grove, W.R. *Phil Mag* **1839**, *14*, 127.

(3) Grove, W.R. *Phil. Mag.* **1839**, *3*, 39.

(4) Atkins, P.W. *Physical Chemistry* 4th ed. W.H. Freeman and Company, New York 1990.

(5) Bockris, J.O'M *Electrochemistry for Cleaner Environments*, Plenum Press, NY, 1972, Chapter 1.

(6) Ostwald, W. *Z. Electrochem.* **1894**, *1*, 122.

(7) Appleby, A.J.; Foulkes, F.R. *Fuel Cell Handbook*, Van Nostrand Reinhold, New York, 1989.

(8) Walsh, P. *J. Power. Sources* **1990**, *29*, 13.

(9) Kordesch, K. V.; Simader, G. R. *Chem. Rev.* **1995**, *95*, 191.

(10) Appleby, A.J.; Richter, G.J.; Selman, J.R.; Winsel, A. in *Electrochemical Hydrogen Technologies Electrochemical Production and Combustion of Hydrogen* Wendt, H. (ed.) Elsevier, 1990, Chapter 7.

(11) Bockris, J.O'M; Wass, J.C. *About the economics of massive hydrogen production at 2010 A.D.* in Proceedings of the 7th World Hydrogen Energy Conference, 1988.

(12) Schrope, M. *Nature* **2001** , *414*, 682.

(13) Bacon, F. T. *Int. J. Hydrogen Energy* **1985**, *10*, 423.

(14) Schlapbach, L.; Zuttel, A. *Nature* **2001**, *414*, 353.

(15) Cameron, D.S. *Plat. Met. Rev.* **2001**, *45*, 146.

(16) Rostrup-Nielsen, J.R. *Phys. Chem. Chem. Phys.* **2001**, *3*, 283.

(17) Geissler, K.; Newson, E.; Vogel, F.; Troung, T-B.; Hottinger, P.; Wokaun, A *Phys. Chem. Chem. Phys.* **2001**, *3*, 289.

(18) Docter, A.; Lamm, A. *J. Power Sources* **1999**, *84*, 194.

(19) Wiese, W.; Emonts, B.; Peters, R. *J. Power Sources* **1999**, *84*, 187.

(20) Ogden, J.M.; Steinbugler, M.M.; Kreutz, T. *J. Power Sources* **1999**, *79*, 143.

(21) Kinoshita, K.; Stonehart, P. in *Modern Aspects of Electrochemistry* Bockris, J. O'M.; Conway, B.E. (eds.) Plenum Press, New York **1977**, *12*, 183.

(22) Bard, A.J.; Faulkner, L.R. *Electrochemical Methods* John Wiley and Sons, 1980.

(23) Bockris, J. O'M *J. Chem. Ed.* **1971**, *48*, 352.

(24) Bockris, J. O'M.; Wroblowa, H. *J. Electroanal. Chem.* **1964**, *7*, 428.

(25) Pletcher, D. *J. Appl. Electrochem.* **1984**, *14*, 403.

(26) Lipkowski, J.; Ross, P.N.(eds.) *Electrocatalysis* Wiley-VCH, 1998.

(27) Tafel, J. *Z. Phys. Chem.* **1905**, *50*, 541.

(28) Bagotzky, V.S.; Skundin, A.M. *Chemical Power Sources*, Academic Press, Inc., London, 1980.

(29) Neidrach, L.W.; Alford, H.R. *J. Electrochem. Soc.* **1965**, *112*, 117.

(30) Liebhafsky, H.A.; Cairns, E.J. *Fuel Cells and Fuel Batteries: A Guide to Their Research and Development*, John Wiley & Sons, Inc., New York, 1968.

(31) Carrette, L.; Friedrich, K. A.; Stimming, U. *Chem. Phys. Phys. Chem* **2000**, *1*, 162.

(32) Hamnett, A. *Phil. Trans. R. Soc. Lond. A* **1996**, *354*, 1653.

(33) Billings, R.E.; Sanchez, M. *Int. J. Hydrogen Energy* **1995**, *20*, 521.

(34) Appleby, A. J. *Phil. Trans. R. Soc. Lond. A* **1996**, *354*, 1681.

(35) Nernst, W. *Z. Elektrochem.* **1899**, *43*, 727.

(36) Yamamoto, O. *Electrochim. Acta* **2000**, *45*, 2423.

(37) *Oxford Dictionary of Chemistry* 3rd ed. J. Daintith (ed.) Oxford University Press, Oxford, 1996.

(38) Park, S.; Vohs, J.M.; Gorte, R.J. *Nature* **2001**, *404*, 265.

(39) Jiang, J.; Virkar, A *J. Electrochem. Soc.* **2001**, *148*, A706.

(40) Hamnett, A. *Phil. Trans. R. Soc. Lon. A* **1996**, *354*, 1653.

(41) Aragane, J.; Murahashi, T.; Odaka, T. *J. Electrochem. Soc.* **1988**, *135*, 844.

(42) Eikerling, M.; Kornyshev, A.A.; Stimming, U. *J. Phys. Chem. B* **1997**, *101*: 10807.

(43) Prater, K. *J. Power Sources* **1990**, *29*, 239.

(44) Watanabe, M.; Uchida, M.; Motoo, S. *J. Electroanal. Chem.* **1986**, *199*, 311.

(45) Srinivasan, S.; Ticianelli, E.A.; Derouin, C.R.; Redondo, A. *J. Power Sources*, **1988**, *22*, 359.

(46) Ticianell, E.A.; Derouin, C.R.; Redondo, A.; Srinivasan, S. *J. Electrochem. Soc.* **1988**, *135*, 2209.

(47) Wilson, M. S.; Gottesfeld, S. *J. Appl. Electrochem.* **1992**, *22*, 1.

(48) Wilson, M. S.; Gottesfeld, S. *J. Electrochem. Soc.* **1992**, *139*, L28.

(49) Wilson, M. S.; Valerio, J. A.; Gottesfeld, S. *Electrochim. Acta* **1995**, *40*, 355.

(50) Liu, R.; Her, W. H.; Fedkiw, P. S. *J. Electrochem. Soc.* **1992**, *139*, 15.

(51) Lefebvre, M.C.; Martin, R.B.; Pickup, P.G. *Electrochem. Solid-State Lett.* **1999**, *2*, 259.

(52) Jordan, L.R.; Shukla, A.K.; Behrsing, Avery, N.R.; Muddle, B.C.; Forsyth *J. Appl. Electrochem.* **2000**, *30*, 641.

(53) Qi, Z.; Lefebvre, M.C.; Pickup, P.G. *J. Electroanal. Chem.* **1998**, *459*, 9.

(54) Taylor, E.J.; Anderson, E.B.; Vilambi, N.R.K. *J. Electrochem. Soc.* **1992**, *139*, L45.

(55) Poltarzewski, Z.; Staiti, P.; Alderucci, V.; Wieczorek, W.; Giordino N. *J. Electrochem. Soc.* **1992**, *139*, 761.

(56) Giorgi, L.; Antolini, E.; Pozio, A.; Passalacqua, E. *Electrochim. Acta* **1998**, *43*, 3675.

(57) Antolini, E.; Giorgi, L.; Pozio, A.; Passalacqua, E. *J. Power Sources* **1999**, *77*, 136.

(58) Lufrano, F.; Passalacqua, E.; Squadrito, G.; Patti, A.; Giorgi, L. *J. Appl. Electrochem.* **1999**, *29*, 445.

(59) Acres, G.J.K.; Frost, J.C.; Hards, G.A.; Potter, R.J.; Ralph, T.R.; Thompsett, D.; Burnstein, G.T.; Hutchings, G.J. *Cat Today* **1997**, *38*, 393.

(60) Lamy, C.; Leger, J-M.; Srinivasan, S. in *Modern Aspects of Electrochemistry* Bockris, J. O'M.; Conway, B.E. (eds.) Plenum Press, New York **2001**, *34*, 53.

(61) Wasmus, S.; Kuver, A. *J. Electroanal. Chem.* **1999**, *461*, 14.

(62) Kordesch, K.; Simander, G. *Fuel Cells and Their Applications*, VCH, New York, 1996.

(63) Kingston, R. *Chemistry in Britain* **2000**, *36*, 24.

(64) McNicol, B. D.; Rand, D. A. J.; Williams, K. R. *J. Power Sources* **1999**, *83*, 15.

(65) Uchida, H.; Mizuno, Y.; Watanabe, M. *Chem. Lett.* **2000**, 1268.

(66) Ren, X. M.; Zelenay, P.; Thomas, S.; Davey, J.; Gottesfeld, S. *J. Power Sources* **2000**, *86*, 111.

(67) Argyropoulos, P.; Scott, K.; Taama, W. M. *J. Power Sources* **2000**, *87*, 153.

(68) Heinzel, A.; Barragan, V. M. *J. Power Sources* **1999**, *84*, 70.

(69) Hampson, N. A.; Willars, M. J.; McNicol, B. D. *J. Power Sources* **1979**, *4*, 191.

(70) Leger, J-M.; Lamy, C. *Ber. Bunsen-Ges. Phys. Chem. Chem. Phys.* **1990**, *94*, 1021.

(71) Leger, J-M. *J. Appl. Electrochem.* **2001**, *31*, 767.

(72) Baldauf, M.; Preidel, W. *J. Power Sources* **1999**, *84*, 161.

(73) Bagotzky, V.S.; Vasilyev, Yu. B. *Electrochim. Acta* **1964**, *9*, 869.

(74) Giner, J. *Electrochim. Acta* **1964**, *9*, 63.

(75) Petry, O.A.; Podlovchenko, B.I.; Frumpkin, A.N.; Lal, H. *J. Electroanal. Chem.* **1965**, *10*, 253.

(76) Cameron, D.S.; Hards, G.A.; Harrison, B.; Potter, R.J. *Plat. Met. Rev.* **1987**, *31*, 173.

(77) Beden, B.; Lamy, C.; Leger, J-M. in *Modern Aspects of Electrochemistry* Bockris, J. O'M.; Conway, B.E.; Whites. R.E. (eds.) Plenum Press, New York **1992**, *22*, 97.

(78) Jarvi, T.J.; Stuve, E.M. in *Electrocatalysis*, Lipkowski, J.; Ross, P.N. (eds.) Wiley-VCH, New York, 1998, Chapter 3.

(79) Franaszczuk, K.; Herrero, E.; Zelenay, P.; Wieckowski, A.; Wang, J.; Masel, R. I. *J. Phys. Chem.* **1992**, *96*, 8509.

(80) W. Vielstich, X.H. Xia *J. Phys. Chem.* **1995**, *99*, 10421.

(81) Tilak, T.V.; Conway, B.E.; Angerstein-Kozlowska H. *J. Electroanal. Chem.* **1973**, *48*, 1.

(82) Li. N.H.; Sun, S.G.; Chen, S.P. *J. Electroanal. Chem.* **1997**, *430*, 57.

(83) Parsons, R.; VanderNoot, T. *J. Electroanal. Chem.* **1988**, *257*, 9.

(84) Xia, X. H.; Iwasita, T.; Ge, F.; Vielstich, W. *Electrochim. Acta* **1996**, *41*, 711.

(85) Clavilier, J.; Lamy, C.; Leger, J-M. *J. Electroanal. Chem.* **1981**, *125*, 249.

(86) Herrero, E.; Franaszczuk, K.; Wieckowski, A. *J. Phys. Chem.* **1994**, *98*, 5074.

(87) Jarvi, T. D.; Sriramulu, S.; Stuve, E. M. *Colloid Surf. A-Physicochem. Eng. Asp.* **1998**, *134*, 145.

(88) McNicol, B.D.; Attwood, P.; Short, R.T. *J. Chem Soc. Faraday Trans 1* **1981**, *77* 2017.

(89) Watanabe, M.; Saegusa, S.; Stonehart, P. *J. Electroanal. Chem.* **1989**, *271*, 213.

(90) Solla-Gullon, J.; Montiel, V., Aldaz, A.; Clavilier, J. *J. Electroanal. Chem.* **2000**, *491*, 69.

(91) Hamnett, A. *Cat. Today* **1997**, *38*, 445.

(92) Gasteiger, H. A.; Markovic, N. M.; Ross, P. N. *J. Phys. Chem.* **1995**, *99*, 8290.

(93) Neidrach, L.W.; McKee, D.W.; Paynter, J.; Danzig, I.F. *J. Electrochem. Tech.* **1967**, *5*, 318.

(94) Oetjen, H. F.; Schmidt, V. M.; Stimming, U.; Trila, F. *J. Electrochem. Soc.* **1996**, *143*, 3838.

(95) W. Lin, J. Wang, R. Savinell *J. Electrochem. Soc.* **1997**, *144*, 1917.

(96) Gasteiger, H.A.; Markovic, N.; Ross, P.N. *J. Phys. Chem.* **1995**, *99*, 16757.

(97) Watanabe, M.; Uchida, M.; Motoo, S. *J. Electroanal. Chem.* **1987**, *229*, 395.

(98) Liu, L.; Viswanathan, R.; Liu, R.; Smotkin, E.S. *Electrochem. Solid-State Lett.* **1998**, *1*, 123.

(99) Liu, R. X.; Iddir, H.; Fan, Q. B.; Hou, G. Y.; Bo, A. L.; Ley, K. L.; Smotkin, E. S.; Sung, Y. E.; Kim, H.; Thomas, S.; Wieckowski, A. *J. Phys. Chem. B* **2000**, *104*, 3518.

(100) Rolison, D.R.; Hagans, P.L.; Swider, K.E.; Long, J.W. *Langmuir* **1999**, *15*, 774.

(101) Long, J.W.; Swider, K.E.; Merzbacher, C.I.; Rolison, D.R. *Langmuir* **1999**, *15*, 780.

(102) Merzbacher, C.I.; Barker, J.G.; Swider, K.E.; Rolison, D.R. *Adv. Colloid Interface Sci.* **1998**, *57*, 76.

(103) Markovic, N. M.; Gasteiger, H. A.; Ross, P. N.; Jiang, X. D.; Villegas, I.; Weaver, M. J. *Electrochim. Acta* **1995**, *40*, 91.

(104) Iwasita, T.; Hoster, H.; John-Anacker, A.; Lin, W. F.; Vielstich, W. *Langmuir* **2000**, *16*, 522.

(105) M. Krausa, W. Vielstich *J. Electroanal. Chem.* **1994**, *379*, 307.

(106) de Souza, J. P. I.; Iwasita, T.; Nart, F. C.; Vielstich, W. *J. Appl. Electrochem.* **1999**, *30*, 43.

(107) Chu, D.; Gillman, S. *J. Electrochem.Soc.* **1996**, *143*, 1685.

(108) Kim, D. I.; Lee, C. H.; Lee, C. W.; Jung, D. H.; Kim, C. S.; Shin, D. R. *J. New Mat. Electrochem. Sys.* **2001**, *4*, 41.

(109) Herrero, E.; Feliu, J. M.; Wieckowski, A. *Langmuir* **1999**, *15*, 4944.

(110) Chrzanowski, W.; Wieckowski, A. *Langmuir* **1998**, *14*, 1967.

(111) Chrzanowski, W.; Kim, H.; Wieckowski, A. *Cat. Letters* **1998**, *50*, 69.

(112) Tremiliosi, G.; Kim, H.; Chrzanowski, W.; Wieckowski, A.; Grzybowska, B.; Kulesza, P. *J. Electroanal. Chem.* **1999**, *467*, 143.

(113) Radmilovic, V.; Gasteiger, H. A.; Ross, P. N., Jr. *J. Catal.* **1995**, *154*, 98.

(114) Frelink, T.; Visscher, W.; Van Veen, J. A. R. *Surf. Sci.* **1995**, *335*, 353.

(115) Frelink, T.; Visscher, W.; Cox, A. P.; Van Veen, J. A. R. *Electrochim. Acta* **1995**, *40*, 1537.

(116) Rauhe, B. R., Jr.; McLarnon, F. R.; Cairns, E. J. *J. Electrochem. Soc.* **1995**, *142*, 1073.

(117) Laborde, H.; Leger, J-M.; Lamy, C. *J. Appl. Electrochem.* **1994**, *24*, 1019.

(118) Gasteiger, H. A.; Markovic, N.; Ross, P. N., Jr.; Cairns, E. J. *J. Electrochem. Soc.* **1994**, *141*, 1795.

(119) Gasteiger, H. A.; Markovic, N.; Ross, P. N., Jr.; Cairns, E. J. *J. Phys. Chem.* **1993**, *97*, 12020.

(120) Herrero, E.; Franaszczuk, K.; Wiecskowski, A. *J. Electroanal. Chem.* **1993**, *361*, 269.

(121) Hable, C. T.; Wrighton, M. S. *Langmuir* **1993**, *9*, 3284.

(122) Meli, G.; Leger, J-M.; Lamy, C. *J. Appl. Electrochem.* **1993**, *23*, 197.

(123) Franaszczuk, K.; Sobkowski, J. *J. Electroanal. Chem.* **1992**, *327*, 235.

(124) Kennedy, B. J.; Hamnett, A. *J. Electroanal. Chem.* **1990**, *283*, 271.

(125) Goodenough, J. B.; Hamnett, A., Kennedy, B. J.; Manoharan, R.; Weeks, S. A. *J. Electroanal. Chem.* **1988**, *240*, 133.

(126) Hughes, V. B.; Miles, R. *J. Electroanal. Chem.* **1983**, *145*, 87.

(127) Beden, B.; Kadirigan, F; Lamy, C.; Leger, J-M. *J. Electroanal. Chem.* **1981**, *127*, 75.

(128) Janssen, M. M. P.; Moolhuysen, *J. Electrochim. Acta* **1976**, *21*, 869.

(129) Surampudi, S.; Narayanan, S. R.;Vamos, E.; Frank, H.; Halpert, G.; LaConti, A.; Kosek, J.; Surya Prakash, G. K.; Olah, G. A. *J. Power Sources* **1994**, *47*, 377

(130) Hogarth, M. P.; Munk, J.; Shukula, A. K.; Hamnett, A. *J. Appl. Electrochem.* **1994**, *24*, 85.

(131) Wasmus, S.; Vielstich, W. *J. Appl. Electrochem.* **1993**, *23*, 120.

(132) Swathirajan, S.; Mikhail, Y. M. *J. Electrochem. Soc.* **1991**, *138*, 1321.

(133) Aramata, A.; Masuda, M. *J. Electrochem. Soc.* **1991**, *138*, 1949.

(134) Iwasita, T.; Nart, F. C.; Vielstich, W. *Ber. Bunsen-Ges. Phys. Chem.* **1990**, *94*, 1030.

(135) McNicol, B. D.; Short, R. T. *J. Electroanal. Chem.* **1977**, *81*, 249.

(136) Watanabe, M.; Motoo, S. *J. Electroanal. Interfacial Electrochem.* **1975**, *60*, 267.

(137) Fonseca, I.T.E.; Proenca, L.F.A. *Environmental Res. Forum* **1996**, *1-2*, 229.

(138) Cathro, K.J. *J. Electrochem. Soc.* **1969**, *116*, 1608.

(139) Grgur, B.N.; Markovic, N.M.; Ross, P.N. *Electrochim. Acta* **1998**, *43*, 3631.

(140) Katayama, A. *J. Phys. Chem.* **1980**, *84*, 376.

(141) Wang, K.; Gasteiger, H. A.; Markovic, N. M.; Ross, P. N. *Electrochim. Acta* **1996**, *41*, 2587.

(142) Motto, S,; Watanabe, M. *J. Electroanal. Chem.* **1980**, *110*, 103.

(143) Gasteiger, H. A.; Markovic, N. M.; Ross, P. N. *Catal. Lett.* **1996**, *36*, 1.

(144) Shropshire J.A. *J. Electrochem. Soc.* **1965**, *112*, 465.

(145) Wang, Y.; Fachini, E. R.; Cruz, G.; Zhu, Y.; Ishikawa, Y.; Colucci, J. A.; Cabrera, C. R. *J. Electrochem. Soc.* **2001**, *148*, C222.

(146) Shen, P. K.; Tseung, A. C. C. *J. Electrochem. Soc.* **1994**, *141*, 3082.

(147) Shukla, A. K.; Ravikumar, M. K.; Arico, A. S.; Candiano, G.; Antonucci, V.; Giordano, N.; Hamnett, A. *J. Appl. Electrochem.* **1995**, *25*, 528.

(148) Shen, P. K.; Chen, K. Y.; Tseung, A. C. C. *J. Electrochem. Soc.* **1995**, *142*, L85-L86.

(149) Troughton, G.L.; Hamnett, A *Bull. Electrochem.* **1991**, *7*, 488.

(150) Ley, K. L.; Liu, R. X.; Pu, C.; Fan, Q. B.; Leyarovska, N.; Segre, C.; Smotkin, E. S. *J. Electrochem. Soc.* **1997**, *144*, 1543.

(151) Reddington, E.; Sapienza, A.; Gurau, B.; Viswanathan, R.;Sarangapini,S.; Smotkin, E. S.; Mallouk, T. E. *Science* **1998**, *280*, 1735.

(152) Gurau, B.; Viswanathan, R.; Liu, R.; Lafrenz, T.; Lye, K.L.; Smotkin, E.S.; Reddington, E.; Sapienza, A.; Chan, B. C.; Mallouk, T. E.; Sarabgapani, S. *J. Phys. Chem. B* **1998**, *102*, 9997.

(153) Arico, A. S.; Creti, P.; Giordano, N.; Antonucci, V.; Antonucci, P. L.; Chuvilin, A. *J. Appl. Electrochem.* **1996**, *26*, 959.

(154) Sinfelt, J. *Bimetallic Catalysis: Discoveries, Concepts, and Applications*, John Wiley & Sons, Inc., New York, 1983.

(155) Breiter, M. W. *J. Electroanal Chem* **1986**,*214*, 547.

(156) Ticanelli, E.; Beery, J. G.; Paffett, M. T.; Gottesfeld, S. *J. Electroanal. Chem.* **1989**, *258*, 61.

(157) Hadzi-Jordanov, S.; Angerstein-Kozlowska, H.; Vukovic, M.; Conway B.E. *J. Electrochem. Soc.* **1978**, *126*, 1471.

(158) Hamnett, A. in *Interfacial Electrochemistry: Theory, Experiment, and Applications,* Wieckowski (ed.) Marcel-Dekker, New York, 1999, p843.

(159) Ross, P.N. Jr in *Electrocatalysis*, Lipkowski, J.; Ross, P.N. (eds.) Wiley-VCH, New York, 1998, Chapter 2.

(160) Lu, C.; Masel, R. I. J. *Phys. Chem. B* **2001**, *105*, 9793.

(161) Iwasita, T.; Nart, F. C.; Vielstich, W. *Ber. Bunsen-Ges. Phys. Chem. Chem. Phys.* **1990**, *94*, 1030.

(162) Frelink, T.; Visscher, W.; Van Veen, J. A. R. *Langmuir* **1996**, *12*, 3702.

(163) Schwarz, J.A.; Contescu, C; Contescu, A *Chem. Rev.* **1995**, *95*, 477.

(164) Toshima, N.; Yonezawa, T. *New. J. Chem.* **1998**, 1179.

(165) Petrow, H.G.; Allen, R.J. *US Patent* 4 044 193, 23 Aug. 1977.

(166) Cahen, D. ; Ibers, J.A. *J. Catal.* **1973**, *31*, 369.

(167) Sinfelt, J.H. *Ann. Rev. Mat. Sci.* **1972**, *2*, 641.

(168) McKee, D.W.; Norton, F.J. *J. Phys. Chem.* **1964**, *68*, 481.

(169) Liu, R.; Her, W. H.; Fedkiw, P. S. *J. Electrochem. Soc.* **1992**, *139*, 15.

(170) Denis, M. C.; Lalande, G.; Guay, D.; Dodelet, J. P.; Schulz, R. *J. Appl. Electrochem.* **1999**, *29*, 951.

(171) Denis, M. C.; Gouerec, P.; Guay, D.; Dodelet, J. P.; Lalande, G.; Schulz, R. *J. Appl. Electrochem.* **2000**, *30*, 1243.

(172) Alerasool, S.; Gonzalez, R. D. *J. Catal.* **1990**, *124*, 204.

(173) Nashner, M. S.; Frenkel, A. I.; Adler, D. L.; Shapley, J. R.; Nuzzo, R. G. *J. Am. Chem. Soc.* **1997**, *119*, 7760.

(174) Gasteiger, H. A.; Ross, P. N.; Cairns, E. J. *Surf. Sci.* **1993**, *293*, 67.

(175) McNicol, B. D.; Short, R. T. *J. Electroanal. Chem.* **1977**, *81*, 249.

(176) Bazin, D.; Mottet, C.; Treglia, G. *Appl. Cat. A Gen.* **2000**, *200*, 47.

(177) Bonnemann, H.; Brijoux, W.; Brinkmann, R.; Dinjus, E.; Joussen, T.; Korall, B. *Angew. Chem.-Int. Edit. Engl.* **1991**, *30*, 1312.

(178) Paulus, U. A.; Endruschat, U.; Feldmeyer, G. J.; Schmidt, T. J.; Bonnemann, H.; Behm, R. J. *J. Catal.* **2000**, *195*, 383.

(179) Schmidt, T. J.; Noeske, M.; Gasteiger, H. A.; Behm, R. J.; Britz, P.; Brijoux, W.; Bonnemann, H. *Langmuir* **1997**, *13*, 2591.

(180) Schmidt, T.J.; Gasteiger, H.A.; Behm, R.J. *Electrochem. Comm.* **1998**, *1*, 1.

(181) Gotz, M.; Wendt, H. *Electrochim. Acta* **1998**, *43*, 3637.

(182) Vogel, W.; Britz, P.; Bonnemann, H.; Rothe, J.; Hormes, J. *J. Phys. Chem. B* **1997**, *101*, 11029.

(183) Schmidt, T. J.; Noeske, M.; Gasteiger, H. A.; Behm, R. J.; Britz, P.; Bonnemann, H. *J. Electrochem. Soc.* **1998**, *145*, 925.

(184) Pan, C.; Dassenoy, F.; Casanove, M.J., Philoppot, K.; Amiens, C; Lecante, P.; Mosset, A. Chaudret, B. *J. Phys. Chem., B* **1999**, *103*, 10098.

(185) Nashner, M. S.; Frenkel, Sommerville, D.; Hills, C.W.; Shapley, J. R.; Nuzzo, R. G. *J. Am. Chem. Soc.* **1998**, *120*, 8093.

(186) Boxall, D. L.; Deluga, G. A.; Kenik, E. A.; King, W. D.; Lukehart, C. M. *Chem. Mat.* **2001**, *13*, 891.

(187) Feldman, L.C.; Mayer, J.W. *Fundamentals of Surface and Thin Film Analysis*, North Holland, New York, 1986.

(188) Rice, C.; Tong, Y. Y.; Oldfield, E.; Wieckowski, A. *Electrochim. Acta* **1998**, *43*, 2825.

(189) Yahnke, M. S.; Rush, B. M.; Reimer, J. A.; Cairns, E. J. *J. Am. Chem. Soc.* **1996**, *118*, 12250.

(190) Antolini, E.; Giorgi, L.; Cardellini, F.; Passalacqua, E. *J. Solid State Electrochem.* **2001**, *5*, 131.

(191) West, A.R. *Solid State Chemistry and its Applications* John Wiley & Sons, Inc., 1984.

(192) Long, J. W.; Stroud, R. M.; Swider-Lyons, K. E.; Rolison, D. R. *J. Phys. Chem. B* **2000**, *104*, 9772.

(193) Hills, C. W.; Nashner, M. S.; Frenkel, A. I.; Shapley, J. R.; Nuzzo, R. G. *Langmuir* **1999**, *15*, 690.

(194) Russell, A. E.; Maniguet, S.; Mathew, R. J.; Yao, J.; Roberts, M. A.; Thompsett, D. *J. Power Sources* **2001**, *96*, 226.

(195) Ross, P. N. *Electrochim. Acta* **1991**, *36*, 2053.

(196) Kokkinidis, G. *J. Electroanal. Chem.* **1986**, *201*, 217.

(197) Ramamoorthy, P.; Gonzalez, R. D. *J. Catal.* **1979**, *58*, 188.

(198) Miura, H.; Gonzalez, R. D. *J. Catal.* **1982**, *74*, 216.

(199) Friedrich, K. A.; Geyzers, K. P.; Linke, U.; Stimming, U.; Stumper, J. *J. Electroanal. Chem.* **1996**, *402*, 123.

(200) Davies, J. C.; Hayden, B. E.; Pegg, D. J. *Electrochim. Acta* **1998**, *44*, 1181.

(201) Davies, J. C.; Hayden, B. E.; Pegg, D. J. *Surf. Sci.* **2000**, *467*, 118.

(202) Davies, J. C.; Hayden, B. E.; Pegg, D. J.; Rendall, M.E. *Surf. Sci.* **2002**, *496*,110.

(203) Tong, Y.; Kim, H.S.; Babu, P.K.; Waszczuk, P.; Wieckowski, A.; Oldfield, E. *J. Am. Chem. Soc.* **2002**, *124*, 468.

(204) Massong, H.; Wang, H. S.; Samjeske, G.; Baltruschat, H. *Electrochim. Acta* **2000**, *46*, 701.

(205) Lin, W. F.; Zei, M. S.; Eiswirth, M.; Ertl, G.; Iwasita, T.; Vielstich, W. *J. Phys. Chem. B* **1999**, *103*, 6968.

(206) Dinh, H. N.; Ren, X. M.; Garzon, F. H.; Zelenay, P.; Gottesfeld, S. *J. Electroanal. Chem.* **2000**, *491*, 222.

(207) Jarvi, T. D.; Madden, T. H.; Stuve, E. M. *Electrochem. Solid State Lett.* **1999**, *2*, 224.

(208) Fachini, E. R.; Cabrera, C. R. *Langmuir* **1999**, *15*, 717-721.

(209) Lamouri, A.; Gofer, Y.; Luo, Y.; Chottiner, G.S.; Scherson, D.A. *J. Phys. Chem. B* **2001**, *105*, 6172.

(210) Watanabe, M.; Motoo, S. *J. Electroanal. Chem.* **1975**, *60*, 267.

(211) Watanabe, M.; Genjima, Y.; Turumi, K. *J. Electrochem. Soc.* **1997**, *144*, 423.

(212) Herrero, E.; Franaszczuk, K.; Wiecskowski, A. *J. Electroanal. Chem.* **1993**, *361*, 269.

(213) Cramm, S.; Friedrich, K. A.; Geyzers, K. P.; Stimming, U.; Vogel, R. *Fresenius J. Anal. Chem.* **1997**, *358*, 189.

(214) Friedrich, K. A.; Geyzers, K. P.; Linke, U.; Stimming, U.; Stumper, J. *J. Electroanal. Chem.* **1996**, *402*, 123.

(215) Friedrich, K. A.; Geyzers, K. P.; Marmann, A.; Stimming, U.; Vogel, R. *Z. Phys. Chemie-Int. J. Res. Phys. Chem. Chem. Phys.* **1999**, *208*, 137.

(216) Lin, W. F.; Zei, M. S.; Eiswirth, M.; Ertl, G.; Iwasita, T.; Vielstich, W. *J. Phys. Chem. B* **1999**, *103*, 6968.

(217) Chrzanowski, W.; Wieckowski, A. *Langmuir* **1998**, *14*, 1967.

(218) Sobkowski, J.; Wieckowski, A. *J. Electroanal. Chem.* **1973**, *41*, 373.

(219) Markovic, N.; Ross, P. N. *J. Electroanal. Chem.* **1992**, *330*, 499.

(220) Petry, O.A.; Frumpkin, A.N.; Lal, H. *J. Electroanal. Chem.* **1965**, *10*, 253.

(221) Frelink, T. ;Vissher, W.; Van Veen, J.A.R. *Surf. Sci.* **1995**, *335*, 360.

(222) Krausa, M.; Vielstich, W. *J. Electroanal. Chem.* **1994**, *379*, 307.

(223) Szabo, F.; Bakos, I. *J. Electroanal. Chem.* **1987**, *230*, 233.

(224) Szabo, F.; Bakos, I.; Nagy, F. *J. Electroanal. Chem.* **1989**, *230*, 269.

(225) Chrzanowski, W.; Wieckowski, A. *Langmuir* **1997**, *13*, 5974.

(226) Chrzanowski, W.; Kim, H.; Wieckowski, A. *Catal. Lett.* **1998**, *50*, 69.

(227) Tremiliosi, G.; Kim, H.; Chrzanowski, W.; Wieckowski, A.; Grzybowska, B.; Kulesza, P. *J. Electroanal. Chem.* **1999**, *467*, 143.

(228) Crown, A.; Wieckowski, A. *Phys. Chem. Chem. Phys.* **2001**, *3*, 3290.

(229) Crown, A.; Moraes, I. R.; Wieckowski, A. *J. Electroanal. Chem.* **2001**, *500*, 333.

(230) Herrero, E.; Feliu, J. M.; Wieckowski, A. *Langmuir* **1999**, *15*, 4944.

(231) Crown, A.; Kim, H.; Lu, G. Q.; de Moraes, I. R.; Rice, C.; Wieckowski, A. *J. New Mat.Electrochem. Syst.* **2000**, *3*, 275.

(232) Waszczuk, P.; Solla-Gullon, J.; Kim, H. S.; Tong, Y. Y.; Montiel, V.; Aldaz, A.; Wieckowski, A. *J. Catal.* **2001**, *203*, 1.

(233) Kim, H.; de Moraes, I. R.; Tremiliosi, G.; Haasch, R.; Wieckowski, A. *Surf. Sci.* **2001**, *474*, L203.

(234) Lin, W. F.; Zei, M. S.; Eiswirth, M.; Ertl, G.; Iwasita, T.; Vielstich, W. *J. Phys. Chem. B* **1999**, *103*, 6968.

(235) Iwasita, T.; Hoster, H.; John-Anacker, A.; Lin, W. F.; Vielstich, W. *Langmuir* **2000**, *16*, 522.

(236) Brankovic, S. R.; McBreen, J.; Adzic, R. R. *J. Electroanal. Chem.* **2001**, *503*, 99.

(237) Brankovic, S. R.; Wang, J. X.; Adzic, R. R. *Electrochem. Solid State Lett.* **2001**, *4*, A217.

(238) de Mongeot, F.B.; Scherer, M.; Gleich, B.; Kopatzki, E.; Behm, R.J. *Surf. Sci.* **1998**, *411*, 249.

(239) Iwasita, T.; Nart, F. C.; Vielstich, W. *Ber. Bunsen-Ges. Phys. Chem. Chem. Phys.* **1990**, *94*, 1030.

(240) Iwasita, T.; Hoster, H.; John-Anacker, A.; Lin, W. F.; Vielstich, W. *Langmuir* **2000**, *16*, 522.

(241) Gasteiger, H. A.; Ross, P. N.; Cairns, E. J. *Surf. Sci.* **1993**, *293*, 67.

(242) Gasteiger, H. A.; Markovic, N.; Ross, P. N.; Cairns, E. J. *J. Electrochem. Soc.* **1994**, *141*, 1795.

(243) Gasteiger, H. A.; Markovic, N.; Ross, P. N.; Cairns, E. J. *Electrochim. Acta* **1994**, *39*, 1825.

(244) Kabbabi, A.; Faure, R.; Durand, R.; Beden, B.; Hahn, F.; Leger, J. M.; Lamy, C. *J. Electroanal. Chem.* **1998**, *444*, 41.

(245) Gasteiger, H. A.; Markovic, N.; Ross, P. N.; Cairns, E. J. *J. Phys. Chem.* **1993**, *97*, 12020.

(246) Gasteiger, H. A.; Markovic, N.; Ross, P. N.; Cairns, E. J. *J. Electrochem. Soc.* **1994**, *141*, 1795.

(247) Chrzanowski, W.; Wieckowski, A. *Langmuir* **1998**, *14*, 1967.

(248) Chrzanowski, W.; Kim, H.; Wieckowski, A. *Cat. Lett.* **1998**, *50*, 69.

(249) Tremiliosi, G.; Kim, H.; Chrzanowski, W.; Wieckowski, A.; Grzybowska, B.; Kulesza, P. *J. Electroanal. Chem.* **1999**, *467*, 143.

(250) WO Patent 97/21256 (12 June 1997).

(251) US Patent 5 523 177 (4 June 1996).

(252) Long, J. W.; Stroud, R. M.; Swider-Lyons, K. E.; Rolison, D. R. *J. Phys. Chem. B* **2000**, *104*, 9772.

(253) Dinh, H. N.; Ren, X. M.; Garzon, F. H.; Zelenay, P.; Gottesfeld, S. *J. Electroanal. Chem.* **2000**, *491*, 222.

(254) O'Grady, W. E.; Hagans, P. L.; Pandya, K. I.; Maricle, D. L. *Langmuir* **2001**, *17*, 3047.

(255) Takasu, Y.; Itaya, H.; Iwazaki, T.; Miyoshi, R.; Ohnuma, T.; Sugimoto, W.; Murakami, Y. *Chem. Comm.* **2001**, 341.

(256) Miura, H.; Taguchi, H.; Sugiyama, K.; Matsuda, T.; Gonzalez, R. D. *J. Catal.* 1990, 124, 194.

(257) Amano, A.; Parravano, G. *Adv. Catal.* **1957**, *9*, 716.

(258) Gray, T.J.; Masse, N.G.; Oswin, H.G. *Adv. Catal.* **1960**, *2*, 1697.

(259) Miura, H.; Gonzalez, R. D. *J. Catal.* **1982**, *74*, 216.

(260) Meng, N.; Ando, Y.; Shinoda, S.; Saito, Y. *Bull. Chem. Soc. Japan* **1999**, *72*, 669.

(261) Gao, X.P.; Kocha, S.; Frank, A.J.; Turner, J.A. *Int. J. Hyd. Energy* **1999**, *24*, 319.

(262) Miller, T. M.; Izumi, A. N.; Shih, Y. S.; Whitesides, G. M. *J. Am. Chem. Soc.* **1988**, *110*, 3146.

(263) Miller, T. M.; McCarthy, T. J.; Whitesides, G. M. *J. Am. Chem. Soc.* **1988**, *110*, 3156.

(264) Miller, T. M.; Whitesides, G. M. *J. Am. Chem. Soc.* **1988**, *110*, 3164.

Chapter 2†

Self-Directing Organometallic Deposition of Ru Adatoms on Pt. Part I. The Hydrogenation of a Ru containing Precursor on a Pt Substrate.

Introduction

The initial target of this work was to develop a reaction that will deposit by adsorption sub-monolayer or multi-layer quantities of Ru adatoms (Ru_{ad}) on the surfaces of blacked Pt gauzes. The resulting rough Pt-Ru_{ad} surfaces will be used to model the high dispersion Pt-Ru particles used in DMFC's. Towards this end, the following describes studies of the hydrogenation of (COD)Ru(η^3-allyl)$_2$ (**1**; COD is 1,5-cyclooctadiene) over the surface of blacked Pt gauzes by H_2(g) in hexanes (eq. 2.1). The primary objectives are to develop a bench-top, clean, and controlled low energy deposition reaction that can be monitored *in situ* and that can be terminated when the desired surface stoichiometry is reached.

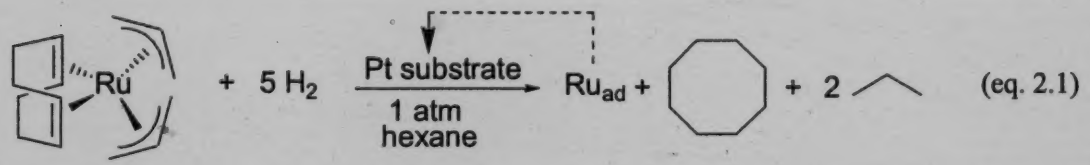

(eq. 2.1)

1

This reaction is conceptually similar to the surface organometallic chemistry (SOMC) work largely carried out by Basset *et al.*,[1-7] and recently applied to other electrocatalysts by Crabb *et al.*.[8-11] Surface organometallic chemistry uses selective surface reactions between organometallic metal containing precursors (e.g.,

---

† Reproduced in part with permission from Lee, C.E.; Tiege, P.B.; Xing, Y.; Nagendran, J.; Bergens, S.H. *J. Am. Chem. Soc.* **1997**, *119*, 3543. Copyright 1997 American Chemical Society. With the exception of the hydrogenation of **1** over Pt black and the Neutron Activation Experiment all work presented in this chapter is that of C.E. Lee.

tetrabutyltin(IV)) in sub-stoichiometric surface ratios on hydrogen saturated catalyst surfaces (e.g., Pt supported on alumina) to selectively deposit metal adatoms.[3] The adsorption of the metal center onto the H_{ads} saturated Pt surface occurs with concomitant loss of the ligands as saturated hydrocarbons. To date, the deposition of Ru_{ad} on Pt surfaces has not been reported by these groups. Gonzalez *et al.* employed a two-step process in which ruthenocene was deposited onto a support containing Pt metal clusters, the Ru containing precursor was then reduced by H_2 at elevated temperatures to produce Pt-Ru supported on silica.[12] Apparent control over the surface composition using these SOMC approaches has been achieved by adjusting the ratio of the amount of organometallic metal source introduced to the number of available sites on the supported clusters of the metal precursor (i.e., limiting-reagent-control). In contrast, the hydrogenation of **1** over Pt is designed to provide in real-time and at low temperatures both the number of surface equivalents Ru_{ad} deposited, and the activity of the evolving surface. That is the hydrogenation will be controlled by the rate of the hydrogenation of **1** on the surface and will therefore occur under reaction-rate-control (*vide infra*).

There are significant advantages to the use of **1** over conventional metal chlorides as the Ru precursor for the deposition of stoichiometric amounts of Ru_{ad} on Pt. First, **1** can be prepared in pure form, and it does not contain components (halide ions, phosphines, carbonyls, or other heteroatoms) that might act as catalyst poisons. Second, **1** is readily soluble in hydrocarbon solvents, and it is the only component of the hydrogenation mixture with a significant UV-vis absorbance. The amount of **1** remaining in solution as the deposition proceeds can therefore be monitored by UV-vis spectrophotometry. Third, the side products of the hydrogenation are saturated hydrocarbons that do not strongly adsorb or poison Pt surfaces. These saturated hydrocarbons can be quantified by gas chromatography (GC) analysis as the hydrogenation proceeds. Thus, the hydrogenation can be carried out and monitored using bench-top techniques.

Three conditions must be satisfied to determine the stoichiometric ratio of Ru_{ad} to Pt as the reaction proceeds. First, the initial surface number of active sites on the surface of the Pt must be known. Second, the reaction must not occur in the absence of Pt (Pt-

Ru_{ad}, or Ru). Finally, the extent of reaction must be measurable. The number of moles of Ru_{ad} deposited can be determined from measurements of either the concentration of **1** or by monitoring the concentration of the saturated hydrocarbon (C_8) products in solution as the reaction proceeds. The number of active sites on the surface of the blacked Pt gauze substrate can be determined using cyclic voltammetry in 1.0 M H_2SO_4(aq) using a standard literature method.[13] The surface stoichiometry (surface composition) at any given point during the hydrogenation of **1** (θ_{Ru}, eq Ru_{ad}) is then the ratio of the number of moles of Ru_{ad} deposited (n_{Ruad}, mol) to the moles of Pt surface ($n_{Ptsurface}$, mol) (eq. 2.2).

$$\theta_{Ru} = \frac{n_{Ruad}}{n_{Ptsurface}} \qquad \text{(eq. 2.2)}$$

In order for the hydrogenation of **1** to produce uniform coverages of Ru_{ad} on Pt substrates (i.e., a narrow distribution of surface compositions among bimetallic particles), the amount of Ru_{ad} deposited must depend on the rate of reaction of **1** at the surface (reaction-rate-control) and not on the rate of diffusion (mass-transport-control) of **1** or H_2(g) to the active sites on the surface. The Pt substrate chosen for the initial studies was a blacked Pt gauze. This use of a rough surface with a high real surface area (number of surface atoms) satisfied two requirements. First, the high real surface area ensures that enough reaction is occurring at low coverages of Pt by Ru_{ad} to allow monitoring by UV-Vis ([**1**]) or by GC ([C_8 products]). There are not enough active surface sites on smooth Pt to monitor the changes in [**1**] or [C_8 products]. Second, use of blacked Pt gauzes eliminated the additional steps of electrode fabrication, the Pt-Ru_{ad} gauzes can be used directly as electrodes.

The deposition of Ru atoms onto the surface is not expected to alter the real surface area of the Pt-Ru_{ad} because Pt and Ru atoms are about the same size (i.e., the metallic radii of Pt and Ru are 139 and 134 pm, respectively).[14] The possibility of surface restructuring was minimized by carrying out Ru_{ad} deposition reactions at low temperatures (i.e., -10°C). This work will determine if by measuring the number of active sites on the blacked Pt gauze before the deposition (*vide infra*) and by monitoring

the extent of hydrogenation of **1** *in situ*, it will be possible to control the surface composition of rough Pt-Ru_{ad}.

Several questions needed to be addressed about this model system before extending it to the preparation of nanoscale electrocatalysts and their application in the anodes of DMFC's (Chapter 4). Is the hydrogenation of **1** effected by Pt or Pt-Ru_{ad} surfaces? Does **1** react with H_2 under these conditions in the absence of Pt? Does the hydrogenation of **1** result in uniformly distributed sub-monolayers of Ru_{ad} on Pt? Does the reaction occur under reaction rate limiting conditions and at a rate that is slow enough to be monitored in real-time? The results of experiments designed to answer these questions are presented here.

Results and Discussion

Electrochemical determination of the real surface area of blacked Pt gauzes. Cyclic voltammetry was used to characterize the surface of the Pt substrate. Figure 2.1 shows the cyclic voltammogram (CV) of a blacked Pt gauze. The morphology of the Pt voltammogram shown in Figure 2.1 is the typical, electrochemical fingerprint response of a clean, polycrystalline Pt surface.[15] Figure 2.1 shows the three distinct regions in the voltammogram; the hydrogen region, the double layer region, and the oxygen region. The cathodic limit is the lowest potential that can be applied to the electrode, and the anodic limit is the highest potential. These limits are determined by the onset of hydrogen or oxygen evolution reactions. During the cathodic sweep in the hydrogen region protons from the electrolyte are reduced to form surface adsorbed hydrogen (H_{ads}). The lower limit is the onset of the hydrogen evolution reaction (HER) at ~ 0 V *vs.* the standard hydrogen electrode (SHE) to ensure maximum saturation of the Pt surface with H_{ads}. During the anodic (positive going) sweep, a portion of the excess H_2(g) formed during the HER and the saturated H_{ads} layer are oxidized to protons. As the potential increases the potential passes through the so-called double layer region between 0.4 and 0.7 V. There are no surface chemical reactions occurring within the in the double layer region. The

charge passed in this region is a result of capacitance charging associated with the formation of adsorbed anions and cations. The oxidation of H_2O begins at ~0.8 V and the so called oxygen region continues until the onset of the oxygen evolution reaction (ORR) at ~ 1.4 V.

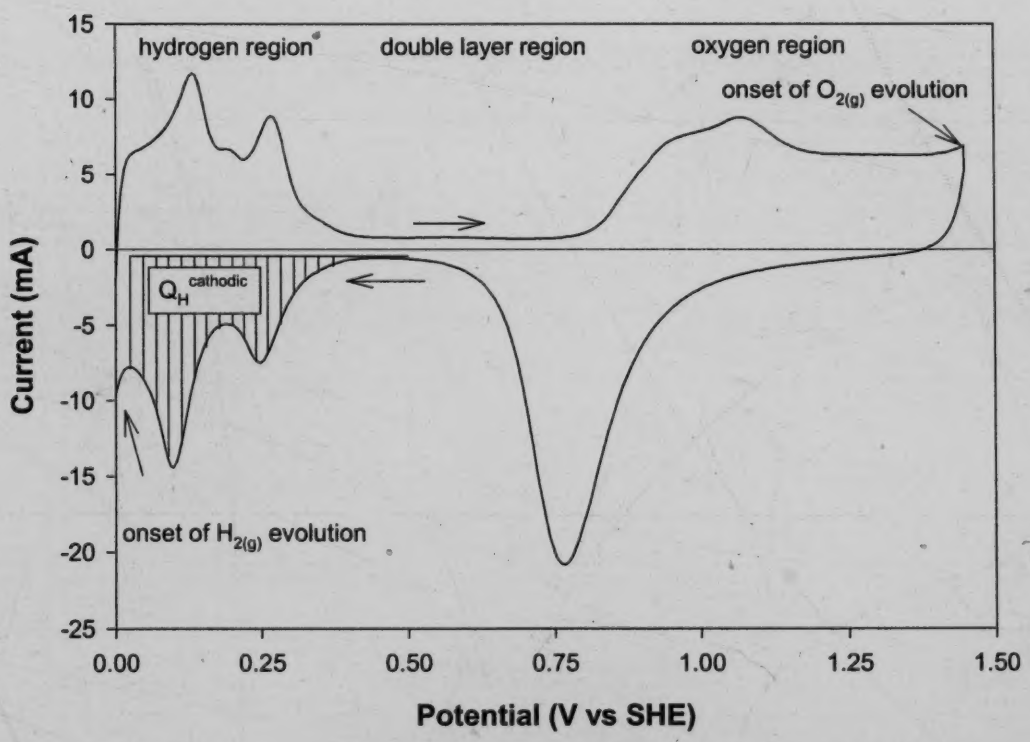

Figure 2.1. A cyclic voltammogram of a blacked Pt gauze electrode at 25 °C in 1.0 M H_2SO_4(aq). The potential was swept in the directions indicated by the arrows at 10 mV/s.

The multiple peaks in the hydrogen region are attributed to the formation of strongly and weakly bound H_{ads} on the individual crystal faces of the polycrystalline Pt surface.[15] The charge passed during the cathodic sweep through the hydrogen region ($Q_{H,cathodic}$, C), is shown as the shaded region in Figure 2.1. The cathodic hydrogen charge is related to the real surface area by eq. 2.3.

$$A_{real}(cm^2) = \frac{Q_{H,cathodic}}{f_s Q_{ap}} \qquad \text{(eq. 2.3)}$$

The cathodic hydride charge overlaps with the hydrogen evolution charge. The measured charge (shaded region of Figure 2.1) must be corrected to account for this overlap. The measured charge is therefore divided by a correction factor that accounts for the charge passed by the onset of the HER. This factor also accounts for the incomplete saturation of the surface with H_{ads}.[13] The accepted value for this correction factor (f_s) is 0.77.[15] The determination of surface area is based on the assumption that each Pt surface atom adsorbs 1 H atom. The surface area of the substrate can be translated into the number of surface Pt atoms (μmol $Pt_{surface}$) using a value of 1.31×10^{15} atoms/cm^2 as the average atomic packing density for a polycrystalline Pt surface.[15] The accepted value for the charge density of polycrystalline Pt surfaces (Q_{ap}) is equal to 210 μC/cm^2.[15] The number of active sites on the blacked Pt gauzes can therefore in this way be measured using benchtop electrochemistry. The surfaces were protected as oxides and kept under pure H_2O for transfers between the electrochemical cells and the vessels used for the hydrogenations of **1** as outlined below.

Preparation of (COD)Ru(π-allyl)$_2$ and Pt substrate. Heterogeneous reactions involving Pt surfaces are sensitive to poisoning and are thereby difficult to reproduce. The presence of trace amounts of strongly adsorbing ligands can poison Pt surfaces. Conditions that avoid the surface poisoning had to be developed for this work. Procedures were devised for the reproducible preparation of the blacked Pt gauze substrates with known real surface areas, for the hydrogenation of **1**, for termination of the hydrogenation, and for the electrochemical characterization of blacked Pt-Ru_{ad} gauzes. The focus was to eliminate contamination of the Pt and Pt-Ru_{ad} surfaces before, during, and after the hydrogenations of **1**. The procedures developed for this reaction are therefore discussed in detail.

The Ru precursor (**1**) was prepared according to a literature procedure.[16] The stability of **1** is reasonable in the absence of O_2(g) when stored at low temperature.

Regardless, it was found that sublimation of **1** immediately prior to use in every reaction was required to ensure reproducibility. The hexane solvent was purified as described in the experimental section. The real surface area of the blacked Pt gauze was determined from the charge passed in the cathodic hydrogen region of cyclic voltammograms recorded in 1.0 M H_2SO_4(aq) as described above.[13] The real surface areas of the blacked Pt gauzes varied from 1600 to 4600 cm^2 (depending on the gauze) corresponding to between 2.5 and 10 μmol Pt surface atoms.

Figure 2.2 illustrates the procedure used to transfer the gauze from the aqueous acid electrolyte to the vessel in which the hydrogenation was carried out without contaminating the surface. First, the surface of the gauze was protected as oxides by

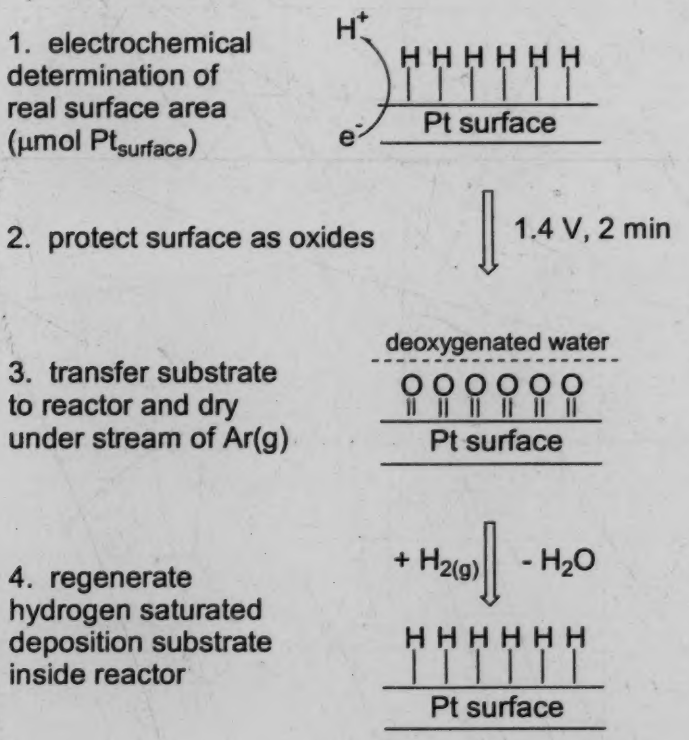
1. electrochemical determination of real surface area (μmol Pt$_{surface}$)
H$^+$
H H H H H H
e$^-$
Pt surface
2. protect surface as oxides
1.4 V, 2 min
deoxygenated water
3. transfer substrate to reactor and dry under stream of Ar(g)
O O O O O O
Pt surface
+ H$_{2(g)}$
- H$_2$O
4. regenerate hydrogen saturated deposition substrate inside reactor
H H H H H H
Pt surface

Figure 2.2. Preparation of a Pt surface for Ru deposition.

holding the potential at 1.4 V vs. SHE for 2 min. Second, the gauze was lifted above the electrolyte and rinsed with purified H_2O under Ar(g). Third, while protected by drops of purified water, the gauze was quickly transferred through air to the hydrogenation vessel. It was found that the Pt surfaces coated with oxides and protected by purified water minimized exposure to atmospheric contaminants. The use of purified H_2O to protect Pt surfaces during transfers in air is an established technique often used in electrochemistry with Pt electrodes.[17] Fourth, the gauze was dried under a stream of Ar(g) and then placed under an atmosphere of H_2(g) The H_2(g) quickly reduces the Pt surface oxides and the H_2O produced was removed by flushing H_2(g) through the reaction vessel for several minutes.

Hydrogenation of (COD)Ru(π-allyl)$_2$. To begin a hydrogenation, a solution of **1** and an internal standard (n-decane) in hexanes was quantitatively transferred to the pre-cooled reactor containing the hydrogen saturated Pt substrate, the substrate was lowered into the reaction solution and the stirring was begun. The reaction mixture was rapidly stirred, and a continuous stream of H_2(g) (~10 ml/min) was bubbled through the solution during the hydrogenation to ensure that mass transfer of H_2(g) to the surface of the gauze was not rate limiting (reaction-rate-limiting conditions rather than mass-transport-limiting conditions).[18, 19, 20] Aliquots were removed at timed intervals and the extent of reaction determined from the amount of saturated hydrocarbon products in solution as determined by GC.

To determine if significant changes in real surface area of the blacked Pt substrate occurred during the these manipulations, a control experiment was performed in which the above procedure was repeated in the absence of **1**. After being immersed in a blank hexanes solution under H_2(g) for a typical time of reaction, the Pt gauze was lifted above the hexanes under H_2(g) in the hydrogenation vessel, the hexanes were removed by cannula from the vessel, and the gauze was dried under a stream of H_2(g). The resulting dry H_{ads} saturated surface was protected under several drops of purified H_2O and then quickly transferred through air to an electrochemical cell containing deoxygenated 1.0 M H_2SO_4 under an Ar(g) atmosphere. The real surface area of the blacked Pt gauze was determined again using the electrochemical method. An insignificant change (a slight

decrease by ~ 6%) in the real surface area of the blacked Pt gauze had occurred during these manipulations, indicating that no irreversible surface rearrangement occurred during the preparation of the Pt substrate. Control experiments (monitored by GC and ^{1}H NMR Spectroscopy) showed that reaction between **1** and H_2 did not occur under these conditions in the absence of Pt. These experiments established that the deposition of Ru_{ad} on Pt is indeed a heterogeneous reaction.

The identities of the products derived from the COD ligand (C_8 products) during the hydrogenation were determined using tandem gas chromatography-mass spectrometry (GC-MS). Propane was identified using GC but not quantified. The identities and relative amounts of the saturated C_8 hydrocarbon products formed during the hydrogenation of **1** depended on the reaction temperature. In all cases cyclooctane was the major C_8 product, cyclooctadiene was not detected in the solution during any of the hydrogenations. The identities of the C_8 products and their relative distributions at 20 and -10 °C are compiled in Table 2.1. At 20 °C cyclooctane (COA), cis-

Table 2.1. The effects of reaction temperature on C_8 product distribution.

Product Identity	Product Distribution	
	20 °C	-10 °C
cyclooctane	89 %	95 %
cis-bicyclo[3.3.0]octane	8 %	5 %
n-octane 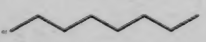	3 %	not detected

bicyclo[3.3.0]octane, and n-octane are produced. At -10 °C, COA and cis-bicyclo[3.3.0]octane are the only C_8 products. The distribution of C_8 products did not change within experimental error over the course of the hydrogenation. The absence of n-octane at - 10 °C indicated that its formation proceeded via a higher energy pathway than hydrogenation of **1**, perhaps by olefin metathesis to form surface alkylidenes.

Figure 2.3 shows plots of the number of surface equivalents of C_8 products vs. time for hydrogenations of **1** carried out at 20 °C and -10 °C. The number of surface

equivalents of C_8 products is relative to the initial number of Pt surface atoms (measured by cyclic voltammetry). At 20 °C, consumption of **1** is too rapid, based on GC analysis, to allow termination at submonolayer coverages of Pt by Ru_{ad}. The rate of the hydrogenation of **1** at -10 °C varies as the reaction proceeds. There was a kinetic burst during the initial stages of the hydrogenations carried out at -10 °C that ended after deposition of 0.2 to 0.5 eq of Ru_{ad}. The size of the burst varied among Pt samples. The rate of hydrogenation slowed after the burst, and then increased as more Ru was deposited on Pt to reach a maximum, constant rate after formation of 1.5 to 1.8 surface equivalents of C_8 products. This rate remained constant until **1** was depleted from solution.

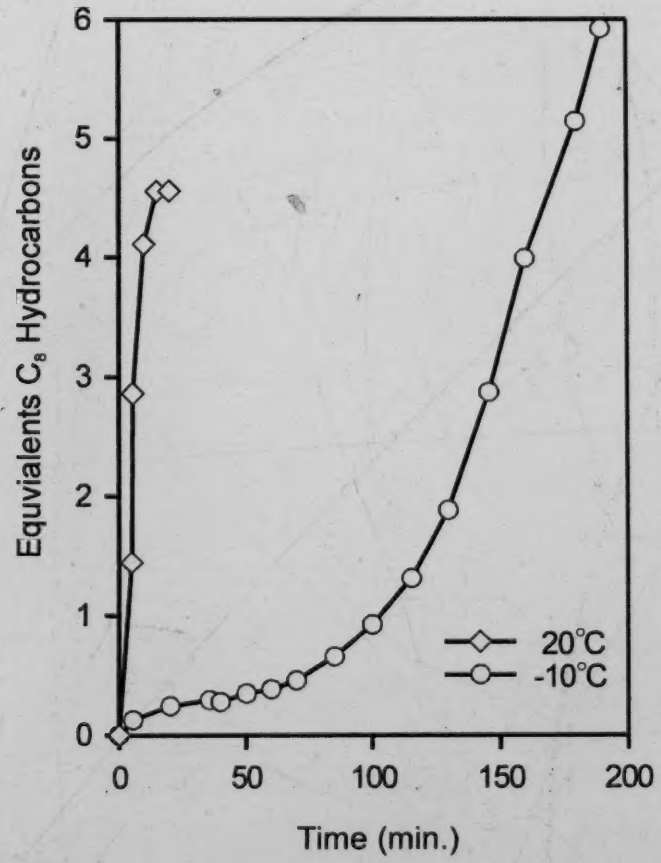

Figure 2.3. Number of equivalents C_8 hydrocarbons formed during hydrogenations of **1** *vs.* time for reactions carried out at 20 and -10 °C.

Figure 2.4 shows a plot of the amount of **1** remaining (determined by UV-Vis spectrophotometry) and the amount of C_8 hydrocarbons formed (GC) in solution during the deposition of between 0 and ~1.8 eq **1** at -10 °C. The rates of consumption of **1** and of formation of C_8 hydrocarbons were the same within experimental certainty at all stages of the hydrogenation. Since there was no observable time lag between consumption of **1**

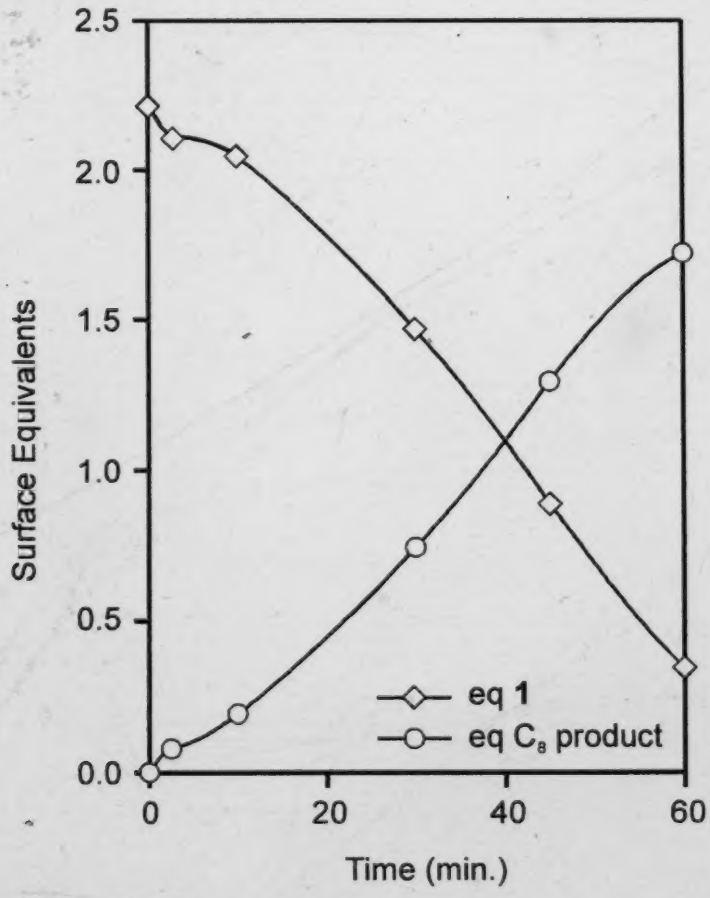

Figure 2.4. Number of equivalents of **1** consumed and total number of equivalents C_8 hydrocarbon products produced in solution *vs.* time for a hydrogenation of **1** carried out at -10 °C.

and the formation of C_8 hydrocarbons in solution the lifetimes of the surface bound hydrocarbons must be short on the time scale of the hydrogenation. The number of eq Ru_{ad} can therefore be determined from the total amount of C_8 product hydrocarbons in solution. It is therefore possible to observe in real-time the amount of Ru_{ad} deposited on the Pt surface by monitoring either the concentration of **1** or the total concentration of C_8 hydrocarbon products in solution.

As the lifetimes of the surface hydrocarbyls appears to be short on the time scale of the hydrogenation, the curves in Figures 2.3 and 2.4 show the actual evolution of the surface's activity toward hydrogenation of **1** as the coverage of Pt by Ru_{ad} increased. Kinetic bursts similar to those observed during low-temperature hydrogenations of **1** (Figures 2.3 and 2.4) were also observed by Whitesides *et al.* during low-temperature hydrogenations of $(COD)Pt(CH_3)_2$ over Pt black carried out under reaction rate limiting conditions.[18] It is reasonable to consider the bursts during hydrogenation of **1** to be a result of a proportion of the active sites on Pt being substantially more active than the others, and that these highly active sites reacted quickly during the initial stages of the hydrogenation. An alternative interpretation is that the initial burst was caused by the surface being saturated with H_{ads} at the beginning of the hydrogenation, and that the decrease in rate after the burst resulted from limitations in mass transport of $H_2(g)$ to the surface. I do not believe that mass transport of $H_2(g)$ limited the rate of hydrogenation after the initial burst because the rate of reaction increased as more Ru was deposited on Pt. The increase in rate after the burst indicated that Ru was more active than Pt and Pt-Ru_{ad} toward hydrogenation of **1**. It appears that the rate increased until all the active sites on Pt were covered by Ru_{ad}. To investigate this possibility several hydrogenations were interrupted after the maximum, constant rate was achieved and the resulting surfaces were analyzed using cyclic voltammetry.

Electrochemical characterization of the Pt-Ru_{ad} Surfaces. The hydrogenations were terminated after the desired amount of Ru_{ad} was deposited on Pt by quickly raising the gauze above the reaction mixture, rinsing the gauze in the reactor with cooled (-10 °C) $H_2(g)$ saturated hexanes, removing the hexane solution from the reactor, and drying the gauze under a stream of $H_2(g)$. The reactor was transferred to a glovebox, and the

gauze, protected by surface hydrides, was transferred through the atmosphere of Ar(g) in the glovebox to an electrochemical cell. The electrochemical cell was removed from the glovebox and placed under the Ar(g) atmosphere of a Schlenk line. 1.0 M H_2SO_4(aq) was transferred to the cell while the gauze was held above the level of the solution. The potential of the gauze was set to 50 mV concurrent with immersion of the gauze into the electrolyte. The controlled potential immersion preserved the reduced surface of the blacked Pt gauze electrode and prevented the adsorption of disadvantageous impurities from the electrolyte that might occur under open circuit conditions.

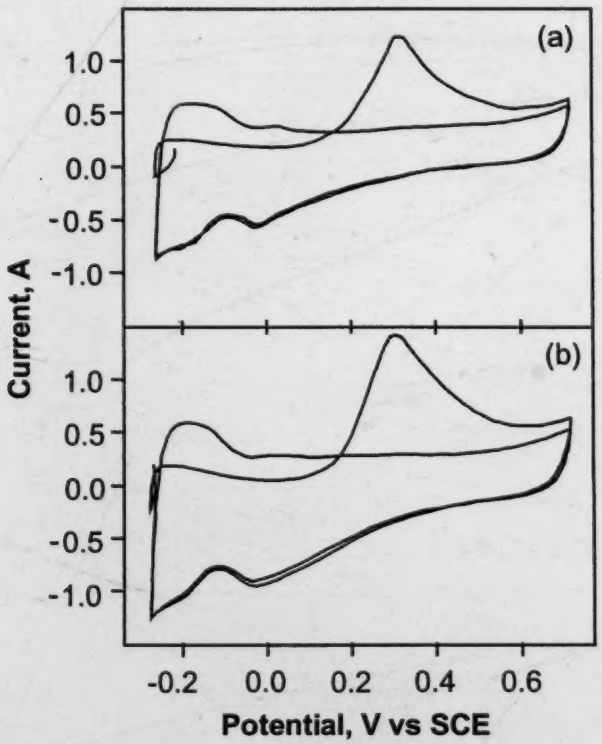

Figure 2.5. (a) Cyclic voltammograms (sweep rate 5 mV/s in 1.0 M H_2SO_4(aq)) of a surface resulting from the deposition of 2.7 eq Ru_{ad}, recorded before and after saturation of the surface with CO_{ads} at 50 mV. (b) Cyclic voltammograms of a blacked Ru electrode recorded under conditions identical with those in (a). (The voltammograms in (a) and (b) are not normalized for surface area.)

A surface resulting from hydrogenation of 2.7 eq of **1** was characterized by CO stripping voltammetry. The electrode was held at 50 mV and CO was bubbled through the electrolyte for 30 min in order to saturate the surface with adsorbed CO (CO_{ads}) and the solution was purged with Ar(g) to eliminate CO from the electrolyte. The potential was swept between the adsorption potential (50 mV), the cathodic limit (0 V) and the anodic potential limit (0.90 V) before and after the saturation of the surface by adsorbed carbon monoxide (CO_{ads}). A similar procedure has been used by others to characterize Pt-Ru surfaces prepared by electrodeposition of Ru and by thermal alloying of the pure metal components.[21, 22] The voltammograms were compared to those of a control blacked Ru surface prepared by electrodeposition of a large excess Ru (~15 eq Ru_{ad}) on a blacked Pt gauze. The resulting voltammograms are shown in Figure 2.5.

The voltammograms of the control blacked Ru surface and the surface resulting from hydrogenation of 2.7 eq of **1** have identical morphologies. The shape of the voltammograms during and after CO_{ads} removal are the same. The position of the CO_{ads} stripping peaks are the same. These results indicate that complete coverage of the blacked Pt gauze by Ru_{ad} occurred.

It is known that a pure Ru surface is not active towards the electrooxidation of CH_3OH at 25 °C.[23, 24] To confirm that the hydrogenation of **1** produces uniform films of Ru_{ad} on Pt, a voltammogram of a surface resulting from hydrogenation of 3.5 eq of **1** was recorded in H_2SO_4(aq) containing CH_3OH. Figure 2.6 shows the resulting voltammograms. Neither was there adsorption of CH_3OH, nor were there appreciable oxidation currents below 0.46 V. This behavior is identical to that observed by Gasteiger *et al.* using a pure Ru surface.[24]

The nearly identical electrochemical responses of the control blacked Ru surface and of the surfaces resulting from hydrogenation of 2.7 and 3.5 eq **1** indicated that the coverage of Pt by Ru_{ad} was essentially complete after adsorption of 1.5 to 1.8 eq Ru_{ad} on the surface of Pt. The observation of constant activity of the surface toward hydrogenation of **1** is an indicator of complete coverage of the Pt substrate by Ru_{ad}. That slightly more than 1 eq Ru_{ad} was required to cover the active sites on Pt was likely due to a combination of factors. These factors include uncertainties in the measured real surface

area of the blacked Pt gauze, hydrogenation occurring on the adsorbed Ru as well as on Pt, the mobility of the Ru atoms on the surface, and the relative affinities of Ru adatoms for Ru and for Pt. The formation of apparently conformal films of Ru_{ad} on a blacked Pt substrate indicates that the reaction is occurring under reaction rate limiting conditions, that is layer by layer growth of the Ru_{ad} film is occurring and that tower formation of Ru_{ad} at submonolayer coverages is not likely. The resulting surfaces are expected to have a reasonably uniform distribution of Ru_{ad} at submonolayer coverages.

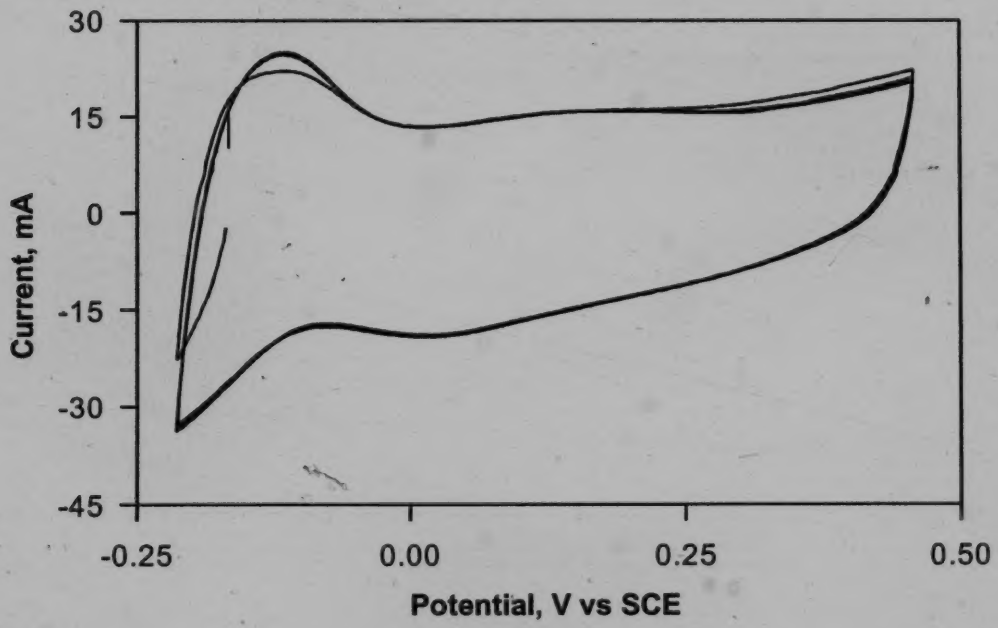

Figure 2.6. Cyclic voltammograms (sweep rate 5 mV/s, $[H_2SO_4] = [CH_3OH] = 0.50$ M, 25 °C) of a catalyst surface generated by the deposition of 3.5 eq Ru_{ad}.

The surface area of the blacked Pt gauze after deposition of 2.7 eq Ru_{ad} was estimated using the charge associated with oxidation of a monolayer of CO_{ads}. The measured surface area was 67% that of the black Pt before hydrogenation of **1**. Oxidation of CO can only be used to approximate the surface area of Ru.[25, 26] These results indicate that no major changes in the number of active surface sites (real surface area) occurred during hydrogenation of **1**. The number of surface equivalents of C_8 products (Figures

2.3 and 2.4) is therefore a measure of the surface stoichiometry of the Pt-Ru_{ad} surfaces resulting from the hydrogenation of **1**. The observation that uniform deposition of Ru_{ad} occurs during the reaction implies that the surface stoichiometry is a reasonable measure of surface composition as defined by eq. 2.2.

Composition of the Ru_{ad} deposit. The amount of Ru_{ad} deposited on Pt after several hydrogenations was determined by anodic stripping of Ru_{ad} from the resulting surfaces. Anodic stripping was carried out in 1.0 M NaOH(aq) at room temperature using a 9 V battery as power source.[27] UV-vis spectroscopy showed that Ru in the resulting electrolyte was mainly in the form of sodium ruthenate. The amount of Ru in solution was determined by inductively coupled plasma spectrophotometry (ICP) and was found to equal the total of cyclooctane, cis-bicyclo[3.3.0]octane, and n-octane in the hydrogenation mixture as determined by GC. These results, taken together with the results of the GC-UV-vis studies shown in Figure 2.4 indicate that little, if any, carbon from COD was trapped by the Ru_{ad} deposit. The chemical composition of the Ru_{ad} deposit was further investigated by hydrogenating ~ 24 eq of **1** over Pt_{black} powder with a specific surface area of 28 m^2/g. The expected molar ratio of Ru to Pt in the resulting powder and the experimental value, according to neutron activation analysis, were the same.

Conclusions

The hydrogenation of **1** in hexanes by hydrogen is effected by Pt surfaces. The hydrogenation results in the adsorption of Ru adatoms onto the surface of Pt (eq. 2.1). Hydrogenation of **1** using $H_2(g)$ on a Pt substrate at -10 °C is the lowest energy processes available for deposition of controlled stoichiometric quantities of Ru adatoms on the surface of a Pt substrate. It appears to allow for the first time generation of a prototypic kinetic bimetallic surface with real time control over the stoichiometry and activity of the evolving surface. This system offers certain advantages over conventional methods of deposition of metal adatoms (e.g., metal atom evaporation, chemical vapor deposition, surface organometallic chemistry, and spontaneous electrochemical deposition), namely,

providing uniform coverage over all exposed sides of a rough, blacked metal surface after adsorption of less than 2 eq Ru_{ad}, allowing for deposition of sub-monolayer amounts of adatoms under reaction-rate control at low temperatures, allowing for use of simple, bench-top equipment and techniques, and use of a Ru precursor (**1**) containing no components that may poison the resulting catalyst surface. Since this deposition proceeded via a reaction with a metal surface, it will in principle allow for self-directed depositions on Pt clusters dispersed on an inert support.

The results presented here indicate that the hydrogenation of **1** can be used to control the surface composition of blacked Pt-Ru_{ad} electrodes. A series of electrodes prepared according to the method described here will be used to evaluate the intrinsic activity of Pt-Ru_{ad} surfaces as a function of their surface composition. These studies and a determination of the optimum surface composition of Pt-Ru_{ad} electrocatalysts for the oxidation of CH_3OH will be discussed in the following chapters.

Experimental Section

General Procedures. Ar(g) (Linde, prepurified) was passed through molecular sieves (Anachemia, activated type 4 Å) prior to use. H_2(g) (Linde, prepurified) and CO(g) (Matheson, ultrahigh purity) were used as received. H_2O was deionized, distilled from alkaline permanganate under N_2(g), and purged with Ar(g) for 30 min prior to use. Hexanes (BDH, HPLC grade) were stirred over concentrated H_2SO_4 for 24 h, passed through Al_2O_3 (grade 1), hydrogenated ($P(H_2) \sim 1$ atm) over Pt_{black} for 24 h, and distilled under Ar(g). Heptane and decane were purified similarly. CH_3OH (BDH, HPLC grade) was distilled from $Mg(OCH_3)_2$ under Ar(g). $(C_2H_5)_2O$ (Calendon) was distilled from K/benzophenone under Ar(g). Cyclohexane-d^{12} was flash distilled from K/benzophenone under Ar(g) and degassed by three freeze-pump-thaw cycles. H_2SO_4 (ACS grade, BDH) was used as received. Rubber septa were extracted for 24 h with HPLC grade hexane in a Soxhlet extractor, and dried under vacuum. All glassware was rinsed with a 1:5 mixture of 30% H_2O_2 in concentrated H_2SO_4, H_2O, a 5% mixture of NH_4OH in C_2H_5OH, and C_2H_5OH then dried in an oven at 100 °C. The reactor used for the hydrogenations was a

2.3 × 10.3 cm Pyrex tube containing a 4 × 14 mm Teflon® coated magnetic stir bar and fitted with a rubber septum pierced with a disposable pipet (used as a H_2(g) inlet) and a glass tube supporting the blacked Pt gauze. The Ru containing precursor ((COD)Ru(π-allyl)$_2$, (**1**)) was prepared by a literature method,[16] then purified by vacuum sublimation. Small portions of **1** were then re-sublimed under vacuum immediately prior to use.

Electrochemical experiments were performed using a Pine Bipotentiostat Model AFCBP1 controlled with Pinechem 2.00 software or using a home built potentiostat equipped with a Hewlett-Packard 7004 chart recorder. Inductively coupled plasma spectroscopy (ICP) was performed using a Perkin-Elmer Optima equipped with an atomic emission detector. Gas chromatography-mass spectrometry (GC-MS) was performed using a VG-7070E with a Varian 6000 GC fitted with a 30 m J&B DB5 column using a MSS data system. Gas chromatography (GC) was performed on a Hewlett-Packard series 530 m × 10 m methyl silicone column, model no. 19057-121, fitted to a Hewlett-Packard 5980A gas chromatograph with a Hewlett-Packard 3392A integrator. ^{1}H NMR spectra were measured on a Bruker AM-400 NMR spectrometer operating at 400.13 MHz.

Electrolytes were purged with Ar(g) for at least 10 min prior to use, and electrochemical experiments were performed under Ar(g) unless stated otherwise. The reference electrode was an anodized silver wire behind a D-porosity glass frit, but potentials are referred to a standard hydrogen electrode (SHE). The counter electrode was a blacked platinum wire behind a D-porosity glass frit.

Blacked Platinum gauze. Platinum gauze (52 mesh, 99.9%, 25 × 25 mm, Aldrich) was threaded with platinum wire (~200 mm in length, 0.127 mm in diameter, 99.9%, Aldrich) and supported by flame sealing the wire leads through 3 mm uranium glass tubing. The gauze was blacked and its surface area determined from the coulometric charge of the hydrogen adsorption region in cyclic voltammograms recorded in 1.0 M H_2SO_4 according to literature procedures.[13] The blacked platinum was then held at 1.4 V for 2 min, rinsed with four 2 mL portions of purified H_2O under Ar(g), and quickly transferred wet through air to the hydrogenation reactor. The blacked platinum gauze was dried with a stream of argon for 3 h, and exposed to a stream of H_2(g) for a further 1 h to reduce the surface oxides and to remove the resulting H_2O.

Hydrogenation of (COD)Ru(π-allyl)$_2$ *over Blacked Platinum gauzes.* Hexanes (15 mL, saturated with H_2(g)) were transferred via cannula to the reactor containing the H_{ads} saturated blacked platinum, and the reactor was immersed into the cooling bath. The blacked Pt was kept above the hexanes until the hydrogenation was begun. A slow stream (~10 mL/min) of H_2(g) was passed through the solution throughout the reaction. Freshly sublimed **1** (10-12 mg) was weighed into a small vial in a drybox, and the vial was capped with a rubber septum. A weighed amount of decane was added to the vial containing **1** using a 5 μL syringe to act as an internal standard for GC analysis. The contents of the vial were dissolved in hexanes and then quantitatively transferred to the reactor with a cannula and with several rinses with hexanes, and the volume of solution in the reactor was brought up to 20 mL. The stir rate was set at 800 rpm (using a calibrated strobe light), the Pt was immersed into the reaction mixture, and timed aliquots (100-300 μL) were cannulated from the reaction mixture. The aliquots were analyzed using GC and UV spectrophotometry. To interrupt the hydrogenation at a desired coverage, the Pt was raised above the solution, and the solution was cannulated out of the reactor. The catalyst surface and the reactor walls were rinsed with four 5 mL portions of hexanes, and the catalyst was dried under a stream of H_2(g) for 30 min.

Control Experiments. The entire hydrogenation procedure was repeated in the absence of **1**. The surface area of the Pt as determined using cyclic voltammetry had decreased by 6% during the course of the procedure. In a separate experiment, H_2(g) ($P(H_2)$ ~1 atm) was bubbled through a hexane (40 mL) solution of **1** (25 mg) for 30 min at room temperature in the absence of Pt. Analysis of the solution by GC showed no reaction occurred. This experiment was repeated in cyclohexane-d^{12} at a higher concentration (39.6 mg of **1** in 2.5 mL of solvent). Analysis by ^{1}H NMR spectroscopy also showed that no reaction occurred after 30 min.

Hydrogenation of (COD)Ru(π-allyl)$_2$ *over* Pt_{black}. In air, Pt_{black} (10-11 mg, Johnson Matthey, fuel cell grade) was weighed into a 3 dram, 21 × 50 mm vial containing a 4 × 14 mm Teflon-coated magnetic stir bar and capped with a rubber septum pierced with two steel needles used as a gas inlet and outlet. The reactor was flushed with argon for 10 min and then placed under an atmosphere of hydrogen gas. Hexanes (~3 mL) were

added via cannula to a 3 dram vial that was capped with a rubber septum and that contained freshly sublimed **1** (42-48 mg, weighed in a drybox). The solution of **1** in hexanes was flushed with a stream of H_2(g) ($F(H_2)$ ~20 mL/min) for 2 min. Hexanes (~1 mL) were added via cannula to the reactor containing the H_2 saturated Pt_{black}, and a stream of H_2(g) ($F(H_2)$ ~20 mL/min) was passed through the hexanes for 1 min while the mixture was stirred at ~400 rpm. The solution of **1** in hexanes was transferred to the reactor with a cannula using an additional ~2 mL of hexanes for rinses. The total volume of the solution in the reactor was brought up to 6 mL. A stream of H_2(g) ($F(H_2)$ ~10 mL/min) was passed through the reaction for the duration of the reaction. After 24 h at room temperature, the solution was drained using a cannula and the contents of the reactor were rinsed with hexanes (three ~5 mL portions). The contents of the reactor were then dried at room temperature under vacuum (~0.01 Torr) for 2 h.

Neutron Activation Analysis. Samples and standards, packed in HNO_3-washed polyethylene 100 mL tubes, were individually irradiated for 300 s at a neutron flux of 1×10^{11} n /cm^2 s in an inner site of the University of Alberta SLOWPOKE II Nuclear Reactor. Following a decay period of 18 min, each sample was counted for 300 s at a sample-to-detector distance of 3 cm using a 34% hyperpure Ge detector attached to an 8k channel PC-based multichannel analyzer. Analysis was performed by the comparator method of INAA using $RuCl_3 \cdot 3H_2O$ and K_2PtCl_6 (98%) as standards. Pt was quantified using the 542.96 and 185.76 keV -ray emissions of ^{199}Pt (T1/2 = 30.8 min) produced via the reaction ^{198}Pt(n, g) ^{199}Pt while Ru was determined using the 724.27 keV -ray emission of ^{105}Ru (T1/2 = 4.44 h) produced via the thermal neutron reaction ^{104}Ru(n, g) ^{105}Ru.

Adsorption and oxidation of CO. A Pt-Ru_{ad} surface was prepared by hydrogenation of 2.7 eq of **1**. The reaction vessel containing the rinsed and dried electrode was transferred to a glovebox, and the electrode was transferred to the electrochemical cell under Ar(g). The cell was removed from the glovebox, flushed with Ar(g), and fitted with two disposable pipets (to be used as gas inlets), with a reference electrode, and with a counter electrode. An Ar(g) purged solution of H_2SO_4 (1.0 M in water) was transferred to the cell via a polyethylene cannula. The potential of the Pt-Ru_{ad}

working electrode was set to -0.19 V concurrent with immersion into the electrolyte, with stirring (700rpm) at room temperature, CO was bubbled through the solution for 30 min followed by bubbling Ar(g) through the solution for 2 min. The stirring was stopped, and the potential of the working electrode was swept at 5 mV/s up to 0.90 V and then down to 0.050 V.

A control blacked Ru electrode was prepared by potentiostatic electrodeposition of Ru on a black Pt electrode at 50 mV for 15 min from a stirred solution of $RuCl_3 \cdot 3H_2O$ (0.005 M) and H_2SO_4 (1.0 M) in water. Using the Coulombic charge passed during the deposition, we calculate that 15 eq of Ru_{ad} was deposited on the electrode surface. The electrode was rinsed with H_2SO_4 and transferred quickly in air to the electrochemical cell, and the oxidation of adsorbed CO was repeated as described above.

Anodic stripping of Ru_{ad}. Several Pt-Ru_{ad} surfaces obtained by hydrogenations of **1** were transferred in air to an electrochemical cell that contained a Teflon® coated stirbar and a 1.0 M solution of NaOH in deoxygenated water (80 mL). The black Pt counter electrode was fitted behind a D-porosity glass frit. The cathode ("+" terminal) of a 9 V battery was connected to the Pt-Ru_{ad} electrode, and the anode ("-" terminal) was connected to the counter electrode. The solution was stirred under argon for 10-30 min as the color of the solution turned orange. The solution was quantitatively transferred to a 100 mL volumetric flask and diluted to volume with 1.0 M NaOH. The amount of Ru in solution was determined using ICP analysis. UV-vis spectra of the solutions indicated that the product of the anodic stripping was sodium ruthenate. Further anodic stripping in fresh electrolyte showed that all the ruthenium was stripped from the electrode by this treatment.

References

(1) Coq, B.; Goursot, A.; Tazi, T.; Diguéras, F.; Salahub, D.R. *J. Am. Chem. Soc.* **1991**, *113*, 1485.

(2) Didillon, B.; Houtman, C.; Shay, T.; Candy, J.-P.; Basset, J.-M. *J. Am. Chem. Soc.* **1993**, *115*, 9380.

(3) Candy, J.-P; Didillon, B.; Smith, E.L.; Shay, T.B.; Basset, J.-M. *J. Mol. Catal.* **1994**, *86*, 179.

(4) Lefebvre, F.; Candy, J.-P.; Santini, C.C.; Basset, J.-M.; *Top. Catal.* **1997**, *4*, 211.

(5) Candy, J.-P.; Didillon, B.; Smith, E. L.; Shay, T.B.; Basset, J.-M.; *J. Catal.* **1998**, *179*, 459.

(6) Humbolt, F.; Didillon, D.; Lepeltier, F.; Candy, J.-P.; Corker, J.; Clause, O.; Bayard, F.; Basset, J.-M. *J. Am. Chem. Soc.* **1998**, *120*, 137.

(7) Humblot, F.; Candy, J.-P.; Le Peltier, F.; Didillon, B.; Basset, J.-M. *J. Catal.* **1998**, *179*, 459.

(8) Crabb, E. M.; Marshall, R.; Thompsett, D.; *J. Electrochem. Soc.* **2000**, *147*, 4440.

(9) Crabb, E. M.; Ravikumar M. K. *Electrochim. Acta* **2001**, *46*, 1033.

(10) Crabb, E. M.; Marshall R., *Appl. Catal. A: Gen.* **2001**, *217*, 41.

(11) Crabb, E. M.; Ravikumar, M. K.; Qian, Y.; Russell, A. E.; Maniguet, S.; Yao, J.; Thompsett, D.; Hurford, M.; Ball, S. C. *Electrochem. Sol. Stat. Lett.* **2002**, *5*, A5.

(12) Miura, H.; Taguchi, H.; Sugiyama, K.; Matsuda, T.; Gonzalez, R.D. *J. Catal.* **1990**, *124*, 194.

(13) Woods, R. *Electroanal. Chem. Interfacial. Electrochem.* **1974**, *49*, 217.

(14) *Tables of Physical and Chemical Constants*; 15th ed.; Kaye, G. W. C.; Laby, T. H., (eds.), Longman, Inc., New York, 1986.

(15) Woods, R. in *Electroanalytical Chemistry: A Series of Advances*, Bard, A.J. (ed), Marcel Dekker, Inc., New York, vol. 9, 1976.

(16) Albert, M. O.; Singleton, E.; Yates, J. E. *Inorg. Synth.* **1989**, *26*, 249.

(17) Clavilier, J.; Faure, R.; Guinet, G. Durand, R. *J. Electroanal. Chem.* **1980**, *107*, 205.

(18) Miller, T. M.; Izumi, A. N.; Shih, Y. S.; Whitesides, G. M. *J. Am. Chem. Soc.* **1988**, *110*, 3146.

(19) Miller, T. M.; McCarthy, T. J. Whitesides, G. M. *J. Am. Chem. Soc.* **1988**, *110*, 3156.

(20) Miller, T. M.; Whitesides, G. M. *J. Am. Chem. Soc.* **1988**, *110*, 3164.

(21) Gasteiger, H. A.; Markovic, N.; Ross, P. N., Jr.; Cairns, E. J. *J. Phys. Chem.* **1994**, *98*, 617.

(22) Richarz, F.; Wohlmann, B.; Vogel, U.; Hoffschulz, Wandelt, K. *Surf. Sci.* **1995**, *335*, 361.

(23) Chu, D.; Gilman, S. *J. Electrochem. Soc.* **1996**, *143*, 1685.

(24) Gasteiger, H. A.; Markovic, N.; Ross, P. N.; Cairns, E. J. *Electrochim. Acta* **1994**, *39*, 1825.

(25) Bett, J.; Kinoshita, K.; Routis, K.; Stonehart, P. *J. Catal.* **1973**, *29*, 160.

(26) Kinoshita, K.; Ross, P. N. J. Electroanal. Chem. **1977**, *78*, 313.

(27) Connick, R. E.; Hurley, R. *J. Am. Chem. Soc.* **1952**, *74*, 5012.

Chapter 3†

Self-Directing Organometallic Deposition of Ru Adatoms on Pt, Part II. Optimization of Pt-Ru_{ad} Surface Composition for the Electrooxidation of Methanol and Adsorbed Carbon Monoxide.

Introduction

In the previous chapter it was found that blacked Pt gauze surfaces effected the hydrogenation of (COD)Ru(π-allyl)$_2$ (**1**; COD is 1,5-cyclooctadiene) in hexanes (eq. 3.1). During the course of the reaction the Ru centre of **1** is deposited onto the surface of

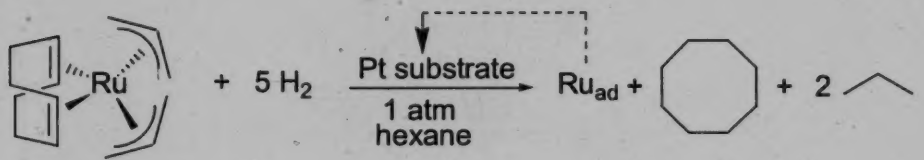

(eq. 3.1)

1

the Pt substrate. This self-directing organometallic deposition of Ru_{ad} provides a convenient method to generate bimetallic Pt-Ru_{ad} surfaces of known surface stoichiometry (surface coverage or surface composition) and number of active surface sites (real surface area). The activity of the Pt-Ru_{ad} surface evolves with the extent of the reaction (i.e., the rate of the hydrogenation of **1** depends non-linearly on the surface composition of the Pt-Ru_{ad} substrate). The hydrogenation of **1** allows for real-time monitoring of the equivalents of Ru adatoms (eq Ru_{ad}) deposited on Pt and the reaction can be terminated at the desired surface stoichiometry. The Pt-Ru_{ad} surfaces prepared by this method can be used to evaluate the intrinsic activity of bimetallic Pt-Ru_{ad} surfaces towards the electrooxidation of CO_{ads} and CH_3OH as a function of their surface

---

† Reproduced in part with permission from Lee, C.E; Bergens, S.H. *J. Phys. Chem. B* **1998**, 102, 193. Copyright 1998 American Chemical Society.

composition (θ_{Ru}, eq Ru_{ad}). The intrinsic activity referred to here is the current measured during electrooxidation CH_3OH per active surface site. Towards this end, the hydrogenation of **1** was used to prepare a series of blacked Pt-Ru_{ad} electrodes with increasing eq Ru_{ad}. The electrooxidation of CH_3OH and adsorbed monolayers of CO (CO_{ads}) by these surfaces in H_2SO_4(aq) was examined to determine the dependence of intrinsic electrocatalytic activity on surface composition. The electrooxidation of CH_3OH was studied under conditions similar to those encountered in the anodes of real direct methanol fuel cells. The systematic variation of θ_{Ru} allowed the identification of an optimum surface stoichiometry for blacked Pt-Ru_{ad} surfaces under conditions similar to those encountered in an operating DMFC.

Results and Discussion

General methods. As discussed in Chapter 2, blacked Pt gauzes were used for the investigations. The hydrogenations of **1** were monitored using gas chromatography (GC) and interrupted when the desired eq Ru_{ad} had been deposited on Pt according to the procedure described in Chapter 2. After a hydrogenation, CO_{ads} stripping voltammetry was performed (as in Chapter 2) followed by several continuous potential sweeps in 0.5 M H_2SO_4(aq) (between potential limits 0.025 and 0.70 V at 5 mV/s). This procedure served to remove as many disadvantageous surface contaminants as possible from the Pt-Ru_{ad} surfaces before performing further electrochemical experiments. The lifetimes and further poisoning of these surfaces are discussed in more detail below.

As discussed previously (Chapter 2) it appears that complete coverage of the active sites on Pt by Ru_{ad} is achieved after hydrogenation of between 1.5 and 2.0 stoichiometric surface equivalents of **1**. That between 1.5 and 2.0 eq Ru_{ad} are required to cover all sites of a blacked Pt gauze indicates that the coverage of Pt by Ru_{ad} is quite uniform. It is therefore likely that the eq Ru_{ad} is an acceptable and representative measure of θ_{Ru} at low coverages (during the early stages of the hydrogenation), when the likelihood of Ru adatoms being deposited only on Pt is statistically high. At later stages

of the hydrogenation, when deposition of Ru adatoms likely occurs on Ru_{ad} as well as on Pt, the eq Ru_{ad} is the upper limit to θ_{Ru}. Beyond this data, there is no information about the distribution of the Ru_{ad} on the Pt surface or about how this distribution changes upon exposure to different conditions and reactants. It is reasonable to conclude from the previous results (complete coverage of Pt by Ru_{ad} at ~1.5 eq Ru_{ad}) stacking of the Ru_{ad} deposit to form towers does not occur to any large extent during the hydrogenation of **1**.

Electrochemical characterization of Ru_{ad} modified blacked Pt gauzes. The cyclic voltammograms of bimetallic Pt-Ru surfaces and Pt surfaces modified by Ru deposition are known to lose resolution in the hydrogen region as the surface coverage of Pt by Ru increases. The change in the morphology of the voltammograms is a result of Ru surface oxidation and reduction processes occurring in the same potential range as the hydrogen region of a pure Pt surface. Figure 3.1 shows cyclic voltammograms of blacked Pt gauzes modified by the deposition of 0, 0.05, 0.30, 0.70, and 3.5 eq Ru_{ad} recorded in 0.5 M H_2SO_4 at 5 mV/s. The current peaks in the hydrogen region become less resolved and increasingly overlap with the enlarging double-layer region as the amount of Ru deposited increases. Quite similar behavior was observed of bulk, shiny alloys of known surface compositions by Ticanelli *et al.*[1] and by Gasteiger *et al.*[2, 3] As was discussed by these and other researchers,[4] the onset of formation of adsorbed oxides on Ru in the positive going sweeps overlaps with the electrooxidation of surface hydrides, resulting in loss of a clear distinction between these processes. It was proposed for bulk Pt-Ru alloys that the increase in the ratio of currents in the double layer to the hydrogen regions with increasing θ_{Ru} results from a progressive lowering of the potential for adsorption of surface oxygen species.[1, 2] It appears that increasing the eq Ru_{ad} adsorbed by Pt during hydrogenation of **1** also causes formation of surface oxides to occur at progressively lower potentials.

Anodic stripping voltammetry of adsorbed carbon monoxide. Numerous investigators have studied the electrooxidation of adsorbed CO (CO_{ads}) over Pt-Ru surfaces.[5] It was shown for bulk Pt-Ru alloys that the potential of the stripping peak of an adsorbed monolayer of CO_{ads} during stripping voltammetry is indicative of θ_{Ru}.[6, 7]

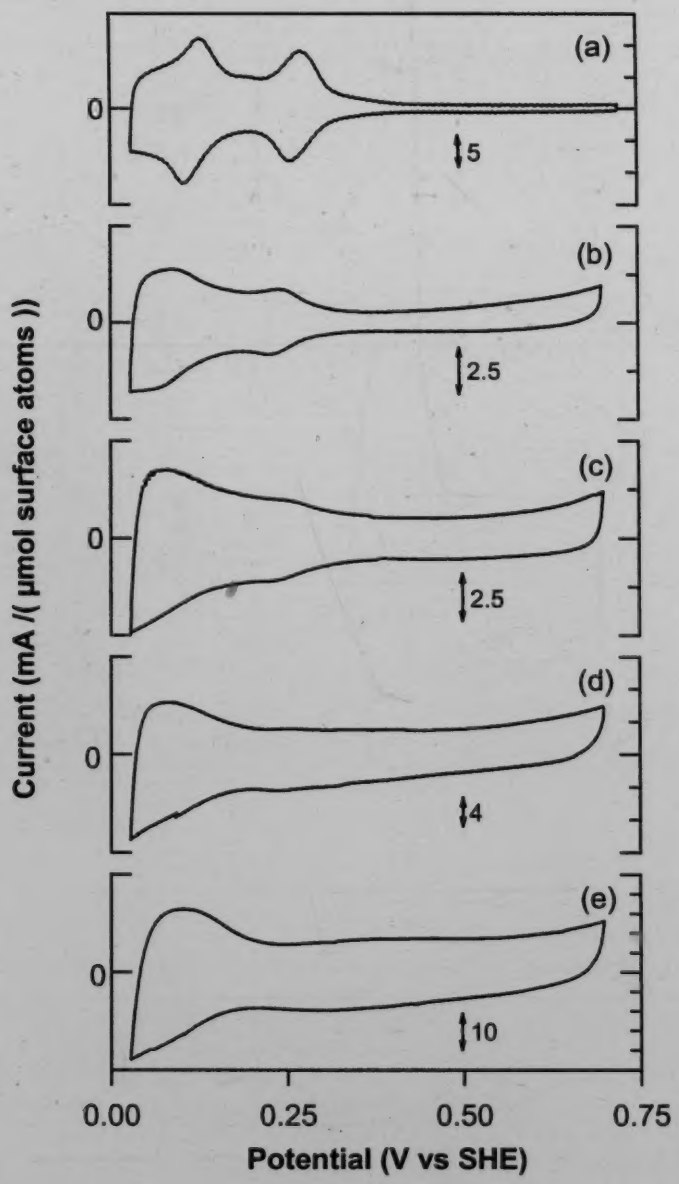

Figure 3.1. Cyclic Voltammograms of blacked Pt gauze electrodes modified by the deposition of: (a) 0, (b) 0.05, (c) 0.30, (d) 0.70, and (e) 3.5 eq Ru_{ad}. These are the stable voltammograms recorded after the electrooxidation of CO_{ads} in 0.5 M H_2SO_4 at 5 mV/s (currents are scaled to illustrate the differences in morphology of the voltammograms).

It was found that θ_{Ru} was ~50% for such surfaces with the highest activity (i.e., lowest stripping peak potential) toward oxidation of CO_{ads}. Frelink *et al.* found that a shift in the CO_{ads} stripping peak to lower potentials by 150-200 mV was caused by electrochemical deposition of small amounts of Ru adatoms (θ_{Ru} ~15%) on Pt.[8] Deposition of more Ru_{ad} did not cause significant further shifts in the CO_{ads} stripping peak potential. Watanabe *et al.* found θ_{Ru} to be ~ 50% at the maximum activity for the potentiodynamic oxidation of CO_{ads} in CO saturated 0.5 M H_2SO_4(aq).[9] The results presented in the literature are different depending on whether alloys or Ru adatom modified Pt-Ru surfaces are used. The reasons for this could be that the distribution of Ru on exposed surface of an alloy is different than on an adatom modified surface, in addition to their relative amounts, the distribution of the Ru on Pt can affect the electrocatalytic activity of these bimetallic surfaces. In addition to the bifunctional mechanism of CO_{ads} electrooxidation (Chapter 1) it is possible that additional electronic effects are observed and that these depend on the bulk composition of the electrocatalyst.

To compare the activities of Ru_{ad} modified blacked Pt gauze surfaces as a function of their surface composition towards the electrooxidation of CO_{ads}, potentiodynamic stripping of CO_{ads} was performed (the procedure used is identical to that described in Chapter 2). A representative CO_{ads} stripping voltammogram and several subsequent potential cycles recorded after the saturation of a 0.05 eq Ru_{ad} surface with CO_{ads} at 75 mV is shown in Figure 3.2. The CO stripping peak potential was 0.543 V, with evidence of a second peak at 0.630 V. The CO stripping peak potential was 0.664 V over a blacked Pt gauze, and 0.559 V over a pure Ru surface (Chapter 2). The presence of 0.05 eq Ru_{ad} on the surface of the electrode causes in decrease in the peak potential for the CO_{ads} stripping of ~120 mV. The effects of Pt-Ru_{ad} surface stoichiometry on the peak potential for CO_{ads} stripping peak potential for a series of Ru_{ad} modified Pt electrodes are summarized in Figure 3.3.

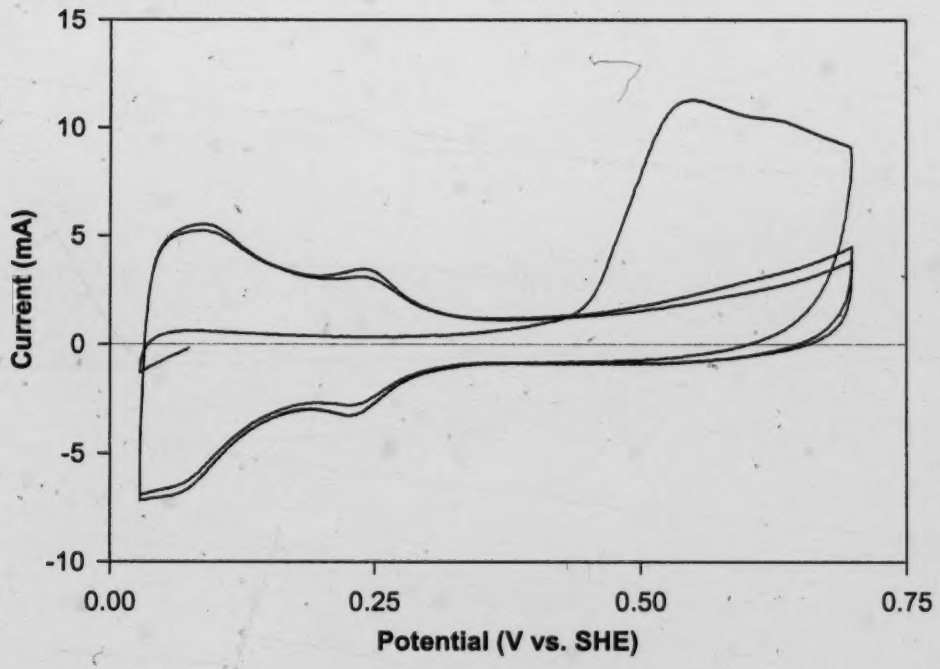

Figure 3.2. The CO stripping voltammogram of a 0.05 eq Pt-Ru_{ad} electrode at 5mV/s.

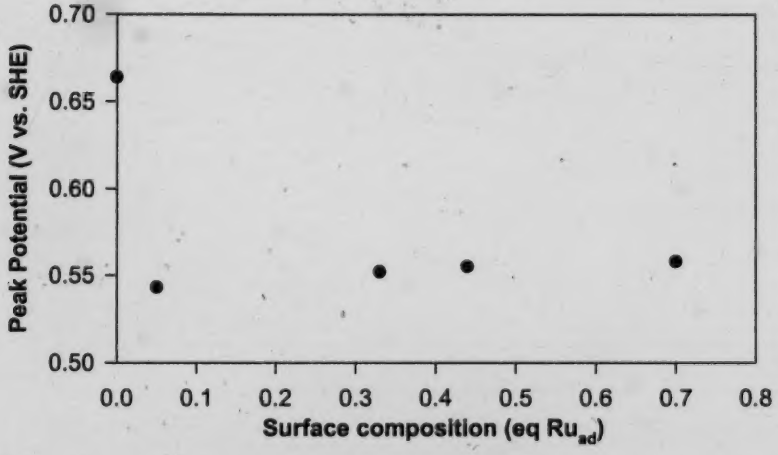

Figure 3.3. A plot of the CO_{ads} stripping peak potentials *vs.* eq Ru_{ad} for a series of Pt-Ru_{ad} electrodes under identical conditions.

In accord with the results of Frelink *et al.* deposition of more Ru_{ad} on Pt by hydrogenation of **1** did not cause significant further shifts in the CO_{ads} stripping peak potential. Our results and those of Frelink *et al.* indicate that the maximum shift in the CO_{ads} stripping peak potential between Pt and Pt-Ru_{ad} occurs at low θ_{Ru} (5 - 15%). These results differ with those from the bulk alloys for which θ_{Ru} at the maximum shift is ~ 50%. These observations allude to an intrinsic difference in reactivity between Pt-Ru_{ad} and Pt-Ru alloys toward oxidation of CO_{ads}. Gasteiger *et al.* provided evidence that the peak potential for CO_{ads} stripping from Pt-Ru alloys depended not only on θ_{Ru} but also on how the Ru atoms were distributed at the surface. They proposed, in accord with the bifunctional mechanism of CO_{ads} and CH_3OH electrooxidation, that the optimum surface composition is 0.5 for CO_{ads} oxidation and significantly lower for the electrooxidation of methanol. The differences between the homogeneous distribution of Ru and Pt surface atoms in an alloy and the heterogeneous distribution of deposited Ru atoms on the electrode surfaces is the primary cause of the divergence in activities toward adsorbed CO as the surface composition is varied. This interpretation is supported by the recent results of Friedrich *et al.* that indicate that sub-monolayers of Ru adatoms electrochemically deposited on Pt(111) exist as islands under adsorbed monolayers of CO.[10] It appears that Ru_{ad} deposited by hydrogenation of **1** on Pt also forms islands under adsorbed monolayers of CO_{ads}. If this proposal is correct, and taking into consideration that deposition of small amounts of Ru_{ad} produces quite active Pt-Ru_{ad} surfaces toward the electrooxidation of adsorbed CO_{ads}, these results imply that the surface mobility of at least one of the intermediates was high on the time scale of the electrooxidation under these conditions. The Vielstich group has examined the electrooxidation of CO_{ads} on Pt(111) modified by the deposition of Ru_{ad} islands, they concluded that the CO_{ads} is mobile on Pt and that oxidation of CO_{ads} to CO_2 occurs at Ru_{ad} islands.[11]

Attempts were made to determine the charge under the CO_{ads} stripping peak for the Pt-Ru_{ad} surfaces. Only an approximate value of the charge could be determined because the upper potential limit of the sweeps (0.70 V) was too low to oxidize all the adsorbed CO_{ads} during the first anodic sweep. The total CO_{ads} stripping charges were estimated by adding in the excess anodic charge passed during the successive positive

going sweeps until the steady potentiodynamic response was obtained. The calculations were based on a saturation coverage of 0.9 for CO_{ads} on Pt and accounted for the transfer of 2 electrons during the electrooxidation of each CO_{ads} to CO_2.[12] The real surface areas of the Pt-Ru_{ad} electrodes estimated from the electrooxidation of CO_{ads} were between 50% and 98% of the known real surface areas of the corresponding blacked Pt gauzes prior to the deposition of Ru_{ad}. It is well known that the use of the CO stripping charge is not an accurate method to determine real Pt-Ru surface areas.[13] This issue is addressed in more detail in Chapter 4. In addition, the summation of the charges over successive positive going sweeps likely added more error to its measured value. Therefore, it is reasonable to conclude that major changes in real surface area do not occur during hydrogenation of **1** over blacked Pt gauzes. Based upon this conclusion the activities of the Pt-Ru_{ad} surfaces toward the electrooxidation of CH_3OH described in the following sections are normalized to the real surface areas of the blacked Pt gauzes measured prior to the deposition of Ru_{ad}. Since small to moderate changes in real surface area cannot be ruled out, the comparisons of normalized activities presented in this work are best taken as approximate measures of the relative intrinsic activities of the Pt-Ru_{ad} surfaces as a function of their surface stoichiometry.

Potentiodynamic oxidation of CH_3OH. Figure 3.4 shows the positive going sweeps obtained with a 0.10 eq Pt-Ru_{ad} surface ($[CH_3OH] = [H_2SO_4] = 0.50$ M, 25 °C, sweep rate = 5 mV/s, sweep range = 0.025 to 0.60 V). The first anodic sweep contains a significant anodic peak at ~0.20 V. Subsequent sweeps do not contain this peak and are appreciably lower in current than the first sweep at all potentials. The peak observed during the first potential sweep in CH_3OH containing electrolyte is due to the dehydrogenation of CH_3OH and accompanying rapid H_{ads} oxidation.[14] The decreases in current after the third sweep were small, indicating the potentiodynamic response had stabilized. Quite similar behavior was observed by Gasteiger *et al.* using a shiny bulk PtRu alloy with (θ_{Ru} = 10%).[2, 3] As was discussed by Gasteiger *et al.*, in reference to results of radiotracer experiments by Horanyi *et al.*,[15] and to results of infrared measurement by Kunimatsu,[16] both the decrease in current and the loss of the hydrogen desorption peak after the first positive going sweep were likely

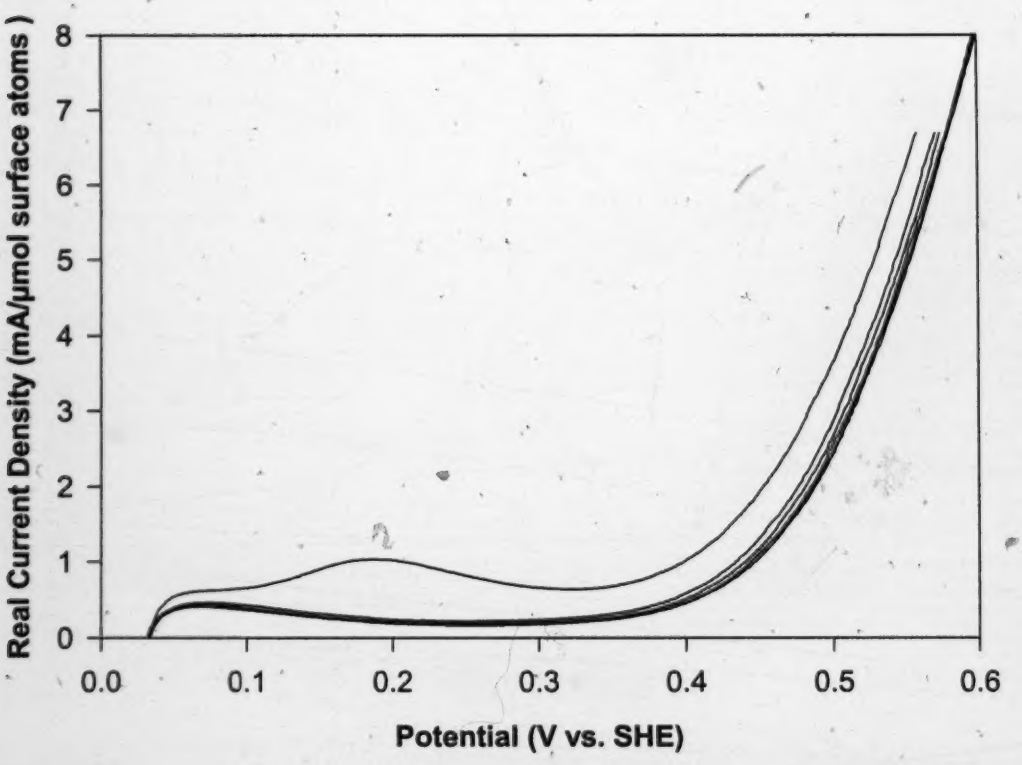

Figure 3.4. Anodic sweeps of CH_3OH electrooxidation over a 0.10 eq Ru_{ad} electrode. The curves are a composite of two experiments containing the first, second, and third sweeps from one and the fourth and fifth sweeps from the other experiment.

caused by an accumulation of surface organic residues from the electrooxidation of CH_3OH. These residues are not significantly desorbed at lower potentials. Figure 3.5 shows the third positive going sweeps (normalized for specific surface area and corrected for (pseudo) capacitive current densities) for Pt and for 0.05, 0.10, 0.30, 0.44, and 0.70 eq Pt-Ru_{ad}. Further decreases in current after the third sweep were small for these surfaces, indicating that the potentiodynamic responses shown in Figure 3.5 approximate the behavior of CH_3OH poisoned surfaces. The onset of oxidation was lower than Pt for all the Pt-Ru_{ad} surfaces. The order of activity was 0.05 > 0.10 > 0.30 ~ 0.44 > 0.70 eq Ru_{ad} > Pt over most of the potential range. The relative activity of Pt increases with potential,

becoming more active than the 0.30, 0.44, and 0.70 eq Ru_{ad} surfaces near the upper limit of the sweeps. This behavior is reminiscent of that obtained by Gasteiger *et al.* using bulk alloys under similar conditions (after 10 sweeps at 20 mV/s).[2, 3] These workers found that θ_{Ru} at maximum activity decreased as the electrode potential increased. The reported order of activity was θ_{Ru} = 33% > 7% > 44% > 0% at 0.45 V and 7% > 33% > 44%> 0% at 0.55 V. Assuming that the eq Ru_{ad} measurements are comparable to those of the θ_{Ru} determined by Gasteiger *et al.*, these results indicate that Pt-Ru_{ad} and bulk, shiny Pt-Ru alloys behave similarly toward the potentiodynamic oxidation of CH_3OH under these conditions.

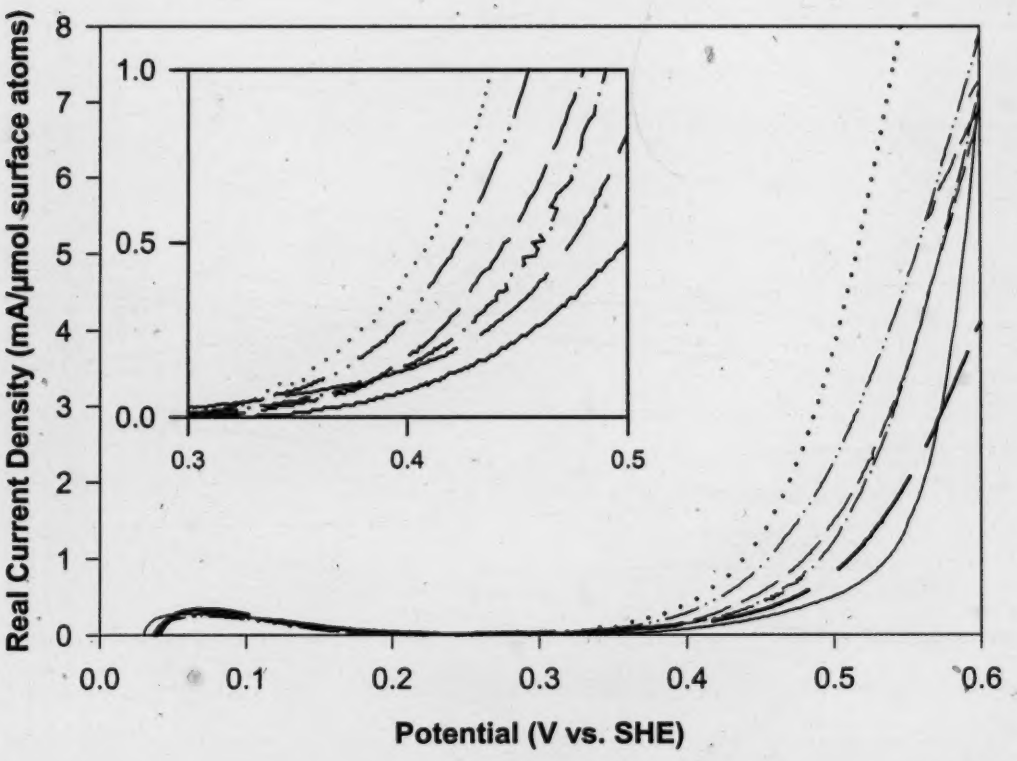

Figure 3.5. Third current-normalized anodic sweeps for the potentiodynamic oxidation of methanol over 0.0 (-),0.05 (- -), 0.10 (- ..-), 0.30 (- .-),0.44 (...), and 0.70 (- --) eq Ru_{ad}.

Potentiostatic oxidation of CH_3OH. Figure 3.6 shows plots of normalized current versus time for the potentiostatic electrooxidation of CH_3OH over Pt-Ru_{ad} surfaces ([CH_3OH] = [H_2SO_4] = 0.50 M, 25 °C, E = 0.40 V at 25 °C). The surfaces all suffered from an initial rapid decrease in current followed by a region of more stable activity, in which the current slowly decreased. This behavior was reported for bulk alloys, and it is interpreted as an initial, rapid dehydrogenation of CH_3OH followed by a slower oxidation of CO_{ads} or related species derived from CH_3OH.[17] The 0.05 eq Ru_{ad} surface was the most active, but it also suffered from the most rapid decrease in activity in the "stabilized" region (t > 2.5 min) of the current-time response. The "stabilized" region is representative of the steady-state activity of these surfaces towards the electrooxidation of CH_3OH. This curve is reproducible: the oxidation was repeated using the same electrode several days later and displayed the same behavior. The activities of two ~0.30 eq Ru_{ad} surfaces (0.30 and 0.32 eq Ru_{ad}, prepared independently) were nearly identical, demonstrating that preparation of $PtRu_{ad}$ by hydrogenation of **1** over Pt is reproducible. Figure 3.7 represents the activities as turnover frequencies (TOF) vs. eq Ru_{ad}. The turnover frequencies were calculated from the moles of CH_3OH consumed per mole of surface site from time = 17 to 25 min (a period of steady-state activity observed after the initial burst). The order of activity among the Pt-Ru_{ad} surfaces was the same as that for the CH_3OH poisoned surfaces toward the potentiodynamic electrooxidation experiments. Surfaces with low eq Ru_{ad} are the most active: the value of the TOF for the 0.10 and 0.05 eq Pt-Ru_{ad} surfaces being between 28 and 50 times that of pure Pt. Our results for the potentiostatic oxidation of methanol are reminiscent of those of Gasteiger *et al.* using bulk alloys (θ_{Ru} = 10% at maximum activity, 25 °C, 0.4 V, 0.5 M CH_3OH, 0.5 M H_2SO_4) and to those of van Veen *et al.*[18] using co-electrodeposited Ru-Pt (θ_{Ru} = 15% at maximum activity, 0.48 V, 0.1 M CH_3OH, 0.5 M H_2SO_4). These similarities indicate that bulk Pt-Ru alloys and Pt-Ru_{ad} surfaces generated by hydrogenation of **1** have similar optimum surface compositions toward CH_3OH electrooxidation under these conditions.

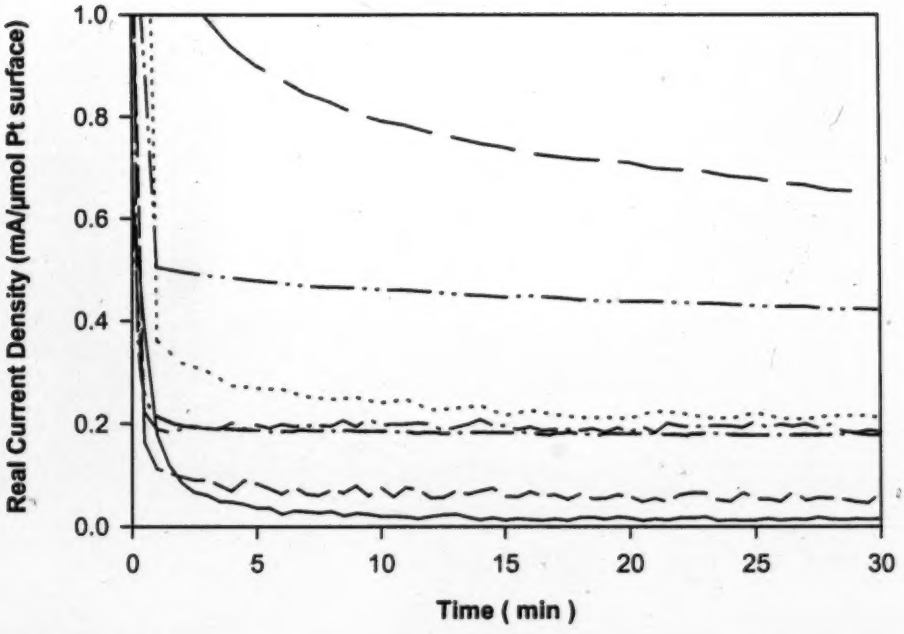

Figure 3.6. Normalized current *vs.* time for the potentiostatic oxidation of methanol over 0.0 (-),0.05 (- -),0.10 (- ..-),0.30 and 0.32 (- .-),0.44 (...), and 0.70 (- --) eq Ru_{ad} at 0.40 V.

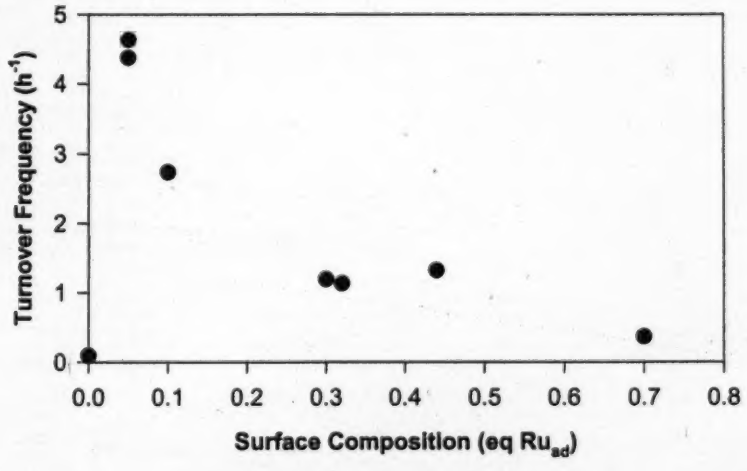

Figure 3.7. Turnover frequencies *vs.* eq Ru_{ad} for the potentiostatic oxidation of methanol over Pt-Ru_{ad} at 0.40 V.

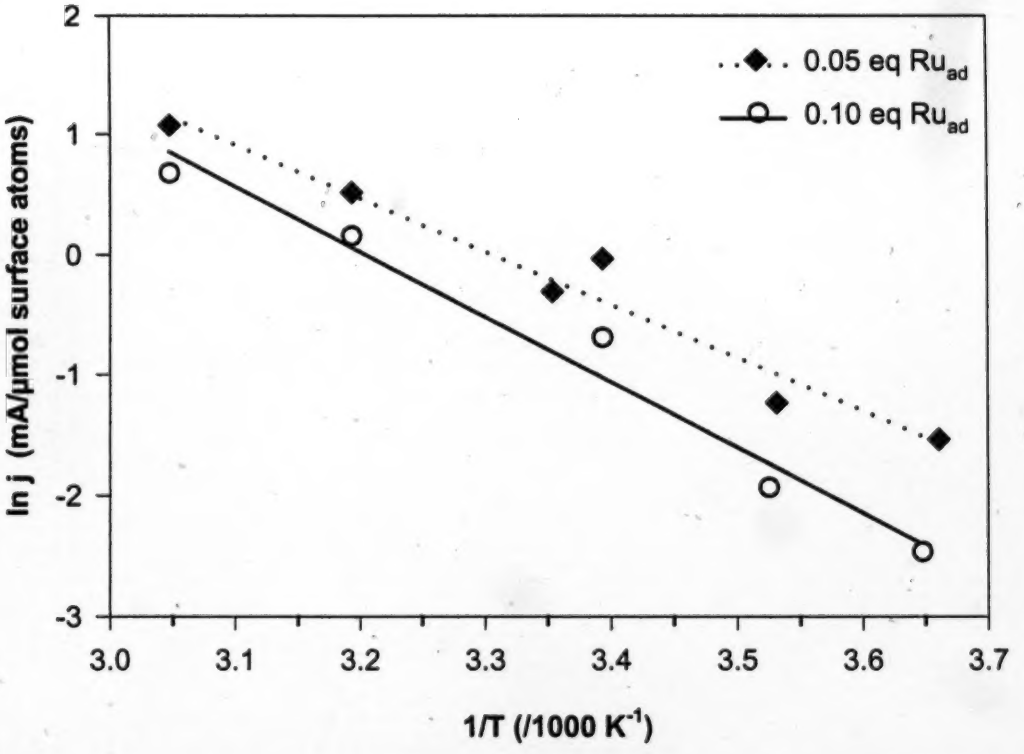

Figure 3.8. Arrhenius plots of ln(j) *vs.* T^{-1} for the potentiostatic oxidation of CH_3OH over 0.05 and 0.10 eq Pt-Ru_{ad} at 0.40 V.

Variable temperature studies. The potentiostatic electrooxidation of ([CH_3OH] = [H_2SO_4] = 0.50 M, 25 °C, E = 0.40 V) was effected using the 0.05 and 0.10 eq Ru_{ad} surfaces at temperatures ranging from 1 to 55 °C. Figure 3.8 shows Arrhenius plots of ln(j) versus T^{-1} using the current measured after 5 min 30 s (i.e. steady-state conditions). Straight lines were obtained with both electrodes, indicating that these surfaces are sufficiently stable to allow for studies of this type. The calculated Arrhenius activation energies were 37 kJ/mol for the 0.05 eq surface and 45 kJ/mol for the 0.10 eq surface. The analogous activation energy over the bulk alloy with θ_{Ru} = 7% was 30 kJ/mol as determined by Gasteiger *et al.*, who postulated that surface migration of adsorbed CH_3OH dehydrogenation fragments was rate determining under these conditions.[19]

Stability of Ru_{ad} modified blacked Pt gauzes. These surfaces could be used for several experiments without appreciable loss of electrochemical activity provided that certain precautions were taken. For example, the 0.10 eq Ru_{ad} surface used for the experiments described in this chapter was also used for the potentiostatic and potentiodynamic electrooxidation of ethanol, ethylene glycol, and d-glucose.[20] The electrode was stored as described below between experiments. Excluding idling in the electrolyte at 50 - 75 mV, this surface was operated electrochemically in the presence of various fuels and at various temperatures for a total of 16 h. As shown in Figure 3.9, this surface exhibited similar activities toward the potentiostatic oxidation of CH_3OH before and after these experiments.

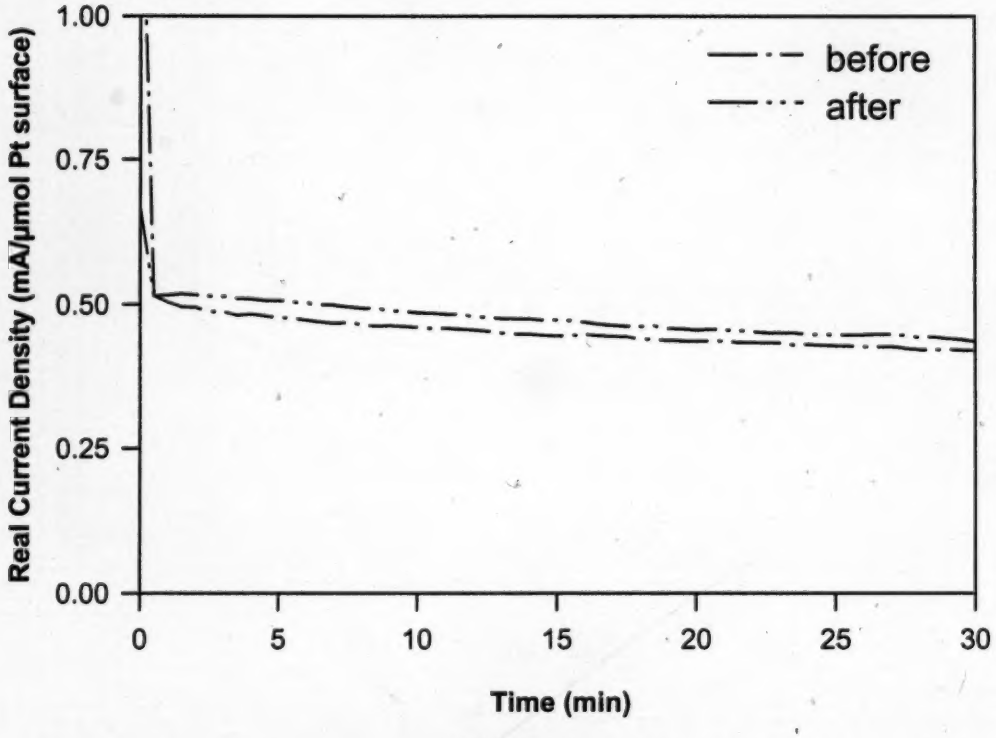

Figure 3.9. Potentiostatic oxidation of CH_3OH over 0.10 eq Pt-Ru_{ad} before and after 16 h of electrochemical activity.

To maintain the activity of these surfaces, it was important to ensure that the potential never exceeded 0.70 V. Dissolution of Ru above 0.90 V can potentially remove the Ru_{ad} from these surfaces. The electrodes were held at 50 to 75 mV whenever in contact with the electrolyte except during the recording of data for experiments. When required, the electrodes could be stored for periods of days by first holding the potential at 50 to 75 mV for at least 2 min, and second, by rinsing the electrode with deoxygenated H_2O, drying the electrode under a stream of Ar(g), and storing it at -30 °C in a drybox freezer. Poisoning by disadvantageous species did not often effect the activities of the surfaces if these and the procedures described previously were followed. A factor in the apparent resistance of these surfaces to trace poisons is their large specific surface areas, which ranged from 2800 to 3700 cm^2. Serious poisoning did occur on occasion (during these studies, as evidenced by a precipitous loss in electrochemical activity and by an absence of any features in the hydride region of voltammograms recorded in 0.5 M H_2SO_4). A procedure that was successful in restoring these poisoned surfaces was to carry out a potentiostatic oxidation of CH_3OH (25 °C, 0.40 V), replace the electrolyte with clean 0.50 M H_2SO_4, and perform continuous potentiodynamic sweeps (5 mV/s, 0.025 to 0.60 V) until the base potentiodynamic response (Figure 3.1) was obtained.

Conclusions

Hydrogenation of **1** over Pt represents a unique method to prepare Pt-Ru_{ad} surfaces as catalysts for the electrooxidation of CH_3OH and CO_{ads}. The results of electrooxidation of CH_3OH and CO_{ads} demonstrate that the hydrogenation produces Pt-Ru_{ad} surfaces of known real surface areas and with reasonable control over the surface stoichiometry. The specific surface area and surface stoichiometry of rough bimetallic surfaces are notoriously difficult to measure and to control, yet knowledge of these values is fundamental to the understanding of how such systems operate as catalysts. Further, the electrochemical activities of the Pt-Ru_{ad} surfaces were noticeably stable (up to 16 h) under the conditions used for this study over a 1 month period, illustrating that certain

metal-metal adatom systems are suitable for long-term studies under the appropriate conditions. Only traces of Ru ions could be detected by inductively coupled mass spectrometry in the electrolytes where electrochemical experiments were carried out. Although the lifetimes of the Pt-Ru_{ad} surfaces under these conditions are unknown, they do not immediately decompose by surface segregation or by dissolution of Ru.

The results reported herein indicate that the eq Ru_{ad} controls the activity of Pt-Ru_{ad} surfaces toward the electrooxidation of CH_3OH and of CO_{ads}. Surfaces with between 0.05 and 0.10 eq Ru_{ad} appear the most active under the conditions used for this study. The apparent control over surface stoichiometry and the knowledge of specific surface area offered by hydrogenation of **1** allows comparisons between these Pt-Ru_{ad} surfaces and the bulk alloys studied by Gasteiger *et al.*[2] On the main, the optimum surface composition of the Pt-Ru_{ad} surfaces prepared by hydrogenation of **1** is comparable to that reported for the shiny bulk Pt-Ru alloys. One notable difference is in their activities toward the electrooxidation of adsorbed monolayers of CO, which may result from differences between the distributions of Ru atoms at the surfaces of Pt-Ru alloys and Pt-Ru_{ad} under these conditions.

The hydrogenation of **1** appears to generate prototypic Pt-Ru_{ad} surfaces with real-time control over the eq Ru_{ad}. Since the hydrogenation requires a Pt surface to occur, it will in principle self-direct the deposition of Ru adatoms (or mixtures of Ru and Pt adatoms) on the surfaces of Pt clusters supported by an inert substrate. In the following chapter the extension of these studies to practical nanoscale Pt-Ru_{ad} particles will be described. The activity and stability of these surfaces will be examined in prototype direct methanol fuel cells.

Experimental Section

Detailed procedures for the preparation, electrochemical characterization, and manipulation of the blacked Pt gauzes, for carrying out and interrupting hydrogenations

of **1**, and for the adsorption and electrooxidation of CO_{ads} were given in Chapter 2. Any alterations or new methods are described below.

The procedure for the purification of the hydrocarbon solvents was changed to the following: hexanes (BDH, HPLC grade) were passed through aluminum oxide (grade I), hydrogenated ($P(H_2)$ ~1 atm) over Pt_{black} for 24 h, and distilled off K(s) via Vigreux column under Ar(g) prior to use. The decane internal standard was purified similarly.

Electrooxidation of CH_3OH on Ru_{ad} modified blacked Pt gauzes. A hydrogenation of **1** was interrupted as described in Chapter 2 after deposition of the desired eq Ru_{ad}. The rinsed and dried catalyst surface was transferred in a drybox to an electrochemical cell. An Ar(g) saturated aqueous solution (90 mL) of H_2SO_4 (0.50 M) and CH_3OH (0.50 M) at 25 °C was transferred to the cell using a Teflon® cannula. The potential of Pt-Ru_{ad} working electrode (WE) was set to 50 mV concurrent with immersion into the electrolyte and then swept to 0.60 V at 5 mV/s.

The potentiostatic oxidations of CH_3OH were carried out in the same electrolyte at 25 °C. The initial potential of the Pt-Ru_{ad} WE was 50 to 75 mV, the potential was stepped to the desired potential to begin the oxidation of CH_3OH for 30 min then the WE potential was returned to 50 to 75 mV.

References

(1) Ticanelli, E.; Beery, J. G.; Paffett, M. T.; Gottesfeld, S. *J. Electroanal. Chem.* **1989**, *258*, 61.

(2) Gasteiger, H. A.; Markovic, N.; Ross, Ir., P. N.; Cairns, E. I. *J. Phys. Chem.* **1993**, *97*, 12020.

(3) Gasteiger, H. A.; Markovic, N.; Ross, Ir., P. N.; Cairns, E. I. *J. Electrochem. Soc.* **1994**, *141*,1795.

(4) Hadzi-Jordanov, S.; Angerstein-Kozlowska, H.; Vukovic, M.; Conway, B. E. *J. Phys. Chem.* **1977**, *81*, 2271.

(5) (a) Niedrach, L. W.; McKee, D. W.; Paynter, J.; Danzig, I. F.; *Electrochem. Technol.* **1967**, *5*, 318. (b) McKee, W. W.; Scarpellino, A. J. *Electrochem. Technol.* **1968**, *6*, 101. (c) Ross. P. N.; Kinoshita, K.; Scarpellino, A. J.; Stonehart, P. *J. Electroanal. Chem.* **1975**, *63*, 97. (d) Watanabe, M.; Motoo, S. *Electroanal. Chem. Interfac. Electrochem.* **1975**, *60*, 275. (e) Gasteiger, H. A.; Markovic, N. M.; Ross, Jr., P. N.; Cairns, E. J. *J. Phys. Chem.* **1994**, *98*, 617. (f) Ianniello, R.; Schmidt, V. M.; Stimming, U.; Stumper, J.; Wallau, A. *Electrochimia Acta* **1994**, *39*, 1863. (g) Gasteiger, H. A.; Markovic, N. M.; Ross, Jr., P. N. *J. Phys. Chem.* **1995**, *99*, 16757. (h) Gasteiger, H. A.; Markovic, N. M.; Ross, Jr., P. N. *J. Phys. Chem.* **1995**, *99*, 8290. (i) Aberdam, D.; Durand, R.; Faure, R.; Gloaguen F.; Hazemann, J. L.; Herreor, E.; Kabbabi, A.; Ulrich, O. *J. Electroanal. Chem.* **1995**, *398*, 43. (j) Richarz, F.; Wohlmann, B.; Vogel, U.; Hoffschulz, H.; Wandelt, K. *Surf. Sci.* **1995**, *335*, 361. (k) Anderson, A. B.; Grantscharova, E. *J. Phys. Chem.* **1995**, *99*, 9149. (l) Shen, P. K.; Chen, K. Y.; Tseung, A. C. C. *J. Electrochem. Soc.* **1996**, *142*, L85. (m) Frelink, T.; Visscher, W.; van Veen, J. A. R. *Langmuir*, **1996**, *12*, 3702. (n) Frelink, T.; Visscher, W.; Cox, A. P.; van Veen, J. A. R.; *Ber. Bunsenges. Phys. Chem.* **1996**, *100*, 599. (o) Napporn, W. T.; Léger, J.-M.; Lamy, C. *J. Electroanal. Chem.* **1996**, *408*, 141. (p) Friedrich, K. A.; Geyzers, K.-P.; Linke U.; Stimming, U.; Stumper, J. *J. Electroanal. Chem.* **1996**, *402*, 123.

(6) Gasteiger, H. A.; Markovic, N. M.; Ross, Jr., P. N.; Cairns, E. J.*J Phys. Chem.* **1994**, *98*, 617.

(7) Richarz, F.; Wohlmann, B.; Vogel, U.; Hoffschulz, H.; Wandelt, K. *Surf Sci.* **1995**, *335*, 361.

(8) Frelink, T.; Visscher, W.; van Veen, J. A. R. *Langmuir* **1996**, *12*, 3702.

(9) Watanabe, M.; Motoo, S. *Electroanal. Chem. Interfacial Electrochem. 1975*, *60*, 275.

(10) Friedrich, K. A.; Geyzers, K.-P.; Linke U.; Stimming, U.; Stumper, J. *J.Electroanal. Chem.* **1996**, *402*, 123.

(11) Lin, W. F.; Zei, M. S.; Eiswirth, M.; Ertl, G.; Iwasita, T.; Vielstich, W. *J. Phys. Chem. B* **1999**, *103*, 6968.

(12) Bett, J.; Kinoshita, K.; Routis, K.; Stonehart, P. *Journal of Catalysis* **1973**, *29*, 160.

(13) Weaver, M. J.; Chang, S.-C.; Leung, L.-W. H.; Jiang, X.; Rubel, M.; Szklarczyk, M.; Zurawski, D.; Wieckowski, A. *J. Electroanal. Chem. 1992*, *327*, 247.

(14) Vielstich, W.; Xia, X.H. *J. Phys. Chem.* **1995**, *99*, 10421.

(15) Horanyi, G.; Wieckowski, A. In *Proceedings ofthe Workshop on Direct Methanol-Air Fuel Cells;* Landgrebe, A. R., Sen, R. K., Wheller, D. J., Eds.; The Electrohemical Society: Pennington, NJ, 1992; Vol. 92-94, p 70.

(16) Kunimatsu, K. *Ber. Bunsen-Ges. Phys. Chem.* **1990**, *94*, 1022.

(17) Watanabe, M; Motoo, S. *Electroanal Chem. 1nterfacial Electrochem.* **1975**, *60*, 267

(18) (a) Frelink, T.; Visscher, W.; van Veen, J. A. R. *Surf Sci.* **1995**, *335*,353. (b) Frelink, T.; Visscher, W.; van Veen, J. A. R. *Langmuir* **1996**, *12*, 3702.

(19) Gasteiger, H. A.; Markovic, N.; Ross, P. N.; Cairns, E. J. *J. Electrochem. Soc.* **1994**, *141*, 1795-1803.

(20) Lee, C.E.; Bergens, S.H. *J. Electrochem. Soc.* **1998**, *145*, 4182.

Chapter 4

Self-Directing Organometallic Deposition of Ru, Part III. Deposition of Ru on a Nanoscale Pt Substrates and the Evaluation of Pt-Ru_{ad} Anode Electrocatalysts in Prototype Direct Methanol Fuel Cells.

Introduction

The results presented in this chapter are an extension of the self-directing organometallic deposition of Ru_{ad}. Nanoscale Pt particles (Pt_{black}) will be used as the substrate in order to prepare practical electrocatalysts for direct methanol fuel cells. The performance of a series of direct methanol fuel cells will be evaluated as a function of their anode electrocatalyst surface compositions. The self-directing organometallic deposition of Ru_{ad} on Pt was described in the previous chapters (Chapters 2 and 3). The surface composition of model Pt-Ru_{ad} electrodes was controlled by monitoring the hydrogenation of (η^4-1,5-cyclooctadiene)Ru(η^3-C_3H_5)$_2$ (**1**) over blacked Pt gauzes, and by terminating the hydrogenation of **1** when the desired surface composition was reached. The optimization of the surface composition of these Pt-Ru_{ad} electrocatalysts for electrooxidation of CH_3OH and adsorbed CO (CO_{ads}) in H_2SO_4(aq) was described (Chapter 3). The intrinsic activity (i.e., current per active site on the electrode surface) of a Pt-Ru_{ad} gauze with a surface composition of ~0.05 eq Ru_{ad} was found to be 50 times higher than that of unmodified blacked Pt towards the electrooxidation of CH_3OH under pseudo-steady-state conditions at 0.40 V *vs.* SHE ([CH_3OH] = [H_2SO_4] = 0.50 M at 25°C). The results from these studies showed that the surface composition of blacked Pt-Ru_{ad} gauzes could be controlled, and that substantial increases in activity towards the electrooxidation of CH_3OH can be obtained if the surface composition is optimized using this methodology. Further, the model Pt-Ru_{ad} surfaces were stable and could be used over extended periods of time.

There are no literature reports of Pt-Ru_{ad} electrocatalysts in prototype DMFC anodes that compare performance on the basis of real current densities using

electrocatalysts with systematically varied surface compositions. Wieckowski *et al.* have recently reported the spontaneous deposition of Ru_{ad} precursors on Pt_{black} and use of the Pt-Ru_{ad} blacks as electrocatalysts for the electrooxidation of CH_3OH.[1] Gottesfeld *et al.* recently reported that the peak potentials observed during CO_{ads} stripping voltammetry could be used to determine the surface composition of Pt-Ru alloy nanoparticles inside a prototype DMFC.[2] The surface composition of the metallic component of these catalysts was estimated by comparing the peak potentials for the potentiodynamic electrooxidation of CO over the Pt-Ru nanoparticles to peak potentials obtained over bulk, atomically smooth Pt-Ru alloys of known surface composition (measured by low energy ion scattering).[2] Unfortunately, there are no alternate methods to measure the surface compositions of the Pt-Ru alloy nanoparticles used by these authors that could confirm the validity of their method. Further, there are no confirmed methods for the preparation of alloyed Pt-Ru nanoparticles that enable systematic variation of surface compositions.

According to Parsons and VanderNoot, adatom modified surfaces are not expected to be stable for use in practical fuel cells.[3] It is apparently assumed to be impractical due to surface enrichment, or dissolution phenomena that result in the loss of Ru from Pt-Ru (adatom modified, or alloy) surfaces in the operating fuel cell. The results presented in Chapters 2 and 3 indicated an impressive degree of stability for Ru_{ad} modified Pt surfaces. The use of Ru adatom modified Pt powders as practical electrocatalysts for DMFC anodes has recently been reported by the Bergens group.[4] It is reasonable to believe that optimization of the surface composition of nanoscale Pt-Ru_{ad} particles in a prototype DMFC can be achieved using this method. Towards this end, the hydrogenation of **1** was carried out in the presence of a nanoscale Pt substrate (Pt_{black}), and a series of Ru_{ad} modified Pt_{black} electrocatalysts (Pt_{black}-Ru_{ad}) with surface composition ranging from 0.05 to 0.68 eq Ru_{ad} were prepared. These Pt_{black}-Ru_{ad} electrocatalysts were characterized using the standard electrochemical techniques of cyclic voltammetry and CO_{ads} stripping voltammetry prior to incorporation into the anodes of prototype DMFC's. The fabrication of electrodes for direct methanol fuel cells using a series of Ru_{ad} modified Pt_{black} powders as the anode enabled the first determination of the optimum surface composition of Pt-Ru_{ad} electrocatalysts in a DMFC. The membrane electrode assemblies were made using a decal transfer method

developed by the Gottesfeld group at Los Alamos National Laboratory.[5] A mechanistic study of the reaction (similar to Chapter 2), and optimization of the surface composition of nanoscale Pt particles (Pt_{black}-Ru_{ad}) towards the electrooxidation of CH_3OH and CO_{ads} using half-cell electrochemical methods (similar to Chapter 3) can be found in thesis work of Yue Xing.[6] A carbon supported Pt substrate (20 wt % Pt/C) was also modified with Ru_{ad} and then characterized using Transmission Electron Microscopy (TEM) and Energy Dispersive X-ray Analysis (EDX).[7]

There are several methods used to mount nanoscale particles for electrochemical analysis, the most common are outlined in brief below. The electrochemical characterization of high dispersion electrocatalysts requires the incorporation of the electrocatalyst into a reproducible and defined electrode structure.[8] The incomplete utilization of the electrocatalyst and limited mass transport to active surface sites complicates interpretation of the results obtained using electrodes that incorporate nanoscale metallic particles (e.g., Pt_{black}). Specifically, incomplete utilization prevents the accurate determination of real surface areas, and mass transport limitations preclude accurate determinations of reaction rates. The fabrication of small gas diffusion electrodes has been used, but the quantitative determination of the amount of active Pt surface is not straightforward. For example, self-supporting electrodes have been prepared by combining carbon supported Pt-Ru powders with a mixture of carbon fibers and Teflon® then heating to high temperatures in order to bind the electrode components together.[9] Using a similar procedure electrodes have been prepared by combining carbon supported Pt-Ru particles with Teflon® then hot-pressing them onto a Ni mesh.[10] As the utilization of the electrocatalysts in porous structures such as these is significantly less than 100 % and cannot be accurately determined, the evaluation of electrocatalysts in such model gas diffusion electrodes is qualitative in nature. An alternate procedure to construct electrodes for electrocatalyst evaluation is to deposit small quantities of nanoscale particles from an aqueous suspension onto a supporting electrode (e.g., Pt, Au, or carbon) in the absence of a restraining film.[1, 9-11] The facile loss of material from the supporting electrode surface causes incomplete electrical contact among the catalyst particles and the supporting electrode. This is the primary limitation to the utility of this method. Niedrach was the first to electrochemically measure the real surface area of

nanoscale Pt_{black}.[14] He used a smooth Pt electrode to support nanoscale Pt particles that were held in place with a sheet of cation exchange membrane equilibrated with 1 M H_2SO_4(aq). A method to incorporate Pt-Ru nanoparticles onto a glassy carbon rotating disk electrode that results in 100 % utilization of the electrocatalyst by attaching the catalyst powder on a glassy carbon electrode using a thin Nafion® film has been reported by Gasteiger *et al.*[15] This method is simple, and reproducible and therefore it was used in the presently described studies.

Results and Discussion

Electrochemical characterization of nanoscale Pt and Pt-Ru_{ad} particles. The procedure developed by Gasteiger *et al.* was used to determine the specific surface areas of the nanoscale Pt substrates and to examine the effects of Ru_{ad} deposition on the electrochemical responses of these substrates.[15] The electrocatalyst particles were held onto the surface of a 1 cm^2 smooth Pt foil by a thin film of Nafion®. The real surface areas of the deposits are significantly higher than the real surface area of the smooth Pt supporting electrode so that the observed electrochemical responses are of the deposits and those of the supporting electrode are effectively masked. The potentials quoted here are in reference to a self-contained hydrogen reference electrode (HRE) with a potential of -0.265 V *vs.* saturated calomel electrode (SCE). The construction of the HRE is described in detail in the experimental section. An upper potential limit of 0.90 V was used whenever necessary to prevent dissolution of Ru into the electrolyte.[16]

Figure 4.1(a) shows the cyclic voltammogram (CV) of a Nafion®-bound Pt_{black} deposit recorded in 1.0 M H_2SO_4(aq). The morphology of the Pt_{black} CV is the same as that observed for a blacked Pt electrode (Chapter 2, Figure 2.1). The real surface areas of several Pt deposits were determined from the charge passed in the hydrogen region during the cathodic sweep, as described in Chapter 2 (according to eq. 2.3). The real surface areas (after subtraction of the real surface area of the smooth Pt support) were then normalized to the masses of the deposits to give the specific surface areas. The average experimental value and the value quoted by the supplier (Johnson Matthey &

Sons, Inc.) for the specific surface area of the Pt_{black} substrate are 28 and 27 m^2/g respectively. Figure 4.1(b) shows the CV of a Nafion®-bound deposit of 20 wt % Pt/C. The specific surface area of the Pt/C deposit was found to be 109 m^2/g Pt metal, similar to the value of 100 m^2/g Pt quoted by the manufacturer (E-tek, Inc.)

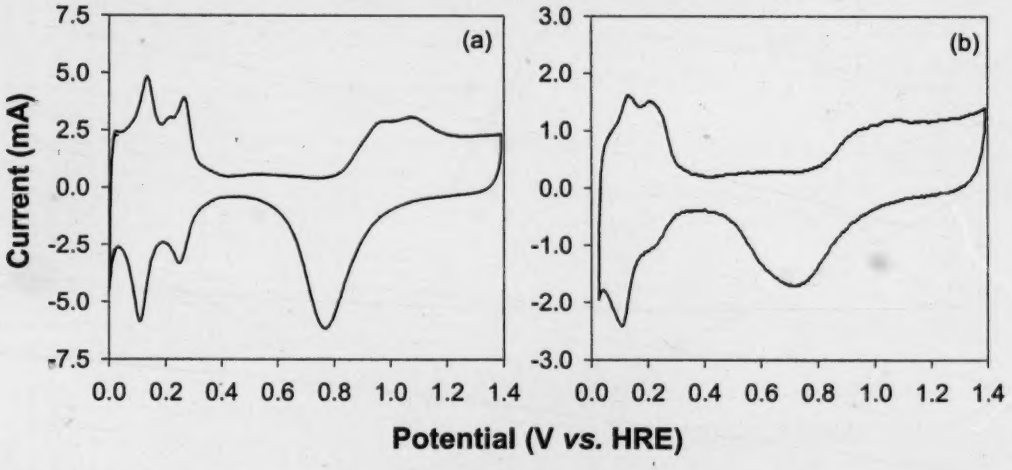

Figure 4.1. Voltammograms of Pt electrocatalyst deposits in 1.0 M H_2SO_4(aq); (a) 0.285 mg Pt_{black} at 50 mV/s, and (b) 0.279 mg of 20 wt % $Pt/C_{Vulcan\ XC\text{-}72R}$ at 20 mV/s.

Self-directing organometallic deposition of Ru_{ad} on Pt_{black}. The procedure used to deposit Ru_{ad} on blacked Pt gauzes (Chapter 2, Figure 2.2) was modified for use with powder substrates. To ensure that the deposition reaction proceeded under reaction rate limiting conditions a higher concentration of **1** was used, relative to the hydrogenations of **1** over the blacked Pt gauzes, and H_2(g) was constantly bubbled through the reaction mixture. The rate of the reaction was slow enough at low temperatures to be monitored by gas chromatography and could be terminated when the desired coverage was realized. The electrochemical pretreatment used to clean and protect the blacked Pt gauzes could not be applied to the nanoscale Pt_{black} or Pt/C substrates. The Pt_{black} substrate was cleaned and protected as oxides under water prior to use.

The use of the high dispersion, unsupported Pt requires careful attention to avoid the simultaneous mixing of the Pt, O_2(g), and H_2(g), since the resulting exothermic reaction may sinter the substrate, resulting in a loss of real surface area. The reduction of

a Pt oxide surface by $H_2(g)$ is very rapid and exothermic, as nanoscale particles cannot conduct heat into the bulk as gauzes can, the oxide protected surface of Pt_{black} was reduced by $H_2(g)$ under H_2O. The H_2O served as a heat-sink, to avoid excessive heating of the Pt powders. The production of a H_{ads} saturated Pt surface, and the complete removal of H_2O from the system was accomplished by cycling the atmosphere between Ar(g), high vacuum, and $H_2(g)$ a number of times. Finally, the reaction vessel was maintained under ~1 atm of $H_2(g)$ and immersed into a -42 °C bath prior to the quantitative addition of a H_2 saturated solution of **1**. Figure 4.2 shows a plot of the surface composition as a function of time during a hydrogenation of **1** over Pt_{black} (taken from the thesis work of Yue Xing).[6] The behavior of the hydrogenation over blacked Pt gauzes (Chapter 2, Figure 2.2) and over Pt_{black} particles (Figure 4.2) is the same.

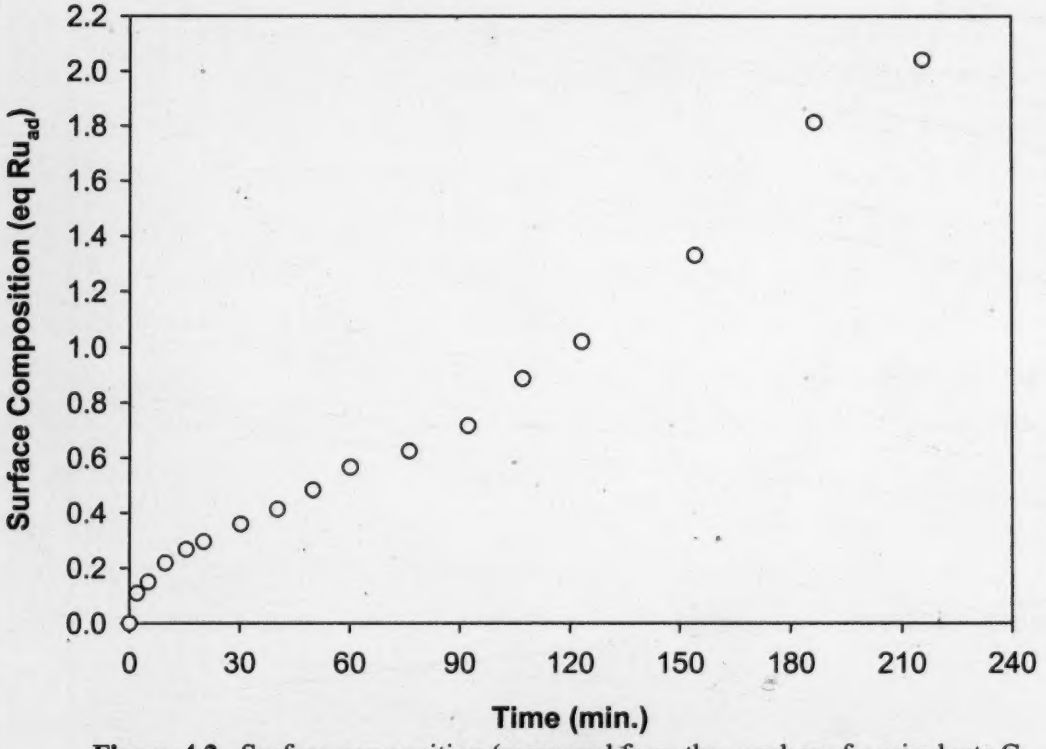

Figure 4.2. Surface composition (measured from the number of equivalents C_8 hydrocarbons in solution) *vs.* time for a hydrogenation of **1** over Pt_{black} at -45 °C.

The Pt_{black}-Ru_{ad} surfaces are saturated with H_{ads} after the deposition is terminated. To avoid sintering of the catalyst powders when they were exposed to the atmosphere, the catalysts were exposed to air at low T and then slowly warmed to room temperature. This exposure to the atmosphere was necessary for fabrication of electrodes for electrochemical characterization and for incorporation into prototype DMFC anodes.

Energy dispersive X-ray analysis of Ru_{ad} modified Pt_{black} and 20 wt % Pt/C. Transmission Electron Microscopy and Energy Dispersive X-ray Analysis were carried out on Pt_{black}-Ru_{ad} and on Pt-Ru_{ad} on carbon (20 wt % Pt on C). The carbon supported Pt substrate contains smaller Pt particles, which therefore have higher ratios of surface to internal atoms, than unsupported Pt_{black}. There were technical difficulties unique to deposition of Ru_{ad} on the supported Pt substrate resulting from the low density of the substrate. The supported Pt/C was activated by the atmospheric cycling procedure used during the final stage of the Pt_{black} substrate pretreatment. The low density of the substrate also caused difficulties with the aliquot removal and termination of the hydrogenation since the Pt/C does not readily settle out of the reaction mixture nor can it be isolated from the reaction solution by filtration. The hydrogenation reaction was therefore terminated by saturating the catalyst surface with CO_{ads} and by diluting the reaction mixture with additional solvent. In order to isolate the Pt-Ru_{ad}/C the reaction mixture was transferred into several small test tubes and centrifuged. The deposition of Ru_{ad} resulted in a Ru coverage of 0.46 eq Ru_{ad} after 30 min at -42 °C according to GC analysis of the reaction mixture. The results of elemental analysis confirmed this result.

The elemental analysis of two Ru_{ad} modified Pt substrates was performed using transmission electron microscope equipped with energy dispersive X-ray analysis (EDX) spectrometer. Table 4.1 summarizes the results of EDX analysis of Pt_{black}-Ru_{ad}

Table 4.1. The bulk compositions of Pt-Ru_{ad} particles determined by EDX and GC.

Surface composition (θ_{Ru}, eq Ru_{ad})	Bulk composition (X_{Ru})	
(GC)	(GC)	(EDX)
0.22 Pt_{black}-Ru_{ad}	0.025	0.042
0.46 Pt-Ru_{ad}/C	0.175	0.186

and of Pt-Ru_{ad}/C. The bulk atomic compositions of Ru (X_{Ru}) of a number of particles were determined from the ratio of peak areas for the Ru K_α (19.278 keV) and Pt K_α (9.441 keV) X-ray emissions. A carbon supported Pt-Ru alloy (20 wt % Pt-Ru/C, 1:1 atomic ratio Ru:Pt) was used as a standard for the elemental analysis. The elemental analysis of individual particles was not possible for any of the samples analyzed due a lack of sensitivity of the EDX and difficulties associated with maintaining the electron beam focused onto a single particle (i.e., a confined area of a only a few nm). Instead, the analysis is of the average bulk composition of a small collection of particles. Unfortunately, the Ru signal from the Ru_{ad} modified Pt_{black} (0.22 eq Ru_{ad}) was too weak to ensure an accurate quantification. The elemental analysis of the carbon supported sample is however, in reasonable agreement with the bulk composition calculated from the specific surface area of the 20 wt % Pt/C substrate (determined electrochemically) and the surface coverage predicted by analysis of the reaction products (determined using GC). It is therefore reasonable to conclude that the GC analysis of the reaction mixture during the hydrogenation of **1** combined with determination of the specific surface area of these nanoscale Pt substrates can be used to determine the surface composition of Ru_{ad} modified Pt nanoparticles. Further experimental evidence for this conclusion from a series of Pt_{black}-Ru_{ad} electrocatalysts was obtained using standard electrochemical techniques and is described in the forthcoming sections.

Electrochemical characterization of Pt_{black}-Ru_{ad}. Exposure of the electrocatalysts to the ambient atmosphere is inevitable during preparation of electrodes from Ru_{ad} modified Pt_{black}. To eliminate interferences caused by the adsorption of disadvantageous surface contaminants during exposure, the cyclic voltammograms of the electrocatalyst deposits were recorded after saturating their surfaces CO_{ads} under controlled potential conditions. The adsorption of CO_{ads} prior to characterization was carried out to displace any disadvantageous surface impurities that had accumulated on with the surface of the Pt_{black}-Ru_{ad} during preparation, isolation, and electrode fabrication. This method of pretreatment of the working electrodes was used previously during the electrochemical characterization of the Ru_{ad} modified blacked Pt gauzes as described in Chapter 3. The use of CO_{ads} surface saturation has recently been used by Clavilier *et al.* to displace surfactant molecules from nanoscale Pt particles.[13]

Figure 4.3. shows the voltammograms of a series of Pt_{black}-Ru_{ad} with surface compositions of 0.053, 0.29, 0.44, and 0.68 eq Ru_{ad}. The voltammograms are scaled to the masses of the deposits to facilitate visual comparisons among them on the basis of their surface compositions (i.e., specific current densities *vs.* potential are plotted).

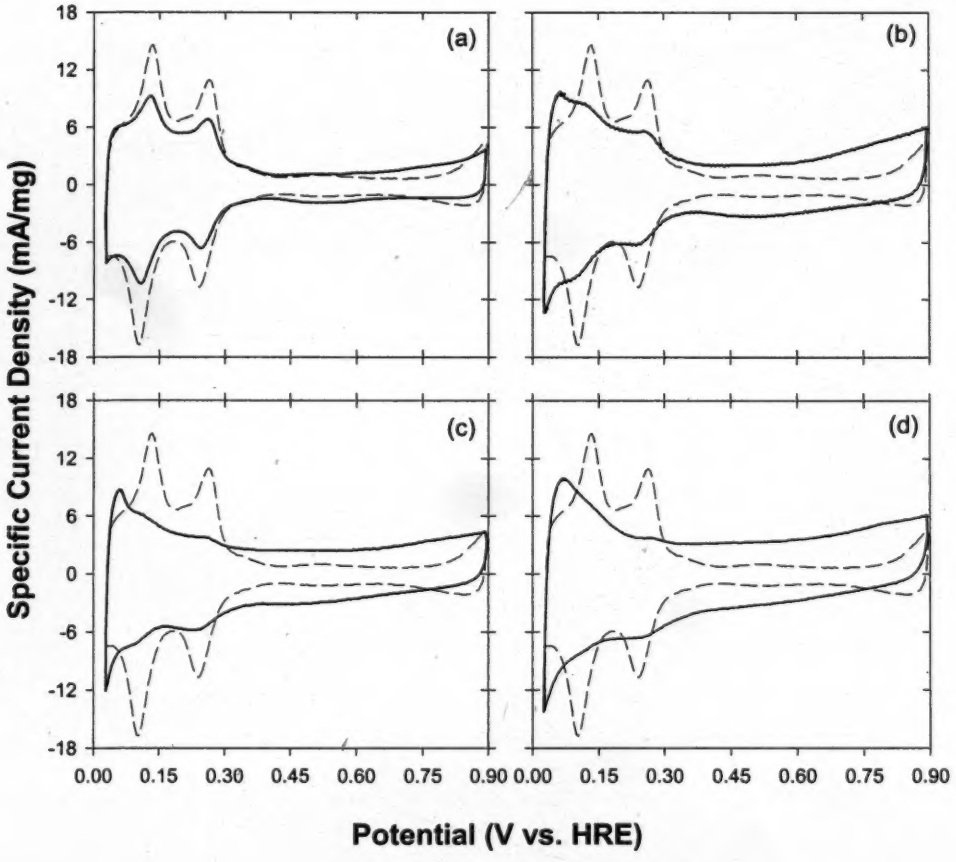

Figure 4.3. Voltammograms of a series of Pt_{black}-Ru_{ad} deposits ((a) 0.053 (b) 0.29 (c) 0.46, and (d) 0.68 eq Ru_{ad}) recorded in 1.0 M H_2SO_4(aq) at 50 mV/s. The dashed lines are voltammograms of a Pt_{black} deposit included as a visual reference.

That the specific current densities in the hydrogen regions of the voltammograms are similar for all of the Pt_{black}-Ru_{ad} deposits indicates that the specific surface areas are also similar, implying that only negligible changes in real surface areas occurred during the

hydrogenation of **1**. The changes in the morphology of the cyclic voltammograms shown in Figure 4.3 are in accord with expectations based on the previous results obtained using the blacked Pt gauze as the deposition substrate (Chapter 3, Figure 3.1). That is, as the amount of Ru_{ad} on the surface increases, the ratio of currents in the hydrogen region to those in the double layer decreases due to the overlap of the hydrogen and oxygen regions of the Ru_{ad} with the hydrogen region of the Pt in the voltammogram.

Wieckowski *et al.* have recently reported the voltammograms of Ru_{ad} modified Pt_{black} prepared using their spontaneous deposition method (Chapter 1).[17] Their voltammograms retain much of the Pt character in the hydrogen region, and it was proposed that this behavior results from the formation of Ru islands on the Pt_{black}, as has been shown to occur the during spontaneous deposition of Ru_{ad} on low index Pt crystals.[18, 19, 20] Voltammograms obtained by Chu and Gilman for nanoscale Pt-Ru alloy particles (of unknown surface composition) prepared by chemical co-reduction of Pt and Ru chlorides although clearly the electrochemical responses of Pt-Ru surfaces are not as well defined as those in Figure 4.2.[21] In addition, due to the method of electrode fabrication they used, their currents can not be normalized to specific current densities and therefore the performance of their electrocatalysts as a function of composition (either surface or bulk compositions) cannot be ascertained. Others have reported voltammograms of Pt-Ru alloys prepared by co-electrodeposition onto Au substrates.[22, 23, 24] The morphologies are poorly defined, and as is usually the case, the surface compositions of these deposits are unknown. The voltammograms obtained by Gasteiger *et al.* on their well-characterized Pt-Ru alloys are the closest match with our own.[25] It is therefore possible that the self-directing organometallic deposition of Ru_{ad} produces Pt_{black}-Ru_{ad} particles that exhibit the electrochemical responses expected of well-defined alloys due to an even distribution of Ru_{ad} on the surface of each individual Pt_{black} particle. In addition, the definition apparent in these voltammograms (Figure 4.2) could be a result of all of the Ru_{ad} being completely reduced to the metallic state during the hydrogenation of **1** and that the less defined voltammograms obtained by others (*vide supra*) are a result of Ru oxide or hydrous Ru oxide surface species being present.

Anodic stripping voltammetry of adsorbed carbon monoxide on Pt_{black} and Ru_{ad} modified Pt_{black} surfaces. These Pt_{black}-Ru_{ad} electrocatalysts were further characterized

using CO_{ads} stripping voltammetry. The relative activities of these surfaces towards CO_{ads} electrooxidation was determined by the position of the CO_{ads} stripping peak as a function of θ_{Ru}. The charge passed during the electrooxidation of CO_{ads} was used to estimate the specific surface areas of the Ru_{ad} modified Pt_{black} electrocatalysts. As mentioned in Chapter 3 the determination of real surface areas using CO_{ads} stripping measurements is not straightforward and therefore an empirical approach using Pt_{black} as a standard was devised (*vide infra*).

Figure 4.4 shows the typical voltammetric response of a Pt_{black} deposit with its surface saturated by CO_{ads}. During the first anodic sweep there is no significant current until the onset of CO_{ads} oxidation at ~0.40 V as a small shoulder, this small shoulder is followed by a large and sharp CO_{ads} stripping peak centered at ~0.78 V. The lack of significant currents between the CO_{ads} adsorption potential and the onset of CO_{ads} oxidation during the first anodic sweep (Figure 4.3) indicates that the surface is saturated with CO_{ads}. Ianniello *et al.* have monitored the anodic stripping of CO_{ads} using differential electrochemical mass spectroscopy (DEMS) and shown that CO_2 production starts at a ~0.40 V.[26] The shoulder has an apparent peak at 0.50 V that has been attributed to the electrooxidation of bridge bonded CO_{ads}.[27] Alternatively, Stonehart suggested that the shoulder is due to the electrooxidation of CO_{ads} by activated H_2O molecules on the surface.[28] Partial splitting of the main peak has also been observed and is thought to arise due to the CO_{ads} electrooxidation on different crystal faces of the Pt surfaces.[27]

As mentioned above, the measurement of the real surface areas of Pt using CO_{ads} stripping voltammetry is not a trivial task. The problems associated with the use of CO_{ads} stripping charges for the determination of real surface areas are primarily due to the difficulty in separating the charges due to Faradaic and non-Faradaic surface processes that occur during the potential sweeps. As a result the saturation coverage of CO_{ads} on Pt is often overestimated according to Weaver *et al.*[29, 30] The saturation coverages of CO_{ads} on low index Pt and polycrystalline Pt are reported to be in the range of 0.6 to 1.0.[30] The situation is complicated further for Pt-Ru surfaces due to the overlap of the hydrogen and oxygen regions in the baseline voltammograms (Figure 4.3), therefore, there is no region

of the voltammogram of a Pt-Ru surface that can be used to accurately determine the baseline response (*vide infra*).

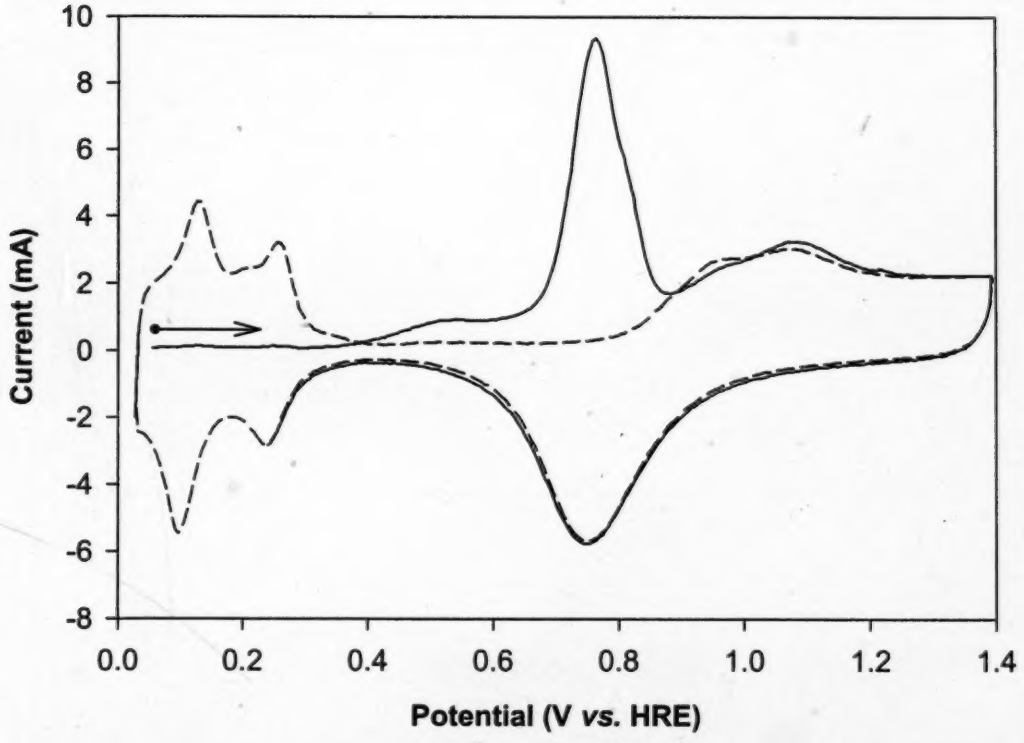

Figure 4.4. Stripping voltammogram of CO_{ads} on a Pt_{black} deposit (0.250 mg) recorded in CO free 1.0 M H_2SO_4(aq) at 50 mV/s. The solid line is the first complete sweep starting at 50 mV (in the direction indicated by the arrow) and the dashed line is the second potential cycle after removal of CO_{ads} from the deposit.

The charge passed during the first anodic sweep (solid line, Figure 4.4) is due to charging the double layer, electrooxidation of CO_{ads}, and oxidation of the surface (Q_{CO+O}). The charge passed during the second anodic sweep (dashed line, Figure 4.4) is due to double layer charging and surface oxidation processes (Q_O). Assuming that the double layer charging is the same in the presence and absence of CO_{ads} and that the extent of surface oxidation is the same at the upper limit the difference between Q_{CO+O} and Q_O is the charge associated with the electrooxidation of CO_{ads} to CO_2. The assumption that the

extent of surface oxidation at the upper potential limit is the same during the first and second sweeps is justified since the cathodic return sweeps are identical in each case.

The charge associated with the electrooxidation of CO_{ads} to CO_2 was determined by integrating the voltammograms from the onset of oxidation (i.e., 0.40 V) to the anodic limit of 1.4 V. The charge passed during the first anodic sweep between 0.40 and 1.4 V gives the value of Q_{CO+O} and the charge passed during the second anodic sweep gives the value of Q_O. The charge attributable to CO_{ads} oxidation (Q_{CO}) is the difference between these two values (eq. 4.1).

$$Q_{CO} = Q_{CO+O} - Q_O \qquad \text{(eq. 4.1)}$$

The charge passed during the CO_{ads} oxidation was compared to the number of surface atoms determined from the charge passed in the cathodic hydrogen region (as described in detail in Chapter 2) using eq. 4.2. The ratio of the number of CO_{ads} molecules oxidized to CO_2 to the total number of surface atoms (R_{CO}) is a measure of the saturation coverage of CO_{ads} on Pt_{black}.

$$R_{CO} = \frac{Q_{CO} / 2}{Q_H / 0.77} \qquad \text{(eq. 4.3)}$$

The average value of R_{CO} determined from several experiments using Pt_{black} deposits as a control was 0.58. This value was subsequently used to relate Q_{CO} measured on a series of Pt_{black}-Ru_{ad} deposits to their real surface areas using a value for the charge per unit of real surface area of 420 $\mu C/cm^2$ according to eq. 4.4.

$$A_{real} = \frac{Q_{CO}}{R_{CO}\ 420\ \mu C / cm^2} \qquad \text{(eq. 4.4)}$$

Figure 4.5 shows the CO_{ads} stripping voltammograms for a series of Pt_{black}-Ru_{ad} deposits. The peak potentials for the oxidation of CO_{ads} are significantly lower on the Pt_{black}-Ru_{ad} deposits than on the Pt_{black} substrate (Figure 4.4). The peaks are broader on

the Ru_{ad} modified surfaces, and at low θ_{Ru} (Figure 4.5(a)) there is evidence of a second peak at a higher potential than the main stripping peak. This second peak appears at 0.78 V, this is the same potential as the main stripping peak observed for Pt_{black}.

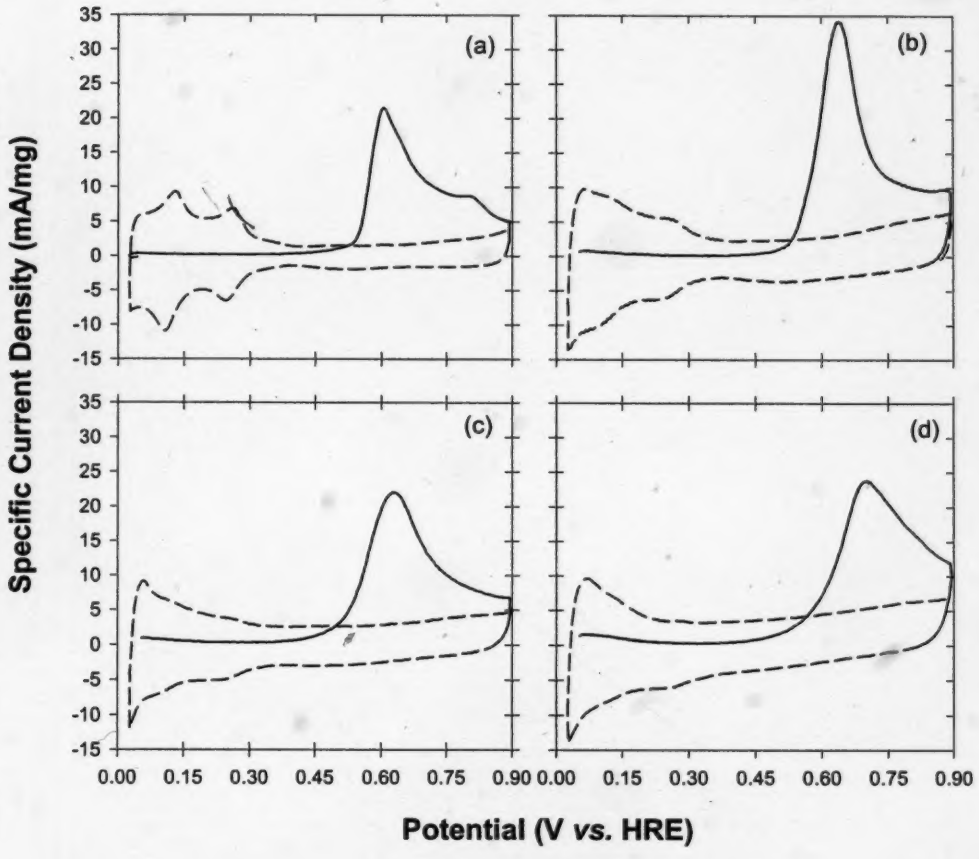

Figure 4.5. Stripping voltammograms of CO_{ads} on a series of Pt_{black}-Ru_{ad} deposits ((a) 0.053, (b) 0.29, (c) 0.46, and (d) 0.68 eq Ru_{ad})) recorded in CO free 1.0 M H_2SO_4(aq) at 50 mV/s. The solid lines are the first potential sweeps from the adsorption potential of 50 mV and the dashed lines are the second complete potential cycles).

The electrooxidation of CO_{ads} commences at ~0.40 V for all of the Pt_{black}-Ru_{ad} electrocatalysts studied (Figure 4.5) as it does for the Pt_{black} (Figure 4.4). In contrast to

the behavior of CO_{ads} stripping on Pt_{black} the peak potentials are approximately 150 mV lower for the Pt_{black}-Ru_{ad} deposits.

Figure 4.6 shows the dependence of the CO_{ads} stripping peak potentials on θ_{Ru} for a series of Pt_{black}-Ru_{ad} deposits. The negative shift of the peak potentials upon the addition of Ru_{ad} to Pt is attributed to an increase in the rate of surface oxide formation at lower potentials on Ru sites relative to Pt sites as discussed in Chapter 3. The straight

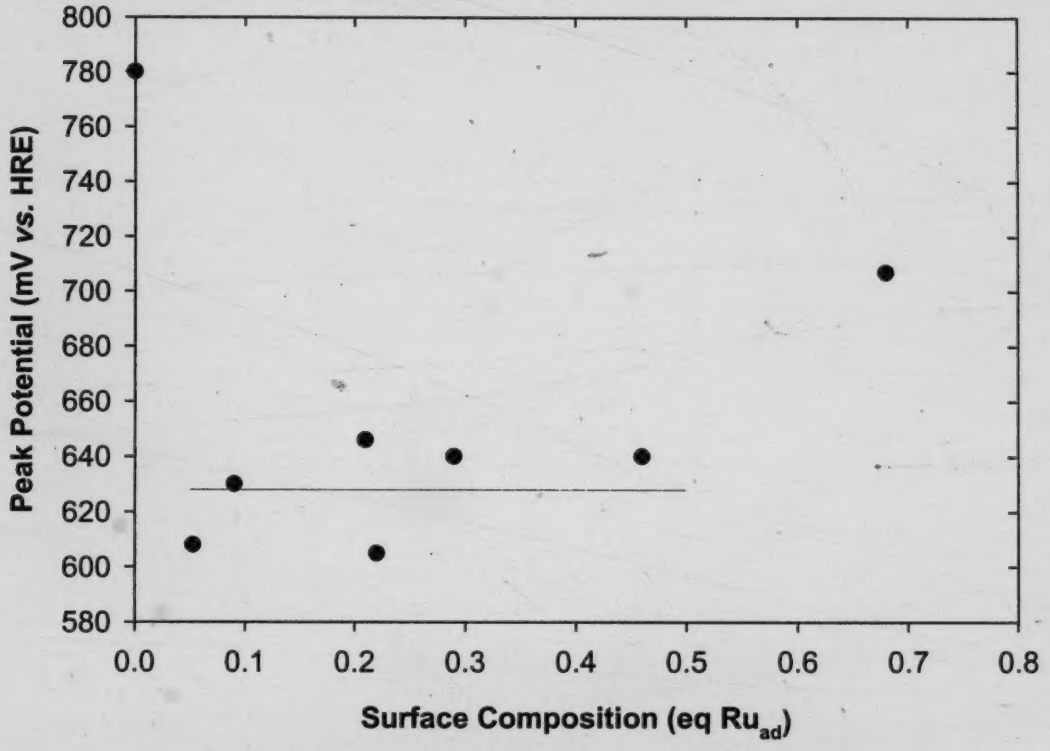

Figure 4.6. Peak potentials for CO_{ads} stripping *vs.* surface composition for a series of Pt_{black}-Ru_{ad} deposits recorded in CO free 1.0 M H_2SO_4(aq) at 50 mV/s.

line in the figure shows the average peak potential for Ru_{ad} coverages between 0.05 and 0.50 eq Ru_{ad}. It is apparent that as θ_{Ru} increases beyond 0.50 eq Ru_{ad} there is a increase in the peak potential. The data plotted in Figure 4.6 indicate a lack of any obvious dependence of the CO_{ads} stripping peak on the surface composition for Ru_{ad} modified Pt_{black} over a broad range of compositions; this is similar to the results presented in Chapter 3.

The peak potentials observed during similar experiments on well-defined alloys and co-electrodeposited alloys exhibit minimum peak potentials at surface compositions of ~50 %.[22, 27] The peak potentials for the electrooxidation of CO_{ads} shift according to the alloy surface composition and the sweep rate used.[27] The magnitude of the peak shift has been used by others to determine the surface composition nanoscale Pt-Ru alloy particles. The use of the CO_{ads} stripping peak potential has been used by Gasteiger *et al.* as a measure of the surface composition of nanoscale Pt-Ru particles using previous results on well-characterized Pt-Ru alloys as a calibration curve.[31] Gottesfeld *et al.* have also used the CO_{ads} stripping peak potential to estimate the surface composition of a commercial electrocatalyst designated as Pt-RuO_x.[32]

There are multiple peaks observed during CO_{ads} stripping that have been attributed to the electrooxidation of CO_{ads} on Pt sites and Pt-Ru sites.[33] Hayden *et al.* have previously observed multiple peaks during the anodic stripping of CO_{ads} from Ru_{ad} modified Pt single crystal surfaces.[34] It is apparent that the effects of θ_{Ru} on the electrooxidation of CO_{ads} are not the same for Pt-Ru alloys and Ru_{ad} modified surfaces. The most likely explanation is that the Ru_{ad} modified surfaces exhibit an island structure (as suggested by Stimming *et al.*) and that the electrooxidation of CO_{ads} may occur on the Pt domains or on the Pt-Ru domains.[35] The situation is different on alloyed surfaces where the distribution of Pt and Ru among surface sites is homogeneous, and therefore one expects the average behavior of all the active sites and the inactive sites to be seen. The results of Gasteiger *et al.* on the well-characterized Pt-Ru alloy surfaces attest to the surface segregation of alloys (equivalent to island deposit formation) as after thermal treatments there was a broadening of their CO_{ads} stripping peaks and evidence of multiple distinct sites for CO_{ads} electrooxidation being formed on the surface.[27] It has also been reported that the formation of Ru islands on Pt surfaces results in multiple CO_{ads} bands in the IR spectra and that for homogeneous alloys only single peaks are observed.[27, 35]

The specific surface areas of the deposits were estimated using the CO_{ads} stripping charge as outlined above for the Pt_{black} deposit. The saturation coverage for CO_{ads} on the $Pt_{black}Ru_{ad}$ surfaces was assumed to be independent of θ_{Ru} and a value of 0.58 was used based on the results obtained using Pt_{black}. The range of the real surface areas measured using CO_{ads} stripping voltammetry is quite large, however, the average specific surface

area of these Pt_{black}-Ru_{ad} deposits was found to be 27.6 m^2/g. The results of Q_{CO} determinations on Pt-Ru_{ad} are not as accurate as those obtained with the hydrogen region of Pt voltammograms due to the lack of a reliable baseline for background corrections. These results imply that the real surface area of the Pt_{black} did not change significantly during the deposition of Ru_{ad}. It appears then that the use of CO_{ads} stripping voltammetry is a reasonable method for the estimation of real surface areas of Pt_{black}-Ru_{ad} electrocatalysts.

Evolution of Ru_{ad} modified Pt_{black} surfaces. An alternate method to estimate changes in the specific surface area of the Pt_{black}-Ru_{ad} electrocatalysts is to remove the Ru_{ad} from the surface and measure the real surface area of the underlying Pt_{black} substrate using the cathodic hydrogen charge. The repetitive potential cycling of Pt-Ru electrodes to an upper potential limit in excess of 0.9 V is known to result in a loss of Ru from the surface.[36] The evolution of Pt_{black}-Ru_{ad} over a range of coverages was examined by repetitive potential sweeps up to an anodic limit of 1.40 V. Figure 4.7 shows the electrochemically induced evolutions of a series of Pt-Ru_{ad} deposits with initial surface coverages ranging from 0.053 to 0.68 eq Ru_{ad}. Similar voltammetric behavior has been reported by Szabo and Bakos.[36]

These measurements are based on the assumption that the potential cycling does not cause the sintering of the particles constituting the deposit. During potential cycling the adatoms are either dissolved into the electrolyte or incorporated into the bulk of the metal particles. During extended periods of potential cycling there was a slow evolution of the electrochemical fingerprints of the Pt-Ru_{ad} surfaces to those expected of Pt_{black}. That the resulting surfaces are pure Pt was further confirmed by repeating the CO_{ads} stripping voltammetry. Peak potentials of ~0.780 V were consistently observed for surfaces that exhibited the electrochemical fingerprints of pure Pt and this is the value expected for a Pt surface under these conditions (Figure 4.3). The specific surface areas of the evolved Pt_{black}-Ru_{ad} deposits were determined from the cathodic hydrogen charges using according to the standard method (Chapter 2) and the results are summarized below in Table 4.5. In all cases the estimates of the specific surface area of the stripped Pt_{black}-

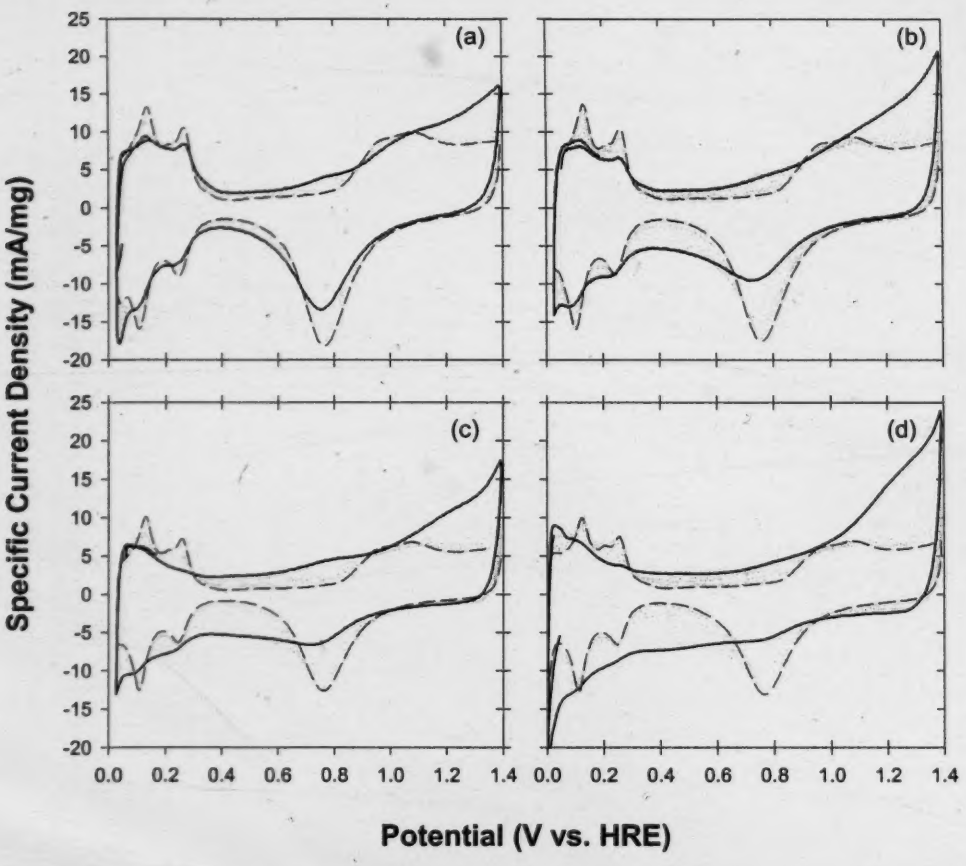

Figure 4.7. Stripping of Ru_{ad} from Pt_{black}-Ru_{ad} deposits during potential cycling in 1.0 M H_2SO_4(aq) at 50 mV/s ((a) 0.053, (b) 0.29, (c) 0.46, and (d) 0.68 eq Ru_{ad}). The solid lines are the initial sweeps, the dashed lines are the final sweeps, and the hairlines show the intervening sweeps.

Ru_{ad} powders were ~20 % lower than the initial specific surface area of the Pt_{black} substrate. The decrease in measured surface area is likely a result of surface annealing during potential cycling to the upper limit of 1.4 V. That the specific surface areas are slightly lower could also be a result of incomplete contact of the deposit to the smooth Pt support after long term potential cycling and/or dissolution of part of the surface.

Evaluation of Pt_{black}-Ru_{ad} electrocatalysts in the anodes of direct methanol fuel cells. A series of Pt_{black}-Ru_{ad} electrocatalysts were incorporated into the anodes of

membrane electrode assemblies that were evaluated using commercial DMFC hardware. These membrane electrode assemblies were prepared using the decal transfer methods.[5] It is well known that the utilization of the electrocatalyst is often significantly less than 100% in a fuel cell electrode.[37] In order to compare the activities of electrocatalysts as a function of their surface composition the utilization of the catalysts inside the operating fuel cell must be known. The electrochemical characterization of the anodes and cathodes of a prototype DMFC enables the evaluation of the intrinsic activity of $Pt_{black}Ru_{ad}$ towards the anodic oxidation of CH_3OH. The anodes and cathode electrocatalysts were characterized using cyclic voltammetry (CV). The optimum surface composition for CH_3OH oxidation inside an operating prototype DMFC was identified. The electrocatalyst loadings for the anodes and cathodes were all ~2 mg/cm^2 and the Nafion® loadings were ~0.6 mg/cm^2.

Electrochemical characterization of thin film anodes and cathodes. The electrodes were conditioned inside the fuel cell (as described in detail in the experimental section) prior to recording their polarization curves. Although the electrochemical characterization of the electrodes was performed after the performance evaluation experiments the results are described first to facilitate the interpretation of the results.

Figure 4.8 shows voltammograms of the anodes and cathodes for a series of membrane electrode assemblies after several days of operation at 90 °C. The voltammograms were recorded at 25 °C in the fuel cell test block as described by Gottesfeld *et al.* (i.e., the working electrode (either the anode or the cathode of the fuel cell) was placed under purified water, and the opposite electrode was used as both counter and reference (R/CE) by placing it under 1 atm of humidified $H_2(g)$).[2] The electrocatalyst utilization factors for the cathodes were used to normalize the polarization curves and thus facilitate comparisons of DMFC performance as a function of θ_{Ru}. The scaled specific current densities are those that would be observed if 100 % of the anode electrocatalyst were electrochemically active.

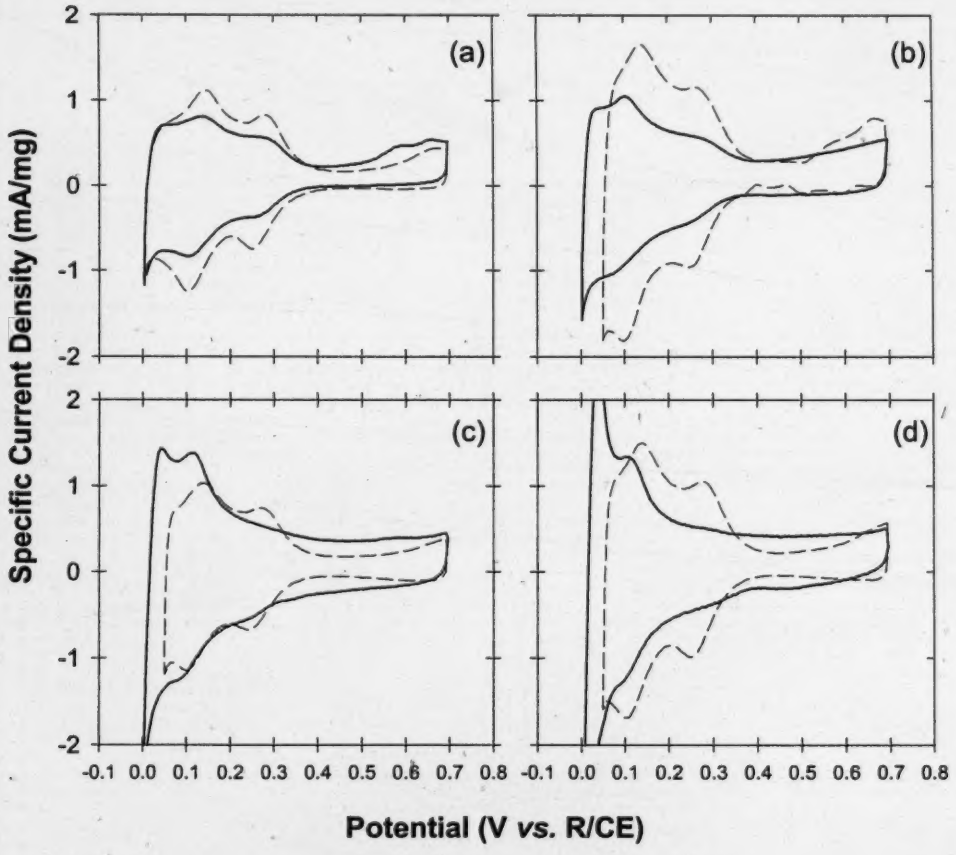

Figure 4.8. Cyclic voltammograms of a series of DMFC anodes (solid lines) and cathodes (dashed lines) at 10 mV/s. The anode surface compositions are (a) 0.0535, (b) 0.29, (c) 0.46, and (d) 0.68 eq Ru_{ad}. The currents are normalized to the mass of the electrocatalyst present.

In order to obtain valid comparisons between DMFC on the basis of the anode electrocatalyst compositions the polarization curves were adjusted to reflect the amount of active electrocatalyst at the anode. The utilization of the cathode catalyst (and presumably also of the anode catalyst) was determined by comparing the initial real surface area of the Pt_{black} to the real surface area of the cathode Pt_{black} measured in the cell (*vide infra*) by cyclic voltammetry. The active fraction of electrocatalyst (i.e., electrocatalyst utilization factor) can only be measured directly for the Pt electrocatalysts.

The real areas of the cathode electrocatalysts were determined from the integrated charge in the hydrogen region of the voltammograms then compared to the values expected from the electrocatalyst loadings and the known specific surface area of Pt_{black} (i.e., 28 m^2/g) to determine the electrocatalyst utilization factors. The utilization factors for the Pt_{black} cathodes range from 40 to 70%. A visual comparison among the voltammograms of the anodes and their corresponding cathodes shows that they are of similar sizes and thus the utilization factors of the anode and cathode electrocatalysts in the same cell were assumed to be similar.

The voltammograms of the thin film anodes exhibit the same trends with increasing θ_{Ru} as seen for the catalysts prior to hot pressing. This is an indication that the Pt_{black}-Ru_{ad} surfaces are stable throughout the MEA fabrication procedure, and during the cell conditioning process. Cyclic voltammograms of the anodes shown in Figure 4.8 are similar to those of the same electrocatalysts prior to incorporation into the fuel cells (Figure 4.4). Thus it appears that these Pt_{black}-Ru_{ad} surfaces do not change their composition during the fabrication of membrane electrode assemblies.

Direct methanol fuel cell polarization and power curves. In order to ensure that accurate comparisons could be made between cells based upon the effects of Ru surface coverage of the anode electrode standard methods were established for the startup, conditioning, performance evaluation, shutdown, and voltammetry of the electrodes. The operating conditions used to compare the performance of direct methanol fuel cells as a function of the anode surface composition were optimized and the following standard conditions were adopted. The anode requires an optimized concentration of methanol and suitable rate of flow of aqueous methanol through the cell in order to ensure that reactants and products are effectively transported to and from the reaction zones. The flow rate used for all polarization curves was 3.5 ml/min of 1.0 M CH_3OH(aq). 1.0 M CH_3OH is the optimum fuel concentration and 3.5 ml/min was the most suitable flow rate. As the concentration of methanol increases the potential at low current densities decreases and the potentials at high current densities increase. The optimum concentration of CH_3OH depends on the instantaneous current load on the cell. The fuel reservoir contained 75 to 100 ml of deoxygenated CH_3OH solution and was kept under an Ar(g) atmosphere. There was sufficient CH_3OH to eliminate any significant change in

the concentration of the fuel solution over several hours of operation under typical current loads. The cathode was operated at elevated pressure and a rapid flow of pure $O_2(g)$ was maintained through it in order to minimize the deleterious effects of CH_3OH crossover. The increased pressure improves the kinetics for the O_2 reduction reaction and the increased flow rate speeds the removal of H_2O and CH_3OH from the cathode reaction zones. The flow rate of $O_2(g)$ was 600 ml/min and the cathode side of the cell was maintained at 20 psig during the performance evaluation of the fuel cells. To record the polarization curves the cell potential was stepped between upper and lower limits in 50 mV increments and the stable current recorded after 30 s. The optimum operating temperature is 90 °C. The geometric area of the fuel cell electrodes is 5 cm^2.

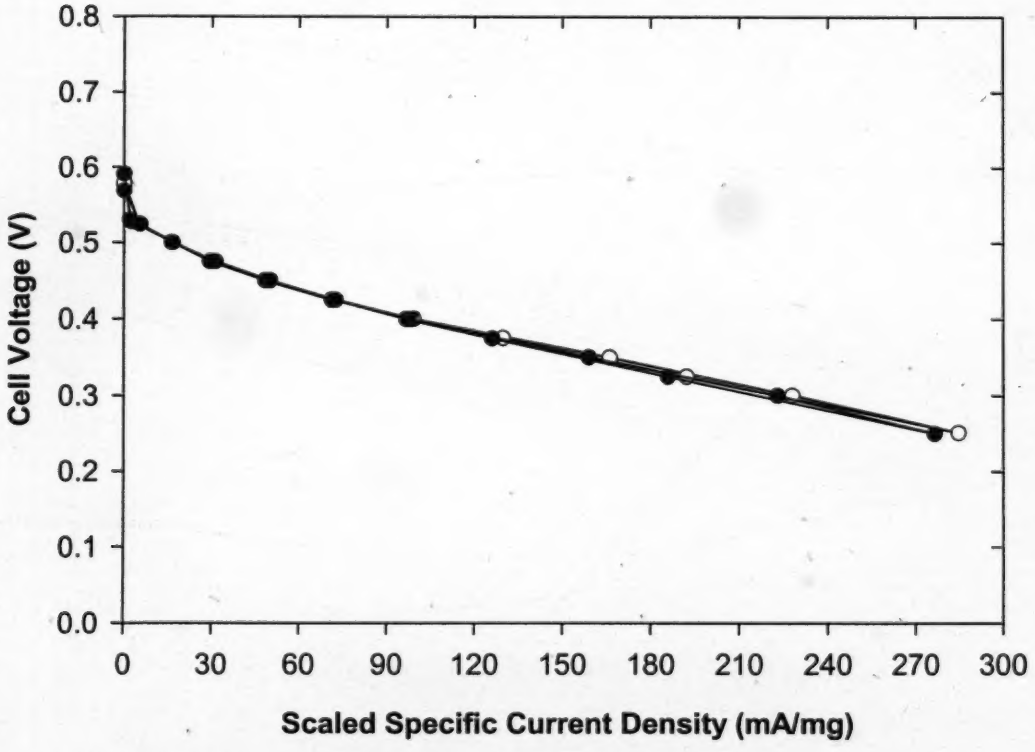

Figure 4.9. Polarization curves recorded at 90 °C for a Pt_{black}-Ru_{ad}(0.29 eq Ru_{ad})//Nafion® 117//Pt_{black} DMFC recorded before (solid circles) and after (open circles) several days of operation. Anode: 1.0 M methanol at 3.5 mL/min. Cathode: 20 psig $O_2(g)$ at 600 mL/min.

Figure 4.9 shows polarization curves for a DMFC with a 0.29 eq Ru_{ad} anode catalyst that was conditioned and operated intermittently for several days under the conditions outlined above. The cell was subjected to daily start-up and shutdown procedures (details are given in the experimental section). Comparison of the polarization curves in Figure 4.9 reveals that they are essentially identical, indicating that once the cell is conditioned its performance is stable and reproducible. Provided that the performance limiting factor is the anode electrocatalyst activity it is reasonable to conclude that the surface composition of the anode electrocatalyst does not change during the operation of the fuel cell. Further evidence for this is shown in Figure 4.10. The figure shows

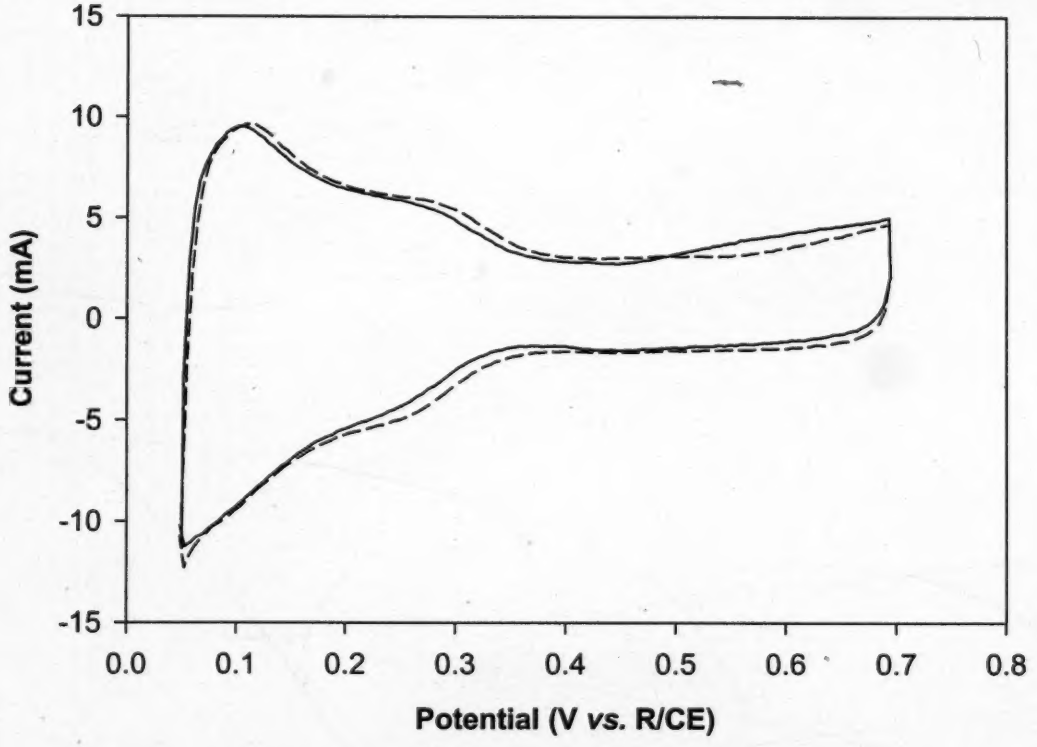

Figure 4.10. Cyclic voltammograms of a 0.29 eq Ruad anode before (solid line), and after (dashed line) several days of intermittent operation. The voltammograms were recorded at 10 mV/s.

voltammograms recorded after the first and final days operation. That the voltammograms are almost identical indicates that there was no change in the surface composition of the anode electrocatalyst during the extended operation of this fuel cell.

The effects of surface composition on DMFC performance. Figure 4.11 shows the polarization curves for a series of Ru_{ad} modified Pt_{black} anode electrocatalysts recorded at 90 °C under standard operating conditions. In order to compare polarization curves as a function of anode surface composition the differences in the electrocatalyst utilization factors must be accounted for. The current densities are quoted in mA/μmol surface atoms and they are scaled to the electrocatalyst utilization factors (*vide supra*).

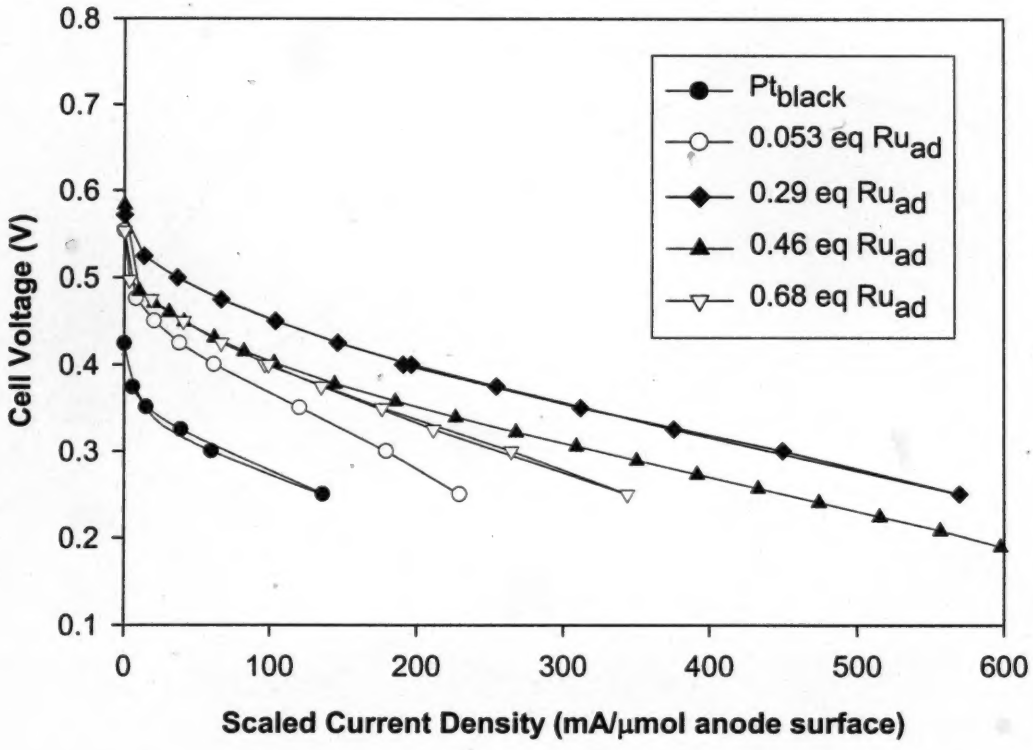

Figure 4.11. Polarization curves for a series of Pt_{black}-Ru_{ad}//Nafion® 117//Pt_{black} DMFC at 90 °C. Anode: 1.0 M methanol at 3.5 ml/min. Cathode: 20 psig O_2(g) at 600 ml/min.

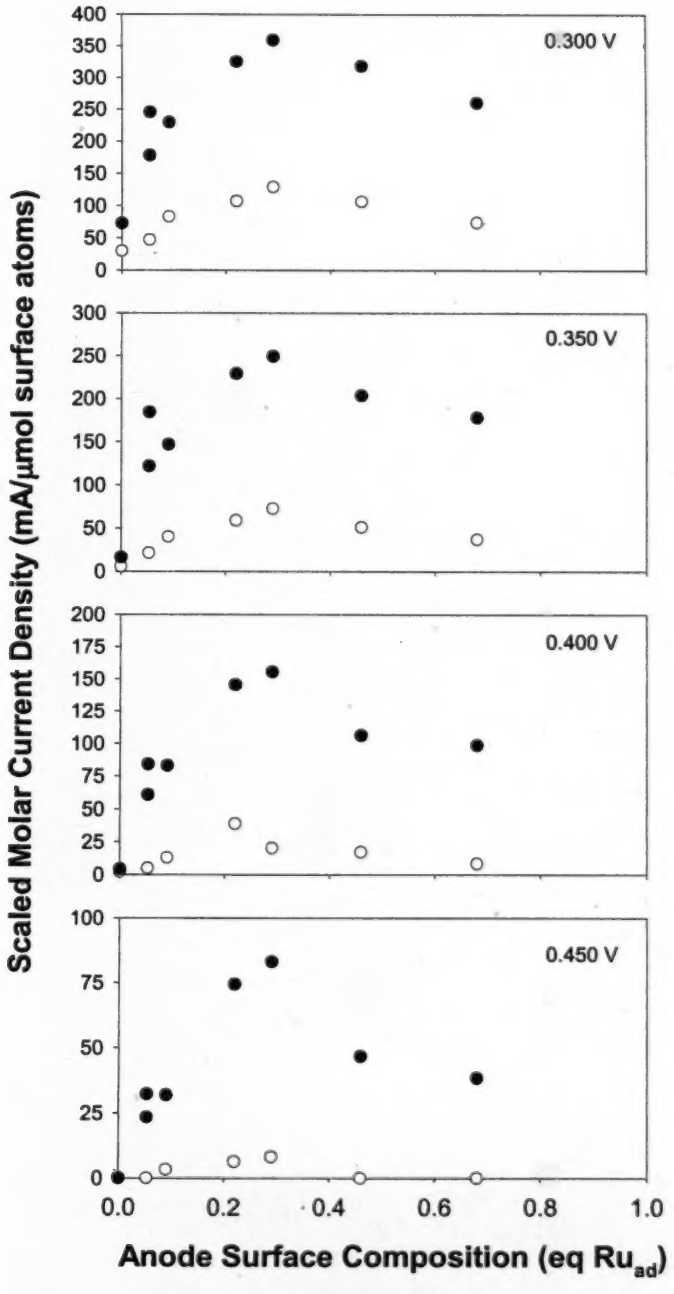

Figure 4.12. The optimum surface composition of Ru_{ad} in operating DMFC (open circles = 60 °C, filled circles = 90 °C).

As expected the Pt_{black} anode exhibits characteristically poor performance. The activity of the Pt_{black}-Ru_{ad} anodes increases in the order: 0.0530 eq Ru_{ad}, 0.29 eq Ru_{ad}. Beyond 0.29 eq Ru_{ad} the performance of the fuel cells begins to decrease with increasing θ_{Ru} and the 0.46 and 0.68 eq Ru_{ad} anode catalysts exhibit similar performance characteristics. The polarization curves reveal a trend towards maximum activity as the surface composition approaches 20 to 30 % Ru_{ad}. This optimum composition is higher than that observed in experiments using Ru_{ad} modified Pt gauze electrodes (Chapter 3). Such an increase in optimum surface composition is likely a result of the elevated operating temperature of the fuel cells relative to the experiments reported in Chapter 3. As was noted in the work of Gasteiger *et. al,* Ru surface atoms are able to adsorb CH_3OH as well as provide the required surface oxide at higher temperatures.[38] The effects of anode composition on a larger number of cells are summarized in Figure 4.12. The scaled specific current densities at 60 and 90 °C are plotted *vs.* the Ru_{ad} coverage for cell voltages ranging from 0.50 to 0.30 V. It is apparent that the relative improvements in performance for the series of coverages examined, relative to Pt_{black} are both temperature and potential dependent, as is already known from the work of Gasteiger *et al.* for pure alloy electrodes.[38] A notable increase in the observed current densities is apparent for anodes with an optimum Ru surface coverages of 20 to 30 %. The optimum Pt_{black}-Ru_{ad} surface composition is ~ 0.30 eq Ru_{ad} at all cell voltages and temperatures studied.

Summary and Conclusions

The self-directing organometallic deposition of Ru_{ad} on Pt substrates can be used to deposit known amounts of Ru_{ad} onto nanoscale Pt particles of known initial specific surface area. The results of CO_{ads} stripping voltammetry on Ru_{ad} modified blacked Pt-Ru_{ad} gauzes and on Pt_{black}-Ru_{ad} particles as well as those obtained from the electrochemically induced evolution of the Pt_{black}-Ru_{ad} electrocatalyst deposits indicated that there were no significant changes in the real surface area of the substrates during the deposition of Ru_{ad}. The assumption that the specific surface area of the Pt_{black} does not change significantly during the self-directing deposition reaction appears to be reasonable. The Pt_{black}-Ru_{ad} powders described in this chapter are the first series of

nanoscale, bimetallic, Pt-Ru particles with known specific surface area and surface compositions to be used in prototype direct methanol fuel cells.

The lifetime of Ru_{ad} atoms on the surface of the Pt_{black} substrates described in this and preceding chapters exceeded all of the experimental time-scales examined thus far. The electrochemical characterization of Ru_{ad} modified Pt_{black} particles can be used to provide rough estimates of the surface compositions of these electrocatalysts according to their electrochemical fingerprints. That potentials in excess of 0.9 V must be applied for a considerable amount of time to remove the Ru_{ad} attests to the stability of these Pt_{black}-Ru_{ad} electrocatalysts. It is not probable that a DMFC anode will reach such a high potential in the absence of some catastrophic cell failure. These results indicate that Ru_{ad} modified Pt_{black} surfaces are stable and are therefore worthy of consideration for further evaluation in prototype DMFC's. In the future, long-term (i.e., months) operation of these DMFC's should be carried out to substantiate the claim of Ru adatom stability on Pt surfaces.

The addition of Ru_{ad} led to an increased performance relative to Pt_{black} at all Ru_{ad} coverages examined. The performance of $Pt_{black}(Ru_{ad})$ electrocatalysts in DMFC using standard operating conditions was examined. The intrinsic activity of Pt_{black}-Ru_{ad} particles for the electrooxidation of CH_3OH depends on the surface coverage of Pt_{black} by Ru_{ad}. The increase in optimum Ru_{ad} content can be attributed to the ability of Ru to activate CH_3OH at elevated temperatures.[38] These results indicate that significant improvements in DMFC anode performance may be realized by reducing the particle sizes and controlling the surface composition.

The self-directing deposition of Ru on Pt can be used to prepare electrocatalysts for direct methanol fuel cells. These Pt-Ru_{ad} surfaces are stable for long periods of time in operating direct methanol fuel cells. The self-directing deposition of Ru_{ad} on Pt enables valid comparisons of intrinsic activities of bimetallic Pt-Ru surfaces with defined surface compositions for CH_3OH oxidation. The optimum surface ratio of Ru to Pt for CH_3OH oxidation in a DMFC is 0.2 to 0.3 equivalents. These Pt-Ru_{ad} catalysts are not subject to surface enrichment during MEA fabrication or their preparation due to the absence of any extreme thermal treatments.

Experimental Section

The details of the electrochemical instrumentation, chemicals and materials used, as well as the standard purification procedures for reagents and solvents are the same as outlined in the experimental sections of the previous chapters. Any exceptions and new experimental procedures are described below.

Chemicals and materials. Hexadecane and octadecyltrichlorosilane were obtained from Aldrich, Inc. Nafion® solution (5 wt % Nafion® in a mixture 2-propanol, 1-propanol, and H_2O) and Pt/C (20 wt% Pt on Vulcan XC-72 carbon powder) were obtained from ElectroChem, Inc. Fuel cell grade Pt_{black} was obtained from Johnson Matthey & Sons, Inc. Pt-Ru/C (1:1 atomic ratio, 20 wt% metal on Vulcan XC-72 carbon powder was obtained from E-Tek, Inc.

The reaction vessels were thick walled glass pressure tubes with an internal diameter of 1.5 cm and a capacity of 25 ml, 4 x 14 mm Teflon® coated magnetic stirbars were placed into the reaction vessels before cleaning them. The reactors were cleaned by filling them with Pirhana (Chapter 2, Experimental Section) and allowing them to soak for 1 h, they were then rinsed with copious amounts of H_2O and dried in an oven at 110 °C. The clean hydrophillic vessels were subsequently rendered hydrophobic by silating them using a dilute solution of octadecyltrichlorosilane in hexadecane according to a literature procedure.[39] The silated vessels were rinsed with hexanes, H_2O, acetone, and finally hexanes again and dried in an oven at 110 °C prior use. This treatment stopped the Pt substrates (Pt_{black} or 20 wt% Pt/C) from sticking to the walls of the reaction vessels during hydrogenations. The reaction vessels had pop-bottle tops and could be sealed using flat rubber septa that were held in place by crimped stainless steel caps. There were 2 small holes though the caps to allow needles to be passed though the rubber septa into the otherwise sealed reaction vessels. All rubber septa were extracted as described in Chapter 2.

The polymer electrolyte fuel cell hardware was a purchased from ElectroChem, Inc. The polarization curves were obtained using an 890 Series Fuel Cell Test System

(Scribner Associates, Inc.). The reported polarization curves are not IR compensated. A JEOL 2010 Transmission Electron Microscope equipped with a Noran energy dispersive X-ray spectrometer, carbon support films on 150 mesh copper grids were obtained from Electron Microscopy Sciences, Inc.

Electrode construction and electrochemical cells. The electrochemical cells were 3-necked 50 ml round bottom flasks. A D-porosity glass frit sealed the end of a glass tube that was inserted through one neck, and served to isolate the counter electrode from the bulk electrolyte. The electrochemical cells and the glass frits were cleaned by rinsing with Pirhana solution and then rinsing with copious amounts of H_2O prior to use. The working electrode support was a 1 cm^2 Pt foil bonded to a 7.5 cm length of 20 gauge Pt wire that was sealed in a 5 cm length of 4 mm diameter glass tube, it was constructed according to an established literature method.[40] The counter electrode (CE) was a partially blacked 15 cm Pt wire coil. A self-contained hydrogen reference electrode was constructed according to modified literature methods.[41, 42] The potential of a charged HRE is ~ 0 V *vs.* SHE and it is stable over periods of 24 h or more. Cyclic voltammograms were recorded in Ar(g) purged 1.0 M H_2SO_4(aq) at room temperature of ~ 20 °C under an Ar(g) atmosphere.

Electrochemical characterization of electrocatalyst powders. The electrocatalyst powders (Pt_{black}, Pt_{black}-Ru_{ad}, and 20 wt% Pt/C, and 20 wt% Pt-Ru_{ad}/C) were supported on a Pt foil and held in place by a thin Nafion® overlayer for electrochemical characterization. The construction of the Pt foil electrode was described in the previous section and the preparation of the complete working electrode is described forthwith. An aqueous suspension of the electrocatalyst powder was prepared (5 mg catalyst in 1.00 mL). The suspensions were sonicated for ~ 1 h prior to use. A disposable micropipet was used to place 50 μL of the suspension onto the Pt foil. The deposit was then dried in an oven for 15 min then allowed to cool back to ambient temperature prior to the application of 50 μL of a 5 wt % Nafion® solution. The solvents were evaporated by returning the electrode to the oven for an additional 15 min and the resulting electrode was allowed to cool to ambient temperature prior to use.

The Nafion® bound deposits were immersed into 1.0 M H_2SO_4(aq), an idle potential of 50 mV applied upon contact of the electrode with the electrolyte prior to

initiating any electrochemical experiments. Cyclic voltammograms of Pt_{black} and 20 wt % Pt/C deposits were recorded at 50 mV/s and 20 mV/s respectively between 50 and 1400 mV *vs.* HRE. The upper potential limit was reduced to 900 mV when Ru_{ad} was present on the electrocatalyst.

Anodic stripping of adsorbed carbon monoxide. The surfaces were saturated with CO_{ads} by bubbling CO(g) through the electrolyte at a constant potential of 50 mV for 10 min. The electrolyte was then purged with Ar(g) for 5 min in order to remove CO from the electrolyte prior to initiating potential sweeps at 50 mV/s.

Deposition of Ru_{ad} on Pt_{black}. The metal powder (~125 mg) was first weighed into reaction tube (in air) then wetted with 1.5 ml of pure water and immersed into an ice bath. A slow dropwise addition of 1.5 ml H_2O_2(aq) (1.5 %) resulted in vigorous gas evolution and the oxidative cleaning of the Pt_{black} powder (substrate). The catalyst was allowed to settle and the majority of the water was removed using a disposable pipet. The reaction flask was sealed with a pop-top and a 20 gauge needle connected to high vacuum was inserted into the vessel and used to remove the remaining water. Prior to total dryness another needle connected to a hydrogen generator was inserted into the reactor. The reactor was then filled with H_2(g) ($P(H_2)$ ~1 atm) then evacuated and flushed with $Ar_{(g)}$, this cycle was repeated until the Pt_{black} powder appeared totally dry. The reactor was finally placed under a H_2(g) atmosphere. The complete removal of H_2O is required prior to proceeding with the reaction due to blockage of the Pt surface by interaction of H_2O(l) with Pt(oxide) and Pt(hydride) surfaces. It is expected that the Pt(oxide) surface will be hydrophillic and the Pt(hydride) surface will be hydrophobic. The repetitive evacuation and refilling with both pure Ar and pure H_2 sped up the drying process. The dried Pt-H_{ads} surface was left under bubbler pressure H_2 prior to the addition of a hexane solution of (COD)Ru(π-allyl)$_2$ and n-decane. The temperature was maintained at - 42 °C using an acetonitrile/CO_2(s) slush bath.[43] Volume of hexane saturated with hydrogen used during the reaction is 15.0 ml. The stir rate used for all of the hydrogenations was 900 rpm (it was measured with a strobe light).

During the hydrogenations aliquots (typically 250 μL) of the reaction mixture could be periodically removed by interrupting the hydrogenation reaction. At the desired coverage the deposition reaction was terminated as follows. The stirring was stopped and

the powder allowed to settle, the supernatant was removed using a 20 gauge cannula (2-5 ml of the supernatant were transferred to a stoppered vial for GC analysis) the solid Pt_{black}-Ru_{ad} was rinsed three times with 5 ml portions of Ar(g) saturated hexanes (brief stirring and allowed powder to settle prior to removing supernatant.).

Deposition of Ru_{ad} on 20 wt% Pt/C. The Pt_{black}-Ru_{ad} was dried under high vacuum and the product stored under Ar(g). The hydrogenation was carried out as follows 20 wt% Pt/C (131.2 mg, 62.22 mol Pt surface), 28 mg Ru precursor and 31.27 mol decane at -42 °C for 30 min. After 30 min the reaction was terminated by purging the solution with CO and a centrifuge was used to isolate the Pt-Ru_{ad}/C powder from a diluted CO saturated reaction solution. GC analysis of a portion of the reaction solution removed after saturating with CO indicated an Ru_{ad} coverage of 0.46 surface equivalents.

Transmission Electron Microscopy and Energy Dispersive X-Ray Analysis. Thin films of Pt_{black}-Ru_{ad} and PtRu/C were cast on carbon films supported by Cu grids (150 mesh). Suspensions of Pt-Ru/C alloy and the (0.27) Pt-Ru_{ad}/C (1.5 mg supported metal powder in 1.5 mL of 2-propanol) and of Pt_{black} (1.5 mg Pt_{black}-Ru_{ad} in 250μL H_2O) were sonicated and periodically shaken for at least 1h prior to use. Carbon film supported by Cu grids (150 mesh) was placed on filter papers and 1 drop (~ 50 μL) of the appropriate suspension was applied and allowed to dry at ambient temperature in air for several hours prior to TEM and EDS analysis. The majority of the droplet spilt over the filter paper and a very small amount of sample was retained on the Cu grid supported C film.

Direct methanol fuel cell hardware and electrochemical testing apparatus. The fuel cell hardware consists of a pair of graphite cell blocks and gold plated current collectors with attached heating pads. There are standard thread holes in the blocks to attach the feed and exhaust for each electrode. There was a 5 cm^2 serpentine flow pattern machined into the center of each of the graphite cell blocks. A membrane electrode assembly and a pair of silicon or Teflon® gaskets are sandwiched between the blocks and current collectors. The assembled components of the fuel cell are held together with 8 bolts passing through holes around the perimeter of the cell. The electrical connections to the cell are on the current collectors for the current measuring circuit and via banana plugs inserted directly into the cell blocks to connect the voltage measuring circuit.

There are small hole drilled into the graphite blocks to insert a thermocouple so that the temperature of the cell can be monitored and controlled using the attached heaters.

A liquid chromatography pump was used to circulate H_2O or 1.0 CH_3OH(aq) through the anode electrode compartment of the cell. The pump was calibrated using a 25 ml graduated cylinder and stopwatch. The pressure of O_2(g) was controlled using a two-stage regulator and measured using a pressure gauge positioned between the cathode exhaust and a back pressure regulating valve. A flowmeter at the end of the cathode exhaust was used to measure the flow rates.

The flow directions were chosen to facilitate the removal of CO_2(g) from the anode and H_2O from the cathode side during the operation of the cell. The system was setup with an Ar(g) purging line in the H_2 and O_2 gas feeds so that either the anode or cathode could be setup for use as the working electrode (WE) for electrochemical characterization without exposing the electrode to the atmosphere.

Preparation of Membrane Electrode Assembly and Operation of the DMFC. The membrane electrolyte assemblies were made using the decal transfer method developed at Los Alamos National Laboratory by the Gottesfeld group.[5, 44, 45] A series of Pt_{black}-Ru_{ad} powders obtained from the hydrogenation of **1** and , Pt_{black} were used as the anode catalysts. The cathode electrocatalyst used throughout was Pt_{black}. To make the catalyst/ionomer ink, the catalyst was first suspended in a small amount of water and agitated in an ultrasonic bath for 30 min to thoroughly wet and disperse the catalyst. There is a tendency for the alcoholic Nafion® solutions to ignite if the catalyst is not wetted with water first. Enough 5 wt% Nafion® solution (ElectroChem, Inc.) was then added to the mixture to give a dry ink composition of 80 wt % electrocatalyst with 20 wt % Nafion® ionomer. The mixtures were sonicated for 2 h to obtain uniformly dispersed inks. The Nafion® 117 membranes were cleaned and converted into the acid form by boiling in 3% H_2O_2 for 1 h, followed by boiling in 0.5M H_2SO_4 for 1 h, and finally boiling in ultra-pure water for 1 h. The cleaned membranes were dried on a heated vacuum table at 60 °C prior to use. The decal blanks prepared from Teflon® Coated Glass Cloth tape (A & M Tape Products, Inc.). A 2 inch piece was reinforced by sticking a 1 inch piece of tape with the grain going perpendicular across the center of the backside of the tape. Short tabs were cut out of the extending ends of the tape. The geometric area of

the blanks was 5 cm^2. The blanks were weighed prior to being placed on a stainless steel plate on top of a hot plate with a surface temperature of 50 to 75 °C. The desired ink was removed from the ultrasound bath and applied to the appropriate blank using a #1 gold sable brush. The brush was cleaned with methanol, H_2O, 2-propanol prior to use. Several coats of the catalyst inks were applied in a perpendicular direction to the previous one. The ink was not allowed to dry completely during the application process. When the desired coverage was obtained (approximated by the amount of ink applied) the decals were placed in covered petrii dishes and heated in an oven at 110 °C for 10 to 15 min. The decals were removed from the oven and allowed to cool to ambient temperature. The change in the mass of the decal and the decal blank was used to determine an accurate value for the electrocatalyst and Nafion® content of the electrodes after being laminated onto the pre-treated Nafion® membranes. The ink loading was determined from the difference in weight of the decal blanks and the painted decals (typically ~ 15 mg) and the electrocatalyst loading was determined from ink loading and the calculated dry composition of the ink. The catalyst inks were painted onto 5 cm^2 Teflon decals to give a metal loading of approximately 2 mg/cm^2. The catalyst inks were transferred from the Teflon decals to the Nafion® membrane by hot-pressing (120 to 127 °C, 1400 to 1500 psi for ca. 2 min). The membrane electrolyte assemblies were then mounted into the fuel cell hardware using 5 cm^2 Teflon® treated Toray® carbon papers (ElectroChem. Inc.) as the electrode backings. Figure 4.13 is a composite of black and white photographs of the hot press apparatus that was constructed in house. Also shown in the figure are photos of a cell block and the same cell block with a Teflon® gasket and a completed MEA laid over top of it. The complete assembled cell with electrical connections and connections to fuel and oxidant inlets and outlets are also shown.

Prior to recording polarization curves the fuel cell electrodes were conditioned. The procedure used to condition the electrodes prior to recording any polarization curves or cyclic voltammograms is as follows. First, Ar(g) purged H_2O was passed through the anode side at 3.5 ml/min, and O_2(g) was passed through the cathode side at ~100 ml/min. After a few minutes the H_2O reservoir was exchanged for one containing ~100 ml of Ar(g) purged, aqueous CH_3OH (1.0 M) that was then pumped through the cell at the same flow rate. The observed open circuit potential increased once the CH_3OH solution

entered the cell then decreased to a stable value of ~0.5 V after a few minutes. The CH_3OH exhaust outlet was transferred from the waste container to the reservoir and feed solution was allowed to circulate under an Ar(g) atmosphere. The CH_3OH solution was periodically replaced during extended periods of fuel cell operation. The cell was heated to 60 °C under open circuit conditions and a current load of 50 mA applied. Under these conditions a stable voltage of 0.35 to 0.45 V was observed. The cell was operated under these conditions for several hours prior to increasing the cathode pressure to 20 psig and the flow rate to 600 ml/min. Prior to recording any polarization curves the cells were conditioned for at least 4 h for the first startup and for 1 to 4 h during longer term cell testing. Steady-state polarization curves were recorded at 60 and 90 °C.

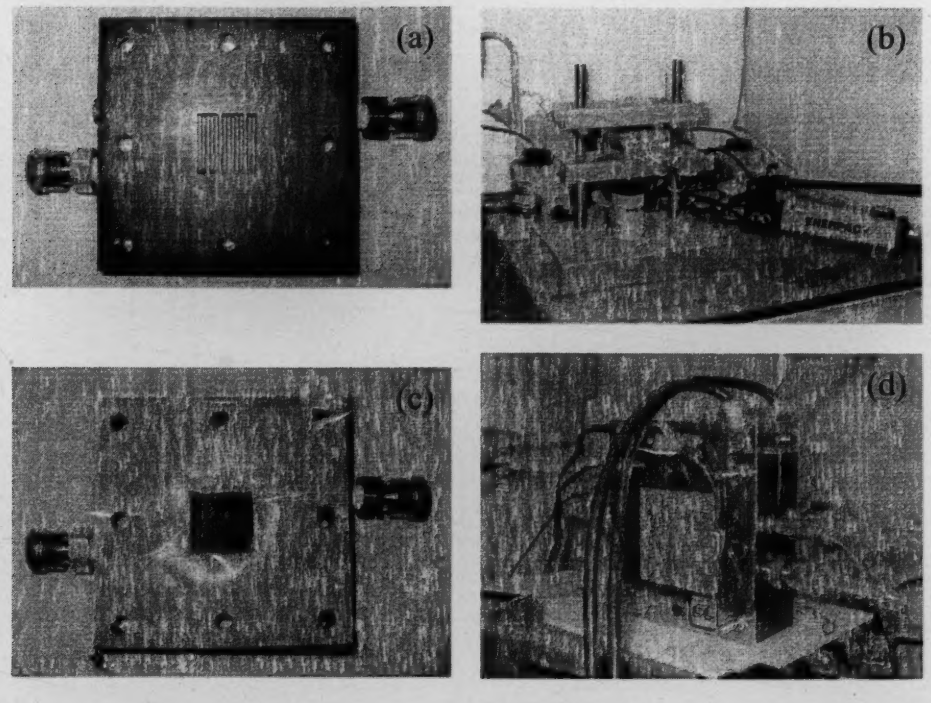

Figure 4.13. Photos of fuel cell hardware and of the heated press used for MEA fabrication; (a) Graphite cell block, (b) heated press showing the heated aluminum blocks, hydraulic press and the power regulators for heating the assemblies, (c) a completed MEA laid over a Teflon® gasket and the cell block shown in (a), and (d) the assembled fuel cell hardware showing connections to test-stand apparatus (not shown), fuel and oxidant feeds.

Electrochemical characterization of fuel cell electrodes. Cyclic voltammograms of the anodes and the cathodes were recorded after conditioning the cells and recording polarization curves at 90 °C. The voltammograms were recorded at 25 °C in the fuel cell test block as described by Gottesfeld *et al.*[2] - the working electrode was placed under H_2O, and the opposite electrode was used as both counter and reference by placing it under 1 atm of humidified $H_2(g)$. In order to perform cyclic voltammetry experiments inside the fuel cell one of the electrodes is made the reference and counter electrode using humidified $H_2(g)$ to provide a stable reference electrode (CE/RE). The working electrode is subjected to deoxygenated H_2O. In order to obtain voltammograms of the fuel cell electrodes the following procedure was used. The O_2 was purged from the cathode side with Ar(g) prior to starting $H_2(g)$ flow. The cathode electrode was humidified passing the $H_2(g)$ through H_2O in a heated gas washing bottle. The anode side was rinsed with deoxygenated H_2O at 3.5 ml/min for 10 - 15 min.

References

(1) Waszczuk, P.; Solla-Gullon, J.; Kim, H. S.; Tong, Y. Y.; Montiel, V.; Aldaz, A.; Wieckowski, A. *J. Catal.* **2001**, *203*, 1.

(2) Dinh, H. N.; Ren, X. M.; Garzon, F. H.; Zelenay, P.; Gottesfeld, S. *J. Electroanal. Chem.* **2000**, *491*, 222.

(3) Parsons, R.; VanderNoot, T *J. Electroanal. Chem.* **1988**, *257*, 9.

(4) Cao, D.; Bergens, S.H. *J. Electroanal. Chem.* **2002**, *533*, 91.

(5) Ren, X. M.; Wilson, M. S.; Gottesfeld, S. *J. Electrochem. Soc.* **1996**, *143*, L12.

(6) Xing, Y. unpublished results.

(7) Starz, K.A.; Auer, E.; Lehmann, Th.; Zuber, R. *J. Power Sources* **1999**, *84*, 167.

(8) Stonehart, P.; Ross, P. N. *Electrochim. Acta* **1976**, *21*, 441.

(9) McBreen, J.; O'Grady, W.E.; Pandya, K.I.; Hoffman, R.W.; Sayers, D.E. *Langmuir* **1987**, *3*, 428.

(10) Pattabiraman, R.; Vasu, K.I. *Bull. Electrochem.* **1993**, *9*, 352.

(11) Rush, B. M.; Reimer, J. A.; Cairns, E. J. *J. Electrochem. Soc.* **2001**, *148*, A137.

(12) Long, J. W.; Stroud, R. M.; Swider-Lyons, K. E.; Rolison, D. R. *J. Phys. Chem. B* **2000**, *104*, 9772.

(13) Solla-Gullon, J.; Montiel, V.; Aldaz, A.; Clavilier, J. *J. Electroanal. Chem.* **2000**, *491*, 69.

(14) Niedrach, L.W. J. *Electrochem. Soc.* **1964**, *111*, 1309.

(15) Schmidt, T. J.; Gasteiger, H. A.; Stab, G. D.; Urban, P. M.; Kolb, D. M.; Behm, R. J. *J. Electrochem. Soc.* **1998**, *145*, 2354.

(16) Hadzi-Jordanov, S.; Angerstein-Kozlowska, H.; Vukovic, M.; Conway, B. E. *J. Phys. Chem.* **1978**, *125*, 1471.

(17) Waszczuk, P.; Solla-Gullon, J.; Kim, H. S.; Tong, Y. Y.; Montiel, V.; Aldaz, A.; Wieckowski, A. *J. Catal.* **2001**, *203*, 1.

(18) Herrero, E.; Feliu, J. M.; Wieckowski, A. *Langmuir* **1999**, *15*, 4944.

(19) Crown, A.; Wieckowski, A. *Phys. Chem. Chem. Phys.* **2001**, *3*, 3290.

(20) Crown, A.; Moraes, I. R.; Wieckowski, A. *J. Electroanal. Chem.* **2001**, *500*, 333.

(21) Chu, D.; Gilman, S. *J. Electrochem. Soc.* **1996**, *143*, 1685.

(22) Richarz, F.; Wohlmann, B.; Vogel, U.; Hoffschulz, H.; Wandelt, K. *Surf. Sci.* **1995**, *335*, 361.

(23) Frelink, T.; Visscher, W.; van Veen, J. A. R. *Surf. Sci.* **1995**, *335*, 353.

(24) Lopez De Mishima, B.A.; Mishima, H.T.; Castro, G. *Electrochim. Acta* **1995**, *40*, 2941.

(25) Gasteiger, H. A.; Markovic, N.; Ross, P. N.; Cairns, E. J. *J. Phys. Chem.* **1993**, *97*, 12020.

(26) Ianniello, R.; Schmidt, V. M.; Stimming, U.; Stumper, J.; Wallau, A. *Electrochim. Acta* **1994**, *39*, 1863.

(27) Gasteiger, H. A.; Markovic, N.; Ross, P. N.; Cairns, E. J. *J. Phys. Chem.* **1994**, *98*, 617.

(28) Stonehart, P. *Electrochim. Acta* **1973**, *18*, 63.

(29) Weaver, M. J.; Chang, S. C.; Leung, L. W. H.; Jiang, X.; Rubel, M.; Szklarczyk, M.; Zurawski, D.; Wieckowski, A. *J. Electroanal. Chem.* **1992**, *327*, 247.

(30) Gomez, R.; Feliu, J.M.; Aldaz, A.; Weaver, M.J. *Surf. Sci.* **1998**, *410*, 48.

(31) Schmidt, T. J.; Noeske, M.; Gasteiger, H. A.; Behm, R. J.; Britz, P.; Brijoux, W.; Bonnemann, H. *Langmuir* **1997**, *13*, 2591.

(32) Waszczuk, P.; Wieckowski, A.; Zelenay, P.; Gottesfeld, S.; Coutanceau, C.; Leger, J. M.; Lamy, C. *J. Electroanal. Chem.* **2001**, *511*, 55.

(33) Tong, Y.; Kim, H.S.; Babu, P.K.; Waszczuk, P.; Wieckowski, A.; Oldfield, E. *J. Am. Chem. Soc.*, **2002**, *124*, 468.

(34) Davis, J. C.; Hayden, B. E.; Pegg, D. J.; Rendall, M. E. *Surf. Sci.* **2002**, *496*, 110.

(35) Friedrich, K. A.; Geyzers, K. P.; Linke, U.; Stimming, U.; Stumper, J. *J. Electroanal. Chem.* **1996**, *402*, 123.

(36) Szabo, S.; Bakos, I. *J. Electroanal. Chem.* **1987**, *270*, 233.

(37) Watanabe, M.; Makita, K.; Usami, H.; Motoo S.; *J. Electroanal. Chem.* **1986**, *197*, 195.

(38) Gasteiger, H. A.; Markovic, N.; Ross, P. N. Jr.; Cairns, E.J. *J. Electrochem. Soc.* **1994**, *141*, 1795.

(39) Miller, T. M.; Izumi, A. N.; Shih, Y. S.; Whitesides, G. M. *J. Am. Chem. Soc.* **1988**, *110*, 3146.

(40) Hills, G.J.; Ives, D.G.J. "The Hydrogen Electrode" in Reference Electrodes: Theory and Practice, Ives, D.G.J.; Janz, G.J. (eds), 1961 Academic Press, Inc. New York.

(41) Gong, S.; Lu, J.; Yan, H. *J. Electroanal. Chem.* **1997**, *436*, 291.

(42) Will, F. G. *J. Electrochem. Soc.* **1986**, *133*, 454.

(43) Casey, M.; Leonard, J.; Lygo, B. Procter, G. *Advanced Practical Organic Chemistry* Blackie Academic and Professional, Great Britain, 1990.

(44) Wilson, M.S.; Gottesfeld, S. *J. Electrochem. Soc.* **1992**, *139*, L28.

(45) Wilson, M. S.; Gottesfeld, S. *J. Appl. Electrochem.* **1992**, *22*, 1.

Chapter 5

Summary and Overview

Hydrogenation of **1** using $H_2(g)$ on a Pt substrate at low temperatures (-10 to -40 °C is the lowest energy processes available for deposition of controlled stoichiometric quantities of Ru adatoms on the surface of a Pt substrate. This reaction allows, for the first time, generation of a prototypic kinetic bimetallic surface with real-time control over the stoichiometry and activity of the evolving surface. The knowledge of the real surface area and surface composition of an electrocatalyst is fundamental to the understanding of how such systems operate as catalysts. This is the first time that real-time control over the ratio of Pt to Ru on the surfaces of nanoscale Pt particles has been described.

This system offers significant advantages over conventional methods of deposition of metal adatoms (e.g., metal atom evaporation, chemical vapor deposition, surface organometallic chemistry, and spontaneous electrochemical deposition), namely, providing uniform coverage over all exposed sides of a rough, metal surfaces after adsorption of less than 2 eq Ru_{ad}, allowing for deposition of sub-monolayer amounts of adatoms under reaction-rate control at low temperatures, allowing for use of simple, bench-top equipment and techniques, and use of a Ru precursor (**1**) containing no components that may poison the resulting catalyst surface. This deposition proceeds via a reaction with a metal surface, as such, allows for self-directed depositions of Ru adatoms (or mixtures of Pt and Ru adatoms) on Pt clusters dispersed on an inert support (e.g., Pt/C).

The determination of the optimum surface composition of Pt-Ru_{ad} electrocatalysts for the oxidation of CH_3OH was described. The optimum surface composition of the Pt-Ru_{ad} surfaces prepared by hydrogenation of **1** was between 0.05 and 0.3 eq Ru_{ad} and depends in part on the nature of the Pt substrate. The optimum ratio of Ru to Pt on the blacked electrodes was 0.05 eq Ruad whereas it increases to 0.30 eq Ru on the nanoscale Pt substrates. The optimum surface composition is comparable to that reported for the

shiny bulk Pt-Ru alloys as described in Chapter 1. One notable difference is in their activities toward the electrooxidation of adsorbed monolayers of CO, which may result from differences between the distributions of Ru atoms at the surfaces of Pt-Ru alloys and Pt-Ru_{ad} under these conditions.

The electrochemical activities of the Pt-Ru_{ad} surfaces were noticeably stable (up to 16 h) under the conditions used for this study over a 1 month period (Chapter 2), illustrating that certain metal-metal adatom systems are suitable for long-term studies under the appropriate conditions. Although the absolute lifetimes of the Pt-Ru_{ad} surfaces under these conditions are unknown, they do not immediately decompose by surface segregation or by dissolution of Ru. The lifetime of Ru_{ad} atoms on the surface of the Pt_{black} substrate exceeds all of the experimental time-scales examined thus far, indeed since this work similar fuel cells have shown stable activities over periods of up to 20 days. These results indicate that Ru_{ad} modified Pt_{black} surfaces are stable and are therefore worthy of consideration for further evaluation in prototype Direct Methanol Fuel Cells.